Analysis of Developmental Epistasis by Chromatin Immunoprecipitation in *Xenopus laevis*

Dissertation zur Erlangung der Doktorwürde des Dr. rer. nat.
an der Fakultät für Biologie der
Ludwig-Maximilians-Universität München

vorgelegt von

Katrin Mansperger

München 2007

Erklärung und ehrenwörtliche Versicherung:

Ich versichere, dass ich die vorliegende Arbeit selbstständig durchgeführt habe und keine anderen als die aufgeführten Hilfsmittel und Quellen benutzt habe.

Hiermit erkläre ich, dass ich mich einer Doktorprüfung anderweitig ohne Erfolg nicht unterzogen habe.

Mündliche Prüfung ablegt am 25. Juli 2007

1. Gutachter: Prof. Dr. Peter Becker

2. Gutachter: Prof. Dr. Heinrich Leonhardt

für meine Eltern

„The final aim of all love intrigues, be they comic or tragic, is really of more importance than all other ends in human life. What it turns upon is nothing less than the composition of the next generation.“

Arthur Schopenhauer, quoted by Charles Darwin

This work gave rise to the following publication:

Linder, B., Mentele, E., **Mansperger, K**., Straub, T., Kremmer, E. and Rupp, R.A. (2007) CHD4/Mi-2beta activity is required for the positioning of the mesoderm/neuroectoderm boundary in Xenopus. *Genes Dev*, **21**, 973-983.

Table of Contents

1 Summary 1

2 Introduction 3

2.1 The live cycle of the African clawed frog *Xenopus laevis* 3

2.2 Determination signals and induction events in *Xenopus laevis* 4

2.2.1 Transcriptional regulation of the muscle determination factor MyoD 6

2.2.2 Canonical Wnt/β-catenin signaling during embryonic development 8

2.2.3 Distinct regulatory input of the SNF2-like chromatin remodeling ATPase CHD4 12

2.3 Epigenetics - from genotype to phenotype 13

2.4 Chromatin 15

2.4.1 Structural features of chromatin 15

2.4.1.1 The nucleosome 16

2.4.1.2 The 30nm fiber 16

2.4.1.3 Higher order chromatin structure 17

2.4.2 ATP-dependent chromatin remodeling 18

2.4.2.1 SWI/SNF-containing chromatin remodeling complexes 19

2.4.2.2 CHD class of remodelers 20

2.4.3 Covalent, post-translational histone modifications 21

2.4.3.1 Acetylation 23

2.4.3.2 Methylation 24

2.4.3.3 Other modifications 27

2.5 Chromatin immunoprecipitation (ChIP) 27

2.6 Objectives 30

3 Materials and Methods 31

3.1 Reagents 31

3.1.1 Fine chemicals 31

3.1.2 Enzymes and proteins 31

3.2 Laboratory Equipment 31

3.3 Antibodies 32

3.3.1 Primary Antibodies 32

3.3.1.1 Primary Antibodies, commercially available or published 32

3.3.1.2 Rat monoclonal antibodies 32

3.3.2 Secondary Antibodies 34

3.3.2.1 Immunocytochemistry *34*
3.3.2.2 Immunofluorescence *34*
3.3.2.3 In Situ Hybridization *34*
3.3.2.4 Western Blot analysis *34*

3.4 Nucleic acids 34

3.4.1 Solutions 34
3.4.2 Size standard 34
3.4.3 Oligonucleotides 35
3.4.3.1 Oligonucleotides for RT-PCR *35*
3.4.3.2 Oligonucleotides for cloning *35*
3.4.3.3 Oligonucleotides for real-time PCR *36*
3.4.4 Plasmids 38
3.4.4.1 Vectors for cloning *38*
3.4.4.2 Plasmids for in vitro transcription *39*
3.4.4.3 Plasmids for dig-labeled RNA in situ hybridization probes *40*
3.4.4.4 Plasmids for recombinant GST-Fusion-Proteins *40*
3.4.4.5 Plasmids for real-time PCR tests *40*
3.4.5 Handling of bacteria 40
3.4.6 Bacteria strains 40

3.5 Molecular biological methods 40

3.5.1 Solutions 40
3.5.2 Isolation of nucleic acids 41
3.5.2.1 Mini-preparation with Qiagen kit *41*
3.5.2.2 Isolation of RNA *42*
3.5.3 Analysis and manipulation of nucleic acids 42
3.5.3.1 Cloning methods *42*
3.5.3.2 Gel electrophoresis of nucleic acids *42*
3.5.3.3 Isolation of DNA fragments from agarose gel *42*
3.5.4 Polymerase chain reaction (PCR) 42
3.5.4.1 PCR amplification of DNA fragments for cloning *42*
3.5.4.2 RT-PCR assay *43*
3.5.4.3 Real-time PCR *43*
3.5.5 *In vitro* transcription 43
3.5.5.1 In vitro transcription for microinjection *43*
3.5.5.2 In vitro transcription of dig labeled RNA probes *44*
3.5.6 RNA *in situ* hybridization 44

3.6 Embryological methods 45

3.6.1 Solutions....45
3.6.2 Experimental animals....45
3.6.3 Superovulation of female *Xenopus laevis*....46
3.6.4 Preparation of testis....46
3.6.5 *In vitro* fertilization of eggs and culture of the embryos....46
3.6.6 Removal of the egg jelly coat....46
3.6.7 Injection of embryos....46
3.6.8 Preparation of animal cap explants....47

3.7 Histological methods....47
3.7.1 Solutions....47
3.7.2 Immunocytochemistry....47
3.7.3 Immunofluorescence on Embryo Sections....48

3.8 Protein analysis....49
3.8.1 Solutions....49
3.8.2 *In vitro* translation....50
3.8.3 Protein extract for SDS-PAGE with StrataClean™ resin....50
3.8.4 Protein extract for SDS-PAGE with StrataClean™ resin and sonication....50
3.8.5 SDS-PAGE and Western Blot Analysis....51
3.8.6 Immunoprecipitation (IP)....51
3.8.7 ChIP-type Immunoprecipitation (ChIP-type IP)....51
3.8.8 Purification of GST-tagged, recombinant proteins....52

3.9 Chromatin Analysis....53
3.9.1 Solutions....53
3.9.2 In Situ Chromatin Immunoprecipitation (ChIP)....54
3.9.3 Douncer ChIP....55
3.9.4 Cesium chloride isopycnic centrifugation....57
3.9.5 Quantification of enriched DNA through ChIP with real-time-PCR....57
3.9.5.1 ΔΔCt Method....57
3.9.5.2 Quantification via standard curves....57

4 Results....58

4.1 Generation of tools for ChIP analyses....58
4.1.1 Antibodies against MyoD....58
4.1.2 Antibodies against Lef1, Tcf1 and Tcf3....61
4.1.2.1 Specificity of the antibodies....67
4.1.2.2 Lef/Tcf protein expression pattern....71

4.2 ChIP Analyses 72
4.2.1 SRF localizes to the *myoD* maintenance enhancer in activin-induced animal cap explants 72
4.2.1.1 Titration of activin containing cell culture supernatant for mesoderm and muscle induction of animal caps 73
4.2.1.2 Optimizing the chromatin shearing conditions 75
4.2.1.3 Quantification of the precipitated DNA via TaqMan technology-based real-time PCR 76
4.2.1.4 SRF is bound to the MyoD maintenance enhancer in activin-treated animal cap explants 80
4.2.2 αLef/Tcf ChIP at the *siamois* and *myf5* loci was irreproducible 81
4.2.3 The switch to the Douncer ChIP protocol helps to remove excessive proteins 83
4.2.3.1 Titration of the chromatin lysate condition 85
4.2.3.2 TaqMan amplicons and method of quantification 88
4.2.3.3 Determination of the amount of antibody 90
4.2.4 Chromatin profiling of the *myoD* locus 91
4.2.5 CHD4 binds to the *sip1* gene 107
4.2.6 ChIP data quality assessment 109

5 Discussion 114
5.1 Technical aspects of ChIP 114
5.1.1 Comparison of ChIP methods 115
5.1.1.1 Preparation of chromatin lysates 115
5.1.1.2 Selection of Antibodies 116
5.1.1.3 ChIP controls 117
5.1.1.4 Real-time PCR techniques 118
5.1.1.5 Abundance of the investigated protein-DNA association 119
5.1.1.6 Quantification and representation of the ChIP data 119
5.1.1.7 Conclusions 121
5.2 Biological results of this project 121
5.2.1 Regulation of the MyoD locus 121
5.2.1.1 Histone ChIP 122
5.2.1.2 αSRF ChIP 125
5.2.1.3 αMyoD ChIP 126
5.2.2 Lef/Tcf transcription factors co-precipitate under ChIP-IP conditions 127
5.2.3 CHD4 binds to the *sip1* locus at exon 1 128
5.2.4 Conclusions 129

5.3 Outlook 130
6 Abbreviations 132
7 References 134
8 Appendix 151

1 Summary

The development of an organism from the fertilized zygote to a multicellular organism is a unidirectional process. It occurs in a spatially and temporally tightly controlled fashion. To understand how the genetic information is interpreted and how the cellular identity is inherited, are major challenges towards the understanding of developmental processes. Epigenetic marks like histone modifications, changes of the protein composition binding to DNA or the remodeling of nucleosomes have been shown to be important for the establishment of tissue-specific transcription profiles.

Chromatin immunoprecipitation (ChIP) is a method to investigate the association of proteins to specific genomic loci. In this study, I have established two protocols for ChIP analyses of *Xenopus laevis* embryos: the In Situ ChIP and the Douncer ChIP. In addition, I have generated several antibodies in collaboration with Dr. Elisabeth Kremmer (GSF München) for ChIP analyses, which were directed against the muscle determination factor MyoD and the Wnt/β-catenin signaling components Lef/Tcf transcription factors Lef1 and Tcf1.

While optimizing of the ChIP protocols, I have analyzed successfully the binding of various transcription factors, chromatin remodeling enzymes and histone modifications on genomic loci of key developmental regulators. With the In Situ ChIP, I have shown that the serum response factor SRF interacts predominantly with the actively transcribed *myoD* gene. Together with other data, this result helps to define a specific role of SRF protein in the stable maintenance of *myoD* transcription, which is essential for proper muscle differentiation.

With the Douncer ChIP protocol, a time course study has been performed in order to understand, when and which histone modification marks appear during muscle cell determination and differentiation on the *myoD* locus. The temporal and spatial distribution of the analyzed histone modification marks was correlated for the most part with the expected patterns. Furthermore, I have demonstrated that direct binding of the chromatin remodeler CHD4/Mi2-β to the 5' part of the *sip1* gene in gastrula stage embryos. This interaction represents a crucial regulatory module, which determines the position along the animal-vegetal axis of the embryo, where the border between the mesodermal and neuroectodermal germ layer will be formed. These examples represent on of

the very few successful ChIP applications for the endogenous proteins in young *Xenopus* embryos, and I hope that my protocols will turn out useful for future investigations of regulatory interactions in this vertebrate model organism.

2 Introduction

2.1 The live cycle of the African clawed frog *Xenopus laevis*

The African clawed frog *Xenopus laevis* has been one of the most favored model organisms for vertebrate experimental embryology over the past decades. Major insights into early embryogenesis like signaling events important for body axis determination or germlayer formation were obtained from studies with *Xenopus* (for review see (Heasman, 2006)).

Regarding embryological studies the major advantage of *Xenopus* over other model organisms like the mouse is that the embryos develop extra-uterine. The super ovulation of the females can be triggered by hormone induction. A female lays from several hundred up to a few thousand eggs per day. Cohorts of eggs can be fertilized *in vitro* at the same time and thus offers the synchrony of clutch. This provides sufficient material to perform large-scale experiments. The embryonic development is rapid. It takes about two days from fertilization to the hatching tadpole. The embryos are relatively large with 1-2mm in diameter. Therefore, they are easy to manipulate, for example by mRNA injection. Furthermore, the embryos can be easily cultured in semi-sterile conditions without external growth factors.

Figure 1 shows an overview of the *Xenopus* live cycle. After fertilization, twelve subsequent cleavage divisions take place. The specific feature of this cleavage phase is that the cells divide very rapidly every 30min. The cell cycle during this first phase consists of only S-phase and M-phase. Except for few loci, no transcription takes place until the so-called mid-blastula transition (MBT) at blastula stage (Niewkoop and Faber stage 8, NF8) five hours post fertilization (hpf). The embryos are staged according to the normal table by Niewkoop and Faber (Niewkoop and Faber, 1994). At MBT, the cell divisions decelerate to about 60-90min, and the cell cycle is separated into the four phases G1, S, G2 and M. During this stage of development, cells are already committed, but not yet determined to their future germ layer. Major cell rearrangements happen during the gastrulation, which starts at about 10hpf. Mesoderm and endoderm move inwards, and the basic bodyplan of the tadpole is established. At

about 15hpf, the neural tube folds up, which gives rise to the brain and the spinal cord. During those stages, also the organs are formed. But they develop a little later during organogenesis at 21hpf. The tadpole hatches at the age of about 48hpf. After about 38 days, changes in the environment, such as nutrient levels, induce the secretion of thyroid hormone. This leads the metamorphosis, which results in effects like the tail destruction, lung enlargement and ossification of the skull. The frogs are sexual mature after about 2 years. This summary is in essence taken from books written by Niewkoop and Wolpert (Niewkoop and Faber, 1994; Wolpert et al., 1998).

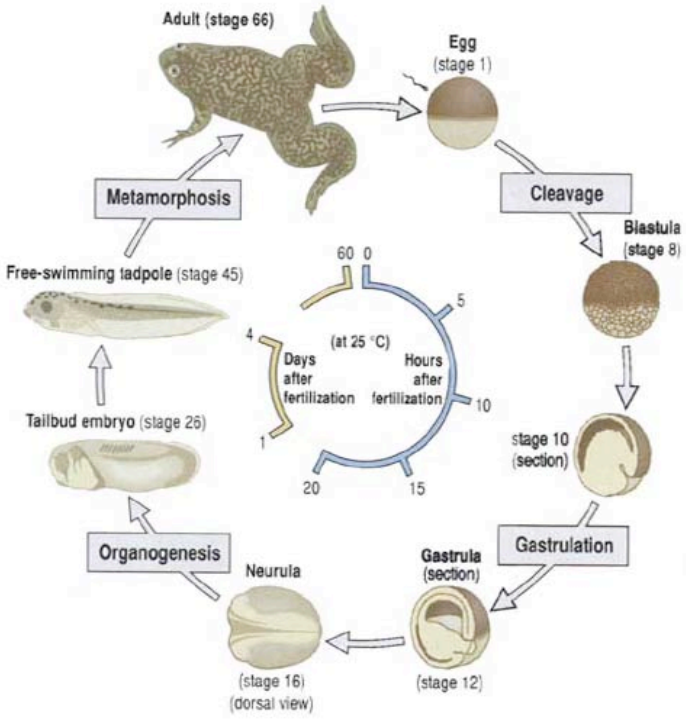

Figure 1: Life cycle of the African clawed frog *Xenopus laevis*

The numbered stages refer to standardized stages of *Xenopus* development (Niewkoop and Faber, 1994). The figure was modified from (Wolpert et al., 1998).

2.2 Determination signals and induction events in *Xenopus laevis*

Developmental studies with *Xenopus laevis* and other amphibians such as newts have made major contributions into the understanding of induction and competence phenomena in vertebrates. In 1925, Hans Spemann and Hilde Mangold performed their pioneering transplantation experiment with newts, whereby they removed the dorsal lip of an early gastrula stage embryo and

transplanted it into the ventral side of a second early gastrula stage embryo. The donor explant then gave rise to a second body axis and Siamese twins formed, which were joined at their bellies. In 1938, Spemann named the dorsal lip the organizer – later called the Spemann organizer – because of its ability to induce and organize the body axis. This induction event is traditionally called the primary embryonic induction (for review see (Gilbert, 2006)). Induction generally refers to the change in fate of a group of cells in response to a signal from other cells. The existence of inductive, diffusible signal molecules was determined a few decades later by transfilter experiments, in which two tissues are separated via a filter to prevent direct cell-cell contact (Grobstein, 1953). In 1986, Horst Grunz and Lothar Tacke showed with this method that the mesoderm inducing activity of *Xenopus laevis* explants can cross a filter with a small pore size (Grunz and Tacke, 1986). Only two years later, Horst Grunz and colleagues as well as Igor Dawid and colleagues purified independently from each other the first secreted growth factor signaling molecule, a protein of the transforming growth factor signaling class β (TGFβ) (Grunz et al., 1988; Rosa et al., 1988).

Besides the necessity of an inducing signal, also the competence of a cell to respond to this signal is important. Major contributions for the understanding of competence phenomena were again derived from studies performed with amphibians. Several groups showed that during development the responsiveness of cells from the ectodermal lineage to inductive signal gets lost (Engländer, 1962; Gebhardt and Nieuwkoop, 1964; Grunz, 1968; Grunz, 1969; Leikola, 1965; Toivonen, 1953). Furthermore, Horst Grunz explored that the competence of ectodermal tissue to respond to various stimuli depends on protein biosynthesis (Grunz H, 1970). In 1989, John Gurdon and colleagues demonstrated with a dissociation experiment that the competence of ectodermal cells to respond to mesoderm inducing signals gets lots over time on the level of single cells (Grainger and Gurdon, 1989). Moreover, Mark Servetnick and Robert Grainger showed with animal cap explants (see Figure-19) that the competence phases of a tissue depend exclusively on its age (Servetnick and Grainger, 1991).

Competence – the ability of cells to respond to an inducing signal – and induction – the change in behavior of a group of cells – are important mechanistic principles of the development from the totipotent zygote to the

multicellular organism. In the subsequent chapters, examples of inductive processes in *Xenopus laevis* will be introduced.

2.2.1 Transcriptional regulation of the muscle determination factor MyoD

A very early link between epigenetic modifications (see chapter 2.3), conversion of cell fate and skeletal muscle development was provided in 1982 by the observation that the treatment of mouse embryonic fibroblasts with the DNA methyltransferase inhibitor 5'-azacytidine converted them frequently into muscle cells (Taylor and Jones, 1982). This led to the cloning of the *myoD* gene (Davis et al., 1987). The basic helix-loop-helix transcription factor MyoD is one of the major determinants of skeletal muscle formation. The *Xenopus* homolog was cloned two years later (Hopwood et al., 1989). At the mid-blastula transition (MBT), which demarcates the onset of zygotic transcription, the *Xenopus myoD* gene is transiently expressed at low levels (Rupp and Weintraub, 1991). This basal gene expression is necessary for the — probably autocatalytic — upregulation of the expression in the preinvoluted mesoderm at the early gastrula stage (see mRNA staining in Figure-2) (Steinbach et al., 1998). It is important to note that in the case of *myoD* the induction occurs on an active rather than an inactive locus. Subsequently, during the neurula und the following tailbud stage, *myoD* expression is maintained in the paraxial mesoderm and in myocytes, respectively (Hopwood et al., 1989). The competence phase for the up-regulation of the *myoD* transcription occurs in a narrow time window of about 90min during the mesodermal competence phase (see Figure-2) (Steinbach et al., 1998). Somatic linker histones gradually replace the maternal linker histone B4 after MBT. The window of mesodermal and myogenic competence is terminated by this replacement at the end of the gastrulation (Steinbach et al., 1997). In mouse, the linker histones also play an important role in the repression of myogenic genes. The somatic linker histone H1b cooperates with the homeobox protein Msx1 in order to repress *myoD* transcription (Lee et al., 2004).

Several growth factor signaling cascades liked sonic hedgehog (SHH), FGF, Wnt or TGFβ have been implicated to be important for the determination of the muscle lineage. Furthermore, also DNA hypomethylation and histone deacetylase (HDAC) activities have been shown to be involved in the induction of *myoD* (for review see (Rupp et al., 2002)). However, a direct link between these

pathways, the epigenetic phenomena and the *myoD* gene has not yet been established.

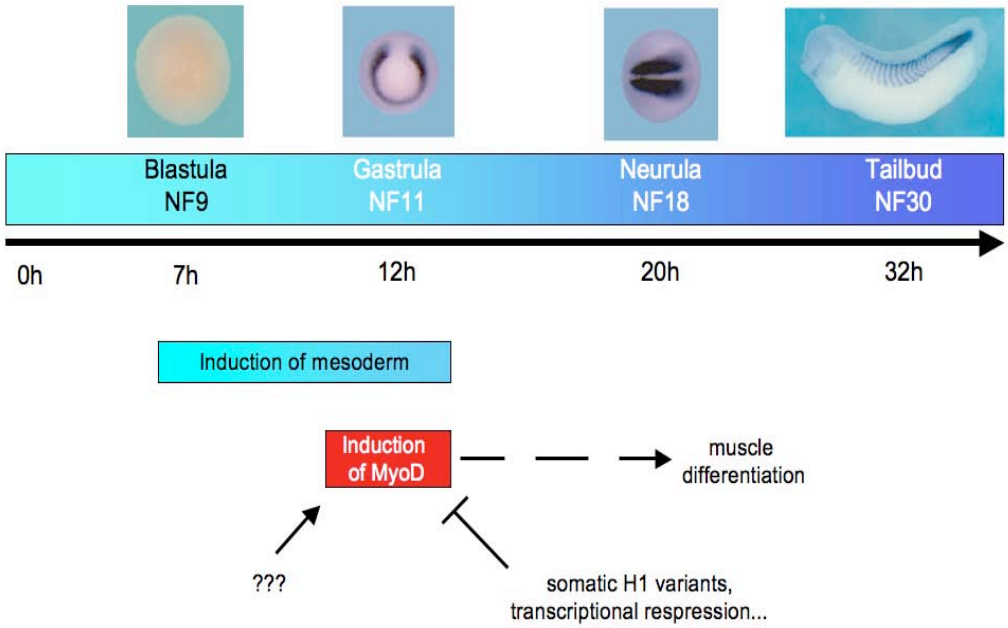

Figure 2: Regulation of *myoD* transcription

The figure describes the timing of the *myoD* induction and expression pattern. The upper pictures show the mRNA expression domains of *myoD*.

To gain further insights into the complex regulation of *myoD* and to understand the specification of the myogenic lineage, the locus of *Xenopus myoD* was analyzed via restriction enzyme-mediated integration (REMI) transgenesis in our lab (Otto, 2000; Xiao, 2003) (see Figure 3). A construct with a Green Fluorescent Protein (GFP) insertion in the first exon was used for this approach. The GFP transgene was able to mimic the endogenous *myoD* expression domain. Analysis of several deletion mutants of the wild type construct mapped two important elements. The deletion mutant of -900bp to -700bp was not able to induce the transcription of the transgene and thus identified it as the induction enhancer. The deletion mutant from -1800 to -1600bp induced the transgene properly, but could not maintain its expression. Therefore, this region of the *myoD* locus was identified as the maintenance enhancer. Further fine-mapping of the induction enhancer via a linker scan approach discovered two regulatory units within the enhancer element: one responsible for the induction and one important for the repression of *myoD*. The

repressive element was also shown to be important for the correct timing of the induction (Xiao, 2003). Yet again, the nucleotide sequences of the inductive and repressive linker scan elements revealed no new direct link to any of the myogenic inducers mentioned above.

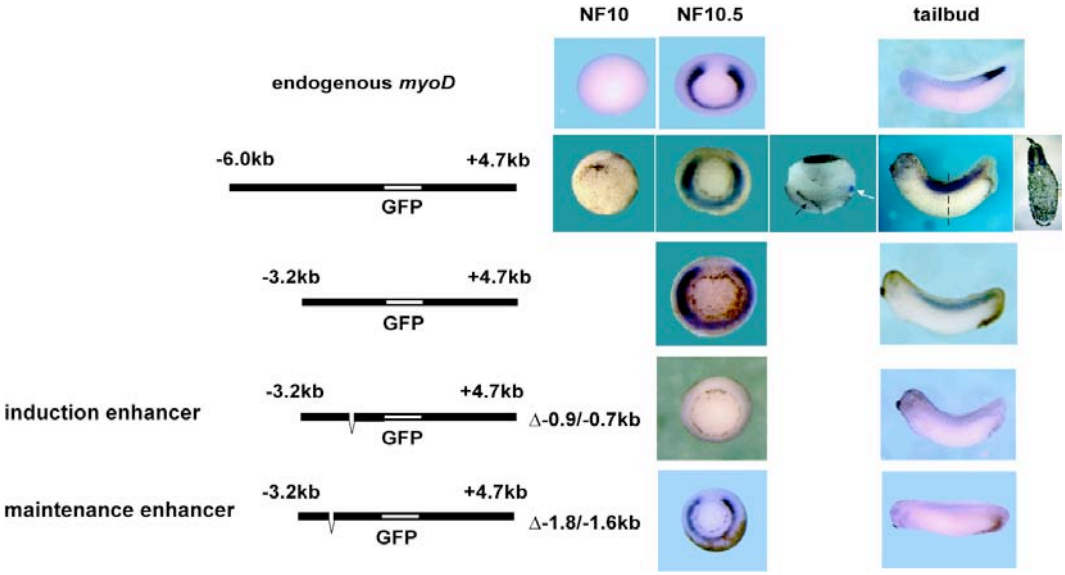

Figure 3: MyoD promoter analysis by REMI-transgenesis

The upper lane shows the endogenous mRNA expression domain of *myoD*. The other lanes show *GFP* mRNA expressions of the *myoD* reporter construct. The transgene with the whole locus is able to mimic the endogenous *myoD* expression domain. Deletion mutants devoid of either the induction or the maintenance enhancer are not able to induce or maintain the transgene expression. The figure was adapted from (Xiao, 2003).

Within the maintenance enhancer, a serum response factor (SRF) binding site, but not adjacent Lef/Tcf or FAST binding sites was shown to be important for the maintenance of the *myoD* transcription. Mutations of this SRF site in the reporter gene construct led to the loss of the transgene in neurula stage embryos (Nentwich, 2003; Xiao, 2003) (for a sketch of the *myoD* locus see Figure 28).

2.2.2 Canonical Wnt/β-catenin signaling during embryonic development

The Wnt signaling pathway is among the most important inductive signaling cascades throughout embryonic development and adulthood. During embryogenesis, it is involved in processes like axis specification, patterning, organogenesis, limb formation, adipogenesis, angiogenesis and stem cell development. During adulthood, it is important for the stem cell maintenance for

example of hair follicles or the gut crypt. Furthermore, it is involved in many types of cancer and Alzheimer's disease (Moon et al., 2002; Stark et al., 2007).

The central signal-transmitting molecule is β-catenin (Figure 4). Besides its signaling function, it is also essential for the formation of cadherin junctions. Binding of the Wnt ligand to the frizzled receptors and its co-receptor Lrp5/6 blocks the destruction complex that contains, amongst other proteins, the glycogen synthase kinase 3 (GSK3) (Figure 9). As a consequence, β-catenin is not phosphorylated, which would otherwise target it to the proteasome. The stabilization of β-catenin allows its translocation into the nucleus, where it binds to transcription factors such as the T-cell factor (Tcf) or lymphocyte enhancer factor (Lef) and activates target gene expression (for review see e.g. (Wang and Wynshaw-Boris, 2004) or http://www.stanford.edu/~rnusse/wntwindow.html).

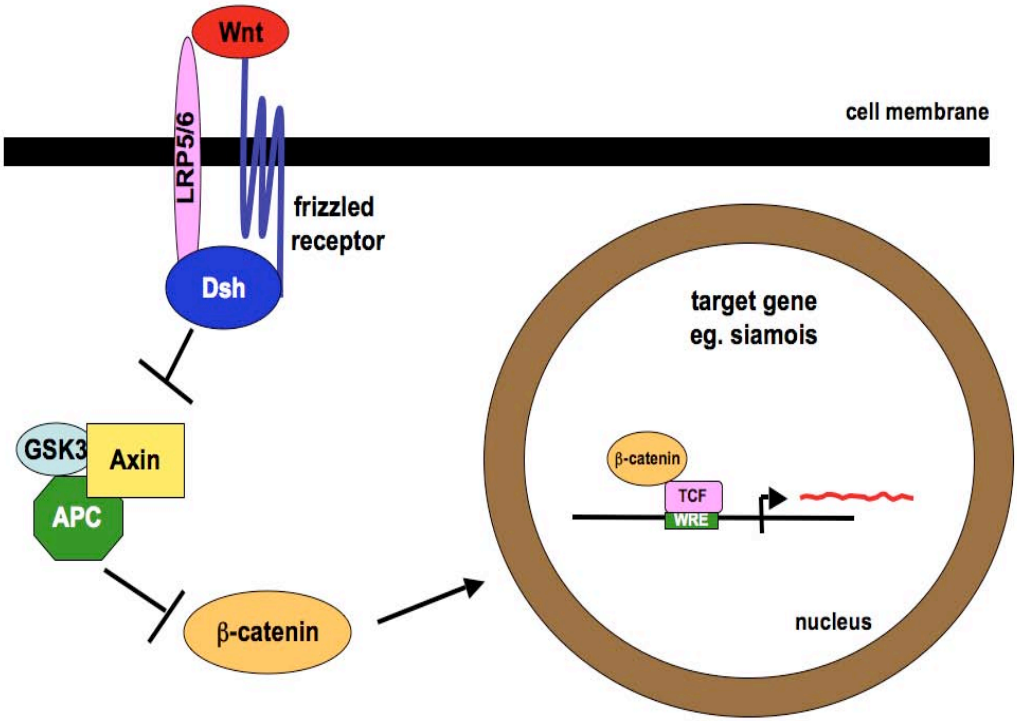

Figure 4: Canonical Wnt/β-catenin signal transduction pathway

The figure describes the signal transduction by inhibition of inhibitory molecules.

During the early *Xenopus* embryogenesis, the canonical Wnt signaling cascade plays different roles during development. It is important for the establishment of the dorso-ventral axis during cleavage stages, for the patterning of the mesoderm during the gastrula and for the patterning of the neuroectoderm

(for review see (Heasman, 2006; Stern, 2005)). Wnt target genes, which are involved in the establishment of the dorso-ventral axis and the Spemann organizer, are the homeobox genes *siamois (sia)* (see Figure 5B), its homolog *twin (xtwn)* and *nodal related 3 (xnr3)* (Brannon et al., 1997; Brannon and Kimelman, 1996; Laurent et al., 1997; McKendry et al., 1997). The responsiveness of the target genes to Wnt signaling is time and space dependent. The Wnt-8 ligand is able to induce an ectopic axis by activating the organizer genes *siamois* and *xnr3* (Christian et al., 1991; Smith and Harland, 1992; Sokol et al., 1991). This induction is time dependent. Overexpression of Wnt8 later than MBT failed to induce *siamois* and *xnr3,* but interfered with the patterning of the neuroectoderm. Furthermore, an activated version of the Lef/Tcf transcription factor Tcf3 was also able to induce an ectopic secondary axis (Darken and Wilson, 2001). This suggests that the Lef/Tcf transcription factors regulate the responsiveness of their target genes and thereby also the competence phase of the axis induction.

Most promoters of Wnt target genes comprise several Wnt response elements, which are bound by Lef/Tcf transcription factors. In the absence of Wnt signaling, the Lef/Tcf proteins are bound to their target sites in conjunction with Groucho-like co-repressors. Upon Wnt stimulation and β-catenin translocation into the nucleus, the Groucho-like co-repressors become displaced and β-catenin together with histone acetyltransferase p300/CBP (Hecht et al., 2000) and ATP-dependent chromatin remodeling ATPase Brg1 (see chapter 2.4.2.1) binds to the Lef/Tcf proteins and thus activates gene transcription (for review see (van Noort and Clevers, 2002)). In *Xenopus*, it could be shown that Brg1 is important for the transcriptional activation of *xnr3* and *siamois* (Singhal, 2005). The *siamois* promoter contains five Lef/Tcf binding sites, of which two have activating and three have repressive function. This demonstrates the complex regulation of the *siamois* gene expression by Lef/Tcf proteins (see Figure 5B) (Brannon et al., 1997).

In addition to its activating function, canonical Wnt signaling is also involved in the repression of genes. An example is the myogenic transcription factor *myf5*. Two distal Lef/Tcf binding sites are important to prevent the *myf5* expression during the gastrula stage at the Spemann organizer (Yang et al., 2002), which has high levels of Wnt signaling (Schohl and Fagotto, 2002) (see Figure 5A).

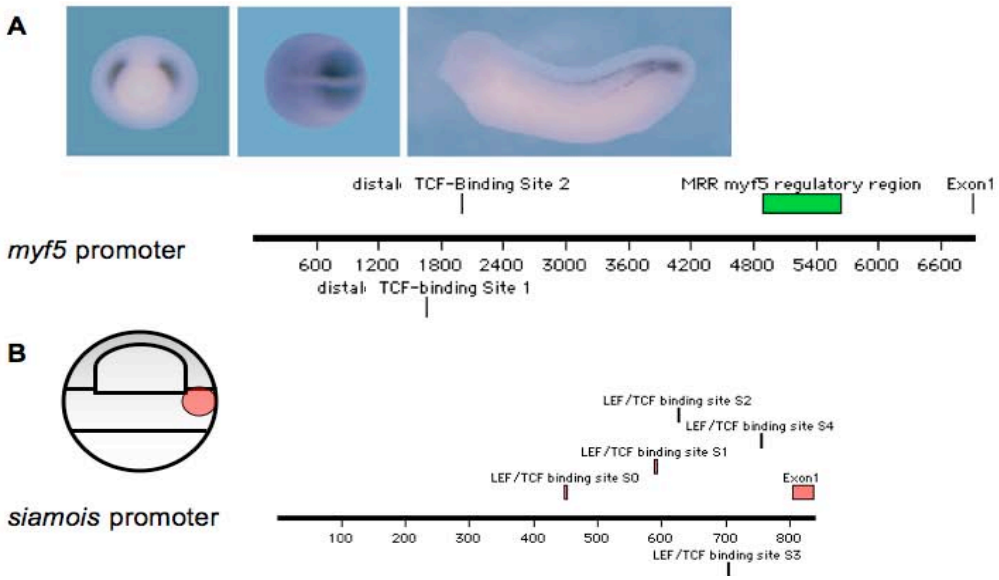

Figure 5: Wnt/β-catenin target genes

A) The bottom panel shows the *myf5* promoter with two distal Lef/Tcf binding sites, a target gene that is negatively influenced by Wnt signaling. The top panel shows the endogenous *myf5* mRNA expression pattern. **B)** shows the positively regulated *siamois* promoter with its five Lef/Tcf binding sites. The cartoon illustrates in red the *siamois* expression domain in the future Spemann organizer in the late blastula stage.

The *Xenopus laevis* Lef/Tcf protein family consists of four members Tcf1, Lef1, Tcf3 and Tcf4 (see Figure 13). The Lef/Tcf genes have distinct, yet in part overlapping mRNA expression domains. Tcf1 and Tcf3 are maternally expressed (Kunz et al., 2004; Molenaar et al., 1998; Roel et al., 2003). Lef1 and Tcf4 are zygotically expressed from the early gastrula stage and from late neurula on in the brain anlage, respectively (Konig et al., 2000; Molenaar et al., 1998).

The Lef/Tcf protein family members possess a N-terminal β-catenin binding domain and a C-terminal DNA-binding HMG box. In addition, Tcf3 and Tcf4a possess a central motif that has repressive function (Pukrop et al., 2001). Furthermore, it could be shown that the individual Lef/Tcf protein family members have distinct roles in the transmission of the Wnt signal throughout development. Lef1 has activating function and is important for the patterning of the mesoderm after the onset of zygotic transcription (Roel et al., 2002). Tcf3 is required for the maternal Wnt signaling during axis specification. It has repressive function and prevents Wnt target gene expression on the future ventral side (Houston et al., 2002; Roel et al., 2002). Furthermore, it is required for the induction of the

mesoderm (Liu et al., 2005). Tcf1 plays a dual role during the maternal Wnt signaling. Ventrally and laterally it prevents target gene activation, whereas dorsally it activates their expression (Standley et al., 2006). Tcf4 plays an important role in the patterning of the midbrain (Kunz et al., 2004).

2.2.3 Distinct regulatory input of the SNF2-like chromatin remodeling ATPase CHD4

Chromatin remodeling, SNF2 domain containing ATPases catalyze the alteration of nucleosome positions (see chapter 2.4.2). In 2004, our laboratory published the screening of 29 members of the SNF2 domain containing protein family for *Xenopus laevis* (Linder et al., 2004). Expression analyses of these proteins revealed that the family members are not ubiquitously expressed, but that they have stage and tissue-specific mRNA expression domains. The chromatin remodeling ATPase CHD4 was further analyzed by gain and loss of function studies in regard to their influence on specific marker genes (Linder et al., 2007). Loss of function experiments with CHD4 reduced the expression domain of the mesodermal marker gene *Xenopus brachyury (Xbra)* and expanded the expression domain of the neuroectoderm marker gene *Smad-Interacting Protein 1 (sip1).* Both genes demarcate the border between the mesoderm and the neuroectoderm. These borders are formed between the germlayers during the gastrulation. How the inducing signals are transformed into these sharp boundaries is still not solved in detail. The current knowledge suggests that the developmentally important genes receive a complex regulatory input. *Xenopus brachyury (Xbra)* is such a gene, which is expressed in response to Nodal/Smad2 and FGF/MAPK signaling. Xbra is induced shortly before gastrulation in the future mesoderm (for review see (Wardle and Smith, 2006)). The typical ring-like transcription domain is generated by activating signals combined with transcriptional repression in areas, where *Xbra* expression is not necessary (Latinkic et al., 1997; Lerchner et al., 2000). The Smad-Interacting Protein 1 (Sip1) is a potential repressor of *Xbra*, since a single bipartite binding site is located in the *Xbra* promoter region (Eisaki et al., 2000; Lerchner et al., 2000; Papin et al., 2002; Verschueren et al., 1999). Sip1 has neural-inducing activity in *Xenopus laevis* animal cap explants (Eisaki et al., 2000; Nitta et al., 2004). In chicken embryos, Sip1 is important for a pathway, which promotes the formation of neurogenesis and suppresses mesoderm (Sheng et al., 2003). In

Xenopus, *Xbra* and *sip1* are initially co-expressed at the beginning of gastrulation, but their domains are quickly separated into neighboring domains, which mark the future mesoderm and neuroectoderm, respectively (Papin et al., 2002). The mechanism, by which this separation happens, is so far unknown. However, our laboratory showed with mRNA *in situ* hybridization experiments and animal cap explanation assays (see Figure 19A) that CHD4 is important for the positioning of the neuroectoderm/mesoderm border, by controlling specifically the Nodal input via Sip1 for the *Xbra* transcription (Figure 6) (Linder et al., 2007).

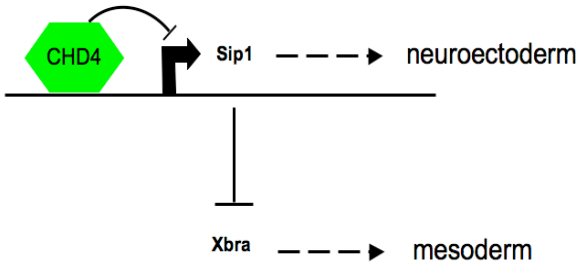

Figure 6: Positioning of the mesoderm/neuroectoderm boundary by Chd4

The cartoon illustrates the regulatory network of the positioning of the neuroectoderm/mesoderm border: CHD4 binds to the *sip1* locus and restricts the expression of the gene. Sip1 on the other hand is involved in the repression of *Xbra*.

2.3 Epigenetics - from genotype to phenotype

The development of a multicellular organism is a unidirectional process, which occurs in a tightly controlled spatial and temporal fashion. It starts with a single, totipotent cell — the fertilized egg. Through subsequent cell divisions, the zygote gives rise to the complex organism. The developmental process leading from a totipotent cell to specialized cell types is called differentiation. This requires multiple preceding events resulting in the committed and finally differentiated cell. The process of commitment is divided into two stages. The first is the specification step, which is reversible. A cell or a tissue is defined as specified, when it can differentiate autonomously in a neutral environment. The second stage of commitment is called determination. Cells are considered to be determined, when they can differentiate autonomously even when placed in a non-neutral environment (for detailed information see (Gilbert, 2006)).

But how is a differentiation profile inherited, based on the fact that all cells of one organism posses the identical genome? The underlying principle of

this cellular memory is called epigenetics. Conrad Waddington coined the term, when he defined epigenetics as “the branch of biology, which studies the causal interactions between genes and their products, which bring the phenotype of the being” (Waddington, 1942). In 1957, he published the epigenetic landscape (Waddington, 1957) (Figure 7). It describes the differentiating cell as a marble rolling along a landscape. At the branches, the marble can choose between two ways. Thereby, it will have made several binary choices until it reaches the bottom of the landscape (for review see (Slack, 2002)).

The current definition of epigenetics is a “bridge between genotype and phenotype — a phenomenon that changes the final outcome of a locus or chromosome without changing the underlying DNA sequence. (…) Cellular differentiation may be considered an epigenetic phenomenon, largely governed by changes in what Waddington described as the epigenetic landscape rather than alterations in genetic inheritance. More specifically, epigenetics may be defined as the study of any potentially stable and, ideally, heritable change in gene expression or cellular phenotype that occurs without changes in Watson-Crick base-pairing of DNA” (Goldberg et al., 2007). The majority of the ongoing epigenetic research concerns the study of covalent histone modification, DNA methylation, nucleosome remodeling and other mechanisms that influence the chromatin structure of a specific gene locus.

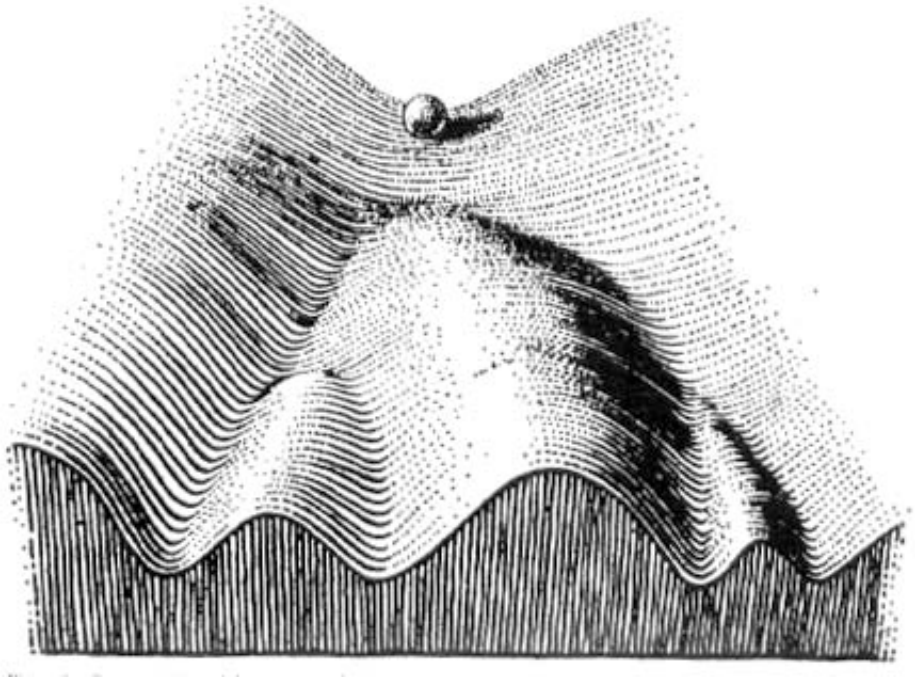

Figure 7: The epigenetic landscape

The marble represents a cell that rolls down a landscape-like surface. At various points the marble can roll into different valleys, *id est* the cell can differentiate into various cell types. So by the time, when the marble has reached the bottom of the landscape, it has made several binary choices (Waddington, 1957).

2.4 Chromatin

2.4.1 Structural features of chromatin

Chromatin is the complex of DNA and proteins found inside the nuclei of eukaryotic cells. The name chromatin originates from the fact that it is easy visible by staining. Walter Flemming coined the term in 1882, which is derived from the Greek word "χρωμα" for color, when he observed the nuclear material by light microscopy (Flemming, 1882). In order to fit the large genome within the dimension of a nucleus, the DNA has to be compacted. The major proteins involved in the compaction of the DNA are the histone proteins, but also other chromosomal proteins are engaged in the compaction. Simplified, three levels of chromatin compaction exist: (I) the nucleosome: DNA wrapping around a histone octamer, (II) the 30nm-fiber: chromatin condensed with the help of linker histones, and (III) the higher order structure of the chromatids (see Figure 8).

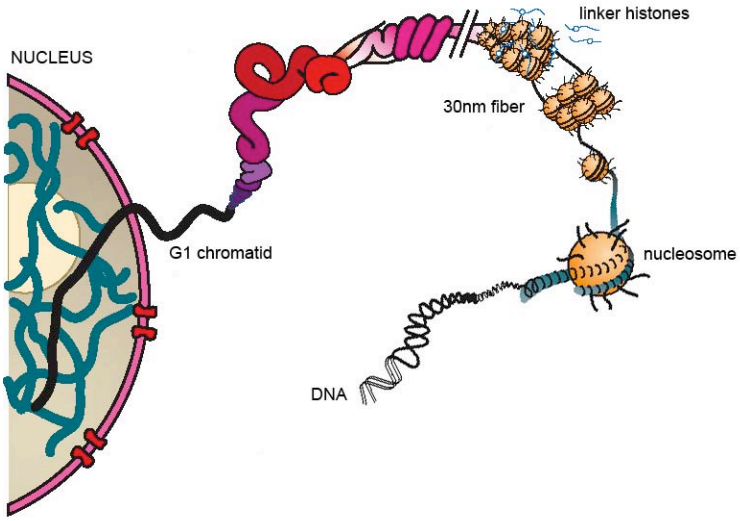

Figure 8: Schematic representation of the DNA packing in the nucleus

The DNA is wrapped around a histone octamer forming the nucleosome. With the help of linker histones, the DNA is further compacted into the 30nm fiber. This stage is followed by several higher orders of compaction. The figure was adapted from (Hansen, 2002).

2.4.1.1 The nucleosome

In 1974, Roger Kornberg suggested that the structural repeating unit within the eukaryotic nucleus would be the nucleosome, as it is defined nowadays (Kornberg, 1974). The final structure of the nucleosome was resolved by Richmond and colleagues more than 20 years later (Luger et al., 1997). The basic repeat element, the nucleosome, consists of 1.65 turns of DNA (=146bp) wrapped around the histone octamer complex. The complex is composed of a central tetramer of the histone proteins H3 and H4 and two dimers of the Histones H2A and H2B. The histone proteins are small basic proteins with an N-terminal domain, a so-called central histone fold domain, and a C-terminal domain. The N-termini and some C-termini reach tail-like out of the globular octamer domain. These tail-like protrusions are major substrates for covalent modifications like methylation, acetylation etc. (see chapter 2.4.3, Figure 9) (for review see (Alberts et al., 2004)). The histone proteins belong to the most conserved protein among all eukaryotes. In addition, many eukaryotic organisms developed specialized histone variants, which differ only in very few amino acids. For example, four vertebrate histone variants for H3 are known: H3.1, H3.2, H3.3 and CENP-A. CENP-A is a H3 variant that is specifically localized at centromers. The variant H3.3 is associated with actively transcribed loci. The roles of H3.1 and H3.2 are less well understood (for review see (Bernstein and Hake, 2006)). These various histone modifications and variants, which are found incorporated into the histone octamer, emphasize the important role that the nucleosomes play in the regulation of gene expression.

2.4.1.2 The 30nm fiber

Adjacent nucleosomes are linked via the so-called linker DNA, which varies in length in a cell- and species-specific manner. Long chains of nucleosomes can be visualized by electron microscopy as a “beads-on-a-string”-structure, but are very unlikely to exist as such in a living cell. Instead, these nucleosome arrays are very tightly compacted in a larger structure, called the 30nm-fiber (for review see (Alberts et al., 2004)). Additional histone proteins, the linker histones, are important for the formation of this structure. The linker histones consist of a central, globular domain and a highly positive charged C-terminal domain. With their globular domain they anchor themselves to the nucleosome. The C-terminal domain binds to the linker DNA (for review see

(Jerzmanowski, 2004)). How the structure of the 30nm-fiber looks like, is still highly debated. Visualization studies with electron microscopy show a various types of zigzag models (for review see (Alberts et al., 2004)). However, recent studies by Rhodes and colleagues suggest a one-start chromatin-fiber model with interdigitated nucleosomes (for review see (Robinson and Rhodes, 2006)).

The linker histones are less conserved than the core histones. Histone variants differ from the conventional histones by slight or significant alterations of the amino acid composition (for review see (Bernstein and Hake, 2006)). The linker histone variants can be divided into maternal and somatic linker histones. They differ mainly in their length and charge of their C-terminal domains. The *Xenopus* maternal linker histone B4 and somatic linker histone H1a share only about 30% sequence identity (Dworkin-Rastl et al., 1994). During early *Xenopus* development until mid-blastula transition (MBT) (also see chapter 2.1), the nuclei contain the oocyte-specific linker histone B4. From MBT onwards until the end of the gastrulation, B4 is replaced by somatic linker histones H1a, H1b and H1c (Dimitrov et al., 1993; Dworkin-Rastl et al., 1994). The replacement of the maternal B4 with the somatic H1a leads *in vitro* to a stronger compaction of the chromatin, which cannot be remodeled anymore (Saeki et al., 2005). Furthermore, maternal linker histones H1M or H1oo have also been described for mammals and other frog species (for review see (Schulze and Schulze, 1995)).

2.4.1.3 Higher order chromatin structure

The DNA of a chromatid undergoes further levels of compaction compared to the 30nm-fiber. Generally, two populations are detectable with light microscopy: the highly condensed heterochromatin and the less condensed euchromatin (Heitz, 1928). Constitutive heterochromatin is referred to as gene-poor regions with very high levels of DNA compaction like telomeres or centromers. Facultative heterochromatin referrers to chromosome regions, which have lost gene expression like inactivated mammalian X-chromosomes or genes that were silenced during differentiation. Euchromatic regions are described as gene-rich with active transcription (for review see (Elgin and Grewal, 2003; Henikoff, 2000)). Changes in gene expressions can alter the relationship between euchromatin and heterochromatin as well as the location of genes within the nucleus. Furthermore, the local organization of genes on a chromatin-loop bordered by boundary elements or even the organization of the whole chromatid

as giant chromosome loops are described to be important for the regulated expression of a gene (for review see (Cremer et al., 2006; Misteli, 2007)).

2.4.2 ATP-dependent chromatin remodeling

For the precise regulation of the gene expression, eukaryotes have evolved an elaborate system. It depends on enzymes that catalyze dynamic changes of the chromatin structure: enzymes that covalently modify histones act in concert with ATP-dependent chromatin remodeling enzymes to alter DNA-histone interactions. These chromatin-altering enzymes play important roles especially during differentiation processes, where they can promote or prevent gene expression (for review see e.g. (Bouazoune and Brehm, 2006)). Furthermore, chromatin remodeling enzymes are important for the chromatin assembly and the maintenance of the chromosome structure (for review see (Langst and Becker, 2001)).

All chromatin remodeling enzymes harbor an ATPase domain with seven motifs that are characteristic for helicases (Eisen et al., 1995). By comparing different yeast helicase-containing chromatin remodeling machineries by a phylogenetic approach (Bork and Koonin, 1993; Eisen et al., 1995; Gorbalenya et al., 1989), they were divided into several SNF2-domain containing subfamilies. The term SNF2 is derived from the yeast helicase SNF (sucrose nonfermenter), which is important for the growth on sucrose and raffinose (for review see (Sudarsanam and Winston, 2000)). As a result of this phylogenetic and many following studies, three major groups of SNF2-domain containing chromatin remodelers were defined SWI/SNF2, ISWI, INO80 and CHD (for review see for example (Becker and Horz, 2002; Bouazoune and Brehm, 2006)). *Xenopus laevis* and human homologues of these remodelers were clustered in a similarity tree and undescribed *Xenopus* homologues were identified by a EST-based screen in our laboratory (Linder et al., 2004).

The mechanism by which the chromatin remodeling enzymes affect the structure of the nucleosome and the nucleosomal array is distinct for each class of remodelers. This can happen either by catalyzing the depositions or evictions of nucleosomes or by alteration of the nucleosome position (for review see (Saha et al., 2006)).

In the subsequent chapters, the SWI/SNF and CHD class of remodelers will be described in more detail.

2.4.2.1 SWI/SNF-containing chromatin remodeling complexes

The yeast SWI/SNF complex was the first described complex with ATP-dependent chromatin remodeling activity (reviewed by (Bouazoune and Brehm, 2006; Stern et al., 1984)). Independently, the *Drosophila* protein Brahma was identified as a dominant negative repressor of Polycomb mutations. This classified it as a member of the Trithorax group of proteins, which are important for the proper maintenance of homeotic gene expressions in *Drosophila* (Kennison and Tamkun, 1988). Later, this protein was found to be highly related to the yeast SWI/SNF remodeling ATPase (Tamkun et al., 1992). Besides an ATP-dependent helicase domain, the SWI/SNF ATPases possess a second characteristic C-terminal domain, the bromodomain, which distinguishes them from ISWI and CHD-like ATPases (Tamkun, 1995). The bromodomain recognizes acetylated lysines on the histone tails (see Figure 10A) (for review see (Zeng and Zhou, 2002)).

Homologues of *Drosophila* Brahma have also been found in vertebrates like *Xenopus* (Gelius et al., 1999), humans (Chiba et al., 1994; Khavari et al., 1993; Muchardt and Yaniv, 1993) and mouse (Randazzo et al., 1994). In these organisms, two SWI/SNF isoforms exist: Brahma and Brg1 (Brahma related gene 1). The compositions of Brahma- and Brg1-containing complexes are variable and depend on the cellular context. Several publications suggested that the mammalian SWI/SNF complexes play a role in the regulation of cell growth. Many tumor cells misexpress or carry mutations in the Brg1 or Brahma genes. Furthermore, Brg1 was shown to interact with the retinoblastoma protein (Rb), cyclin E and BRCA1, a gene, which is frequently mutated in breast cancer. Most studies support a role of these complexes in the activation of transcription. However, some studies also implicate a role in transcriptional repression (for review see (Becker and Horz, 2002; Bouazoune and Brehm, 2006)). Knockout of either murine Brahma or Brg1 are both viable, since they can compensate for each other (Bultman et al., 2000). In *Xenopus,* Brg1 was described to play an important role in the β-catenin dependent determination of the secondary body axis (Singhal, 2005). In addition, Brg1 is required for neurogenesis by mediating the transactivation of the bHLH transcription factors neurogenin and neuroD (Seo et al., 2005a; Seo et al., 2005b).

2.4.2.2 CHD class of remodelers

The first chromodomain-containing chromatin remodeling ATPase, murine CHD1, was cloned by the laboratory of Rick Perry (Delmas et al., 1993). Subsequently, related proteins have been identified in other eukaryotes. The common feature of the CHD protein family is a pair of chromodomains in addition to the SNF2-related ATPase domain. The chromodomain is named after proteins, which are involved in the regulation of chromatin (chromatin organization modifiers) (Paro and Hogness, 1991). The best studied chromodomain is the one of the heterochromatin protein 1 (HP1), which binds to di- or trimethylated lysine 9 one histone H3 (Grewal and Jia, 2007). Based on protein sequence features and a phylogenetic analysis, the CHD ATPases were grouped into three subclasses (Woodage et al., 1997). Among the second CHD protein subclass are the best-studied CHD proteins CHD3 (Mi-2α) and CHD4 (Mi-2β). They contain two PHD fingers in addition to the chromodomain. PHD fingers are named after the plant homeodomain and are a highly specialized methyl-lysine binding domains (see Figure 10A) (for review see (Mellor, 2006b)). Later, CHD4 was shown to be the chromatin-remodeling ATPase of the NuRD complex. In addition to Mi2, the NuRD complex consists of other subunits: the histone deacetylases HDAC1/2 and the histone H4-interacting proteins RbAP46/48. Furthermore MTA, p66/68 and MBD protein family members, which bind to methylated DNA, were later identified as components of the complex (Brackertz et al., 2002; Brackertz et al., 2006; Feng et al., 2002; Feng and Zhang, 2001; Fujita et al., 2004; Fujita et al., 2003; Wade et al., 1999). Taking these facts together, the NuRD complex is not only able to detect epigenetic modifications like methylation of DNA, but it also combines two different chromatin remodeling strategies: histone modification activity and ATP-dependent nucleosome remodeling activity (Becker and Horz, 2002).

The Mi2 protein containing complexes have various functions throughout *Drosophila* development. A prime function of the *Drosophila* NuRD complex appears to be the prevention of the inappropriate function of developmental transcription programs (Bouazoune and Brehm, 2006). In other model organisms and in cell culture systems, the NuRD complex was also shown to be involved in cell-type specific transcriptional repression (Fujita et al., 2004; Fujita et al., 2003; Unhavaithaya et al., 2002; von Zelewsky et al., 2000).

However, the NuRD complex was also shown to be important for maintaining an active transcription cycle of a estrogen-receptor activated gene (Mellor, 2006a).

2.4.3 Covalent, post-translational histone modifications

Besides the ATP-dependent alteration of the nucleosome position, another way of nucleosome remodeling are covalent, post-translational epigenetic modifications of the core histones. The modifications can either be acetylation, methylation, phosphorylation, ubiquitination or biotinylation of mainly the N-termini of the core histones (Figure 9). To shorten the spelling for the histone modification, the Brno nomenclature will be used, which was set out at the first meeting of the Epigenome Network of Excellence (NoE), at the Mendel Abbey in Brno, Czech Republic: Trimethylation of lysine 4 on Histone H3 will be written for example as H3K4me3 (for review see (Turner, 2005)). Many proteins have been identified that put these modifications in place and/or recognize specifically the one or the other modification (for review see(Kouzarides, 2007; Nightingale et al., 2006)).

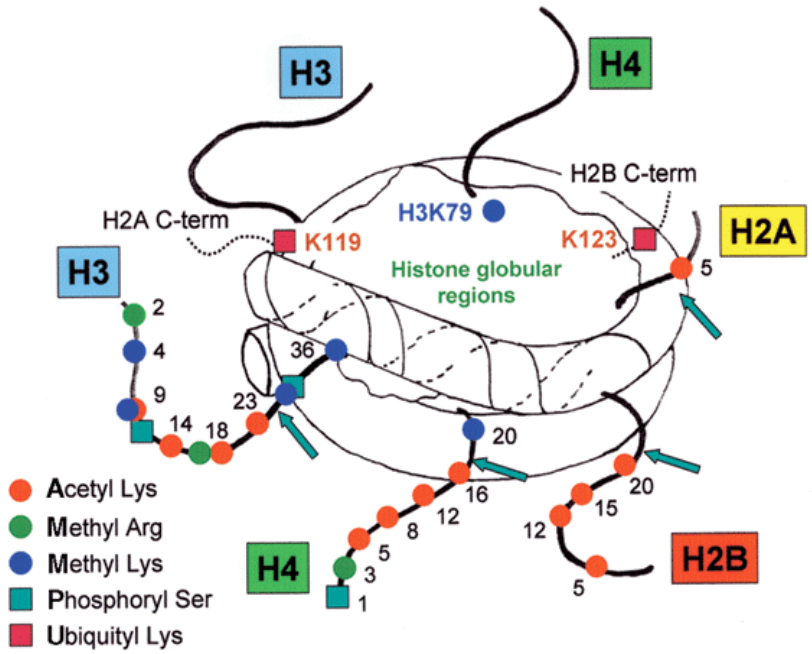

Figure 9: Histone modifications on the nucleosome core particle

The arrows mark the N-terminal, tail-like protrusions of the four core histones. The picture was adapted from (Turner, 2005).

Depending on the position, the quality and the combination, histone modifications have different implications in regard to gene expression. The majority of the histone modifications can be correlated with active transcription, repression and cell cycle stages. Figure 10 gives an overview of the histone modifications on Histone H3 with their corresponding enzymes that read, set and remove them. The color code of Figure 10B (red for repressive function and blue for activating function) and interactions of the different chromatin modifying enzymes illustrates the complexity for the epigenetic regulatory pathways. Some factors regulate or inhibit each other and thereby form a complex network of interactions. Figure 10A shows factors that bind to the corresponding modifications (for review see (Mellor, 2006a)). Furthermore, the histone modifications do not occur in isolation, they rather appear in a combinatorial fashion. Modifications either depend on or antagonize each other. The majority of the modifications is either correlated with active or repressed gene expression. Even hierarchies of histone modifications were postulated (for review see (Allis CD, 2007)).

The finding that most of the histone modifications are correlated with different chromatin states like active or silent gene expression resulted in the proposal of the histone code hypothesis. It is proposed to be a code consisting of histone modifications, which regulate the accessibility and the functional state of the underlying DNA (Jenuwein and Allis, 2001). Further more, Brian Turner suggested the existence of an epigenetic code, which he described as “the way in which the potential for expression of genes in a particular cell type is specified by chromatin modifications put in place at an earlier stage of differentiation” (Turner, 2007). Whether this epigenetic code exists and whether the histone modifications are cause or consequence of changes in gene expression is still under debate.

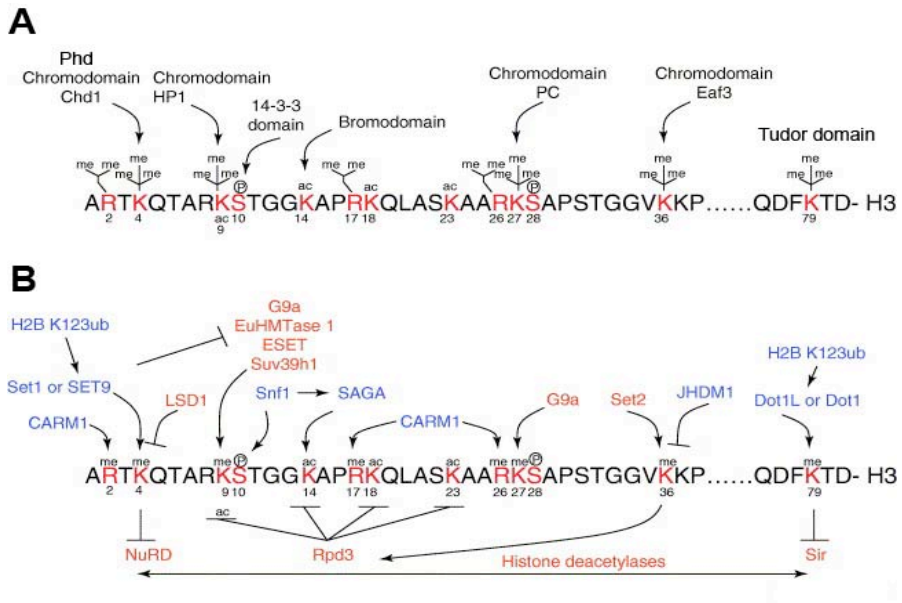

Figure 10: Histone modifications on the N-terminus of Histone H3

The figure shows the IUPAC code of the amino acid sequence of the N-terminus of Histone H3. The modified amino acids are marked in red. The numbers underneath mark the position of the amino acid. me: methylation, ac: acetylation. **A)** shows the factors with their domains that are known to bind to the modifications. **B)** shows the enzymes that modify the residues. Enzymes associated with activating events are marked in blue; those associated with repressive events are marked in red. This figure was adapted from (Mellor, 2006a).

2.4.3.1 Acetylation

Acetylation of histones was first described in the early 1960ies. It was shown that acetylated histones do not inhibit the *in vitro* RNA synthesis as non-acetylated histones do (Allfrey et al., 1964; Phillips, 1963). Acetylation is placed on lysines of the N-termini of H3 and H4 and is correlated with active RNA transcription (for review see (Nightingale et al., 2006)). Histone acetylation alters the chromatin structure by weakening the interactions between the core histones and the DNA. Other studies have proven that the transcriptional activation of a gene due to histone acetylation is brought about by specific binding factors. Bromodomain proteins like Brahma or Brg1 have been shown to bind to acetylated lysines with high affinity (see Figure 10A) (for review see (Fischle et al., 2003)).

The enzymes that are responsible for the acetylation of the histones are the histone acetyltransferases (HATs). HATs are parts of multimeric complexes. Based on sequence similarities, HATs are grouped into several subfamilies. The Gcn5/PCAF family functions as a co-activator for a specific subset of transcriptional activators and contains besides the HAT domain a

conserved bromodomain. Another family is called p300/CBP. The members of this family harbor a more extended HAT domain than the PCAF family members and are more globally involved in transcriptional regulation (for review see (Santos-Rosa and Caldas, 2005)).

The acetylation of the lysine residues is reversible, and the turnover rate of this modification is very rapid. It occurs within a few minutes (Waterborg, 2001). The deacetylation is governed by histone deacetylases (HDACs). These enzymes are also part of multimeric complexes, which are involved in transcriptional repression. In addition, the HDACs were found in complexes together with HAT and thereby form a local equilibrium of histone acetylation (Yamagoe et al., 2003). The HDACs are grouped into three major subclasses. Class I HDACs are nuclear proteins that are expressed in many tissues. Class II HDACs are larger in size, are expressed tissue-specifically and shuttle between the nucleus and the cytoplasm. Class III HDACs differ in their catalytic mechanism. Their enzymatic activity depends on the cofactor NAD+. HDACs are found to be overexpressed in a variety of tumors (for review see (Santos-Rosa and Caldas, 2005)) and are therefore targets for chemotherapy. A critical component of the class I HDAC activity is a zinc-ion in the enzymatic pocket. This site is the main target for anti-cancer drugs and HDAC inhibitors TSA and SAHA (Finnin et al., 1999)

2.4.3.2 Methylation

Histone methylation has been described about 40 years ago (Murray, 1964). Arginine and lysine residues can be mono-, di- or tri methylated. Methyl groups are transferred to arginine residues by protein arginine methyltransferases (PRMTs) (see Figure 10A) and have either activating or repressive function. The methyltransferases PRMT1 and CARM1 are involved in transcriptional activation. Their recruitment is mediated by transcription factors. Furthermore, they were shown to interact with HATs to form co-activator complexes. PRMT5 in contrast is involved in repression (for review see (Santos-Rosa and Caldas, 2005)). In very recent studies, CARM1 was shown to regulate pluripotency (Torres-Padilla et al., 2007) and to be involved in the coupling of transcription and mRNA processing (Cheng et al., 2007). The histone methylation marks have long been considered as stable marks due to their much lower turnover rate compared to the histone acetylations. Mechanisms for the removal

of methylated histones like histone replacement or tail clipping were discussed (Klose et al., 2007). For the first time, the enzymatic demethylation of an methylated arginine residue was described by Kouzarides and colleagues in 2004 (Cuthbert et al., 2004). They showed that the peptidyl arginine deiminase 4 (PDI4) converts arginine to citrulline and thereby antagonizes arginine methylation.

Histone lysine methylation is set by histone methyltransferases (HMT). The common catalytic HMT domain is the so-called SET domain. Several well-characterized lysine residues are highly conserved. H3K4, H3K36 and H3K79 methylations are correlated with active transcription, whereas H3K9, H3K27 and H4K20 methylations are correlated with non-transcribed regions. Therefore, the transcriptional state of a locus can be classified according to the present histone methyl marks (Kouzarides, 2007).

H3K4 methylation is catalyzed in mammals (humans) by the Trithorax-related SET1 domain containing protein family MLL (mixed lineage leukemia) with its members MLL1, MLL2, MLL3, MLL4, SET1A and SET1B. H3K4me3 is strongly correlated with active RNA polymerase II transcription and histone acetylation and peaks at the promoter regions. H3K4me2 in vertebrates is found on promoter regions together with trimethylation, while in yeast it is spread throughout genes in either a transcriptionally poised or active state. Recently, H3K4me1 was described to be associated with enhancer regions in human cell lines (for review see (Heintzman et al., 2007)). Methylation marks can be read by proteins containing a chromodomain or a PHD finger (see Figure 10A). An example is CHD1, which binds H3K4 methylation via its chromodomain and mediates ATP-dependent chromatin remodeling (for a detailed review see (Ruthenburg et al., 2007)).

H3K9 methylation is implicated in gene repression as well as the formation of heterochromatin found in telomeres or centromers. The HMTs Suv39-protein family members Suv39h, G9a, EST/SETB1 and EuHMTaseI sets this epigenetic mark (Santos-Rosa and Caldas, 2005). H3K9me-mediated repression is usually facilitated by the Heterochromatin Protein 1 (HP1) (for review see (Kouzarides, 2007)). The recruitment of Suv39h to promote the formation of pericentric heterochromatin is mediated by short heterochromatic RNAs (shRNAs). In contrast, sequence-specific DNA-binding transcriptional

repressor proteins facilitate the recruitment to euchromatic promoters (for review see (Lee et al., 2005)).

H3K27 methylation is involved in transcriptional silencing. H3K27me1 can be found in pericentric heterochromatin, whereas H3K27me3 is a characteristic of the facultative heterochromatin of the inactive X chromosome (Lee et al., 2005). Furthermore, H3K27 methylation is engaged in the silencing of euchromatic gene loci.

This methylation mark is set by the HMTase Enhancer of Zeste (E(z)) of the Polycomb group of protein (PcG). Three PcG complexes (PRC) are described for *Drosophila* and mammals: PRC1 with E(z), Esc (extra sex combs, human homolog: EED), Su(z)12 (suppressor of zeste) and Nurf55 (in humans: RbAp46/48; PRC2 with Pc (Polycomb), polyhomeotic (Ph), Psc (posterior sex combs) and dRING as well as several other factors; the third complex is called PhoRC including Pho (polyhomeotic) and dSfmbt protein. Neither PRC1 nor PRC2 core complexes contain proteins that specifically bind to DNA. Pho is the only known sequence specific DNA binding protein. It was shown to interact with PCR2 (for a detailed review see (Schuettengruber et al., 2007)).

The vertebrate Pho homolog is called Ying-Yang1 (YY1) (Brown et al., 1998). The *Xenopus* YY1 is expressed throughout the embryonic development (Ficzycz et al., 2001; Kwon and Chung, 2003; Morgan et al., 2004). It was shown to be important for neural, neuronal and heart-muscle development (Latinkic et al., 2004; Morgan et al., 2004; Satijn et al., 2001). In pluripotent embryonic stem cell lines, H3K27me3 and EED are found in concert with the activation marks H3K4me2,3 and H3K9ac on promoters of developmentally important genes like *msx1* or *sox2.* This is so far exclusively described for mouse and human (Azuara et al., 2006; Bernstein et al., 2006) and suggests an important role of PcG proteins during embryonic development.

In 2004, the first lysine demethylase LSD1 was discovered. This paved the way for the discovery of many other demethylating enzymes. Two distinct catalytic subunits have been described so far: LSD1 domain and JmjC domain. LSD1 acts as a demethylase for H3K4 methylation; if present in complexes with the androgen receptor, it can also remove methyl groups of H3K9. Furthermore, H3K9 methylation can also be removed by a variety of enzymes containing a JmjC domain like JHDM2A (Klose et al., 2007; Kouzarides, 2007). However, the precise regulatory function of these demethylases is still unclear.

2.4.3.3 Other modifications

Apart from acetylation and methylation, further modifications of histones include phosphorylation, ubiquitination, ADP-ribosylation, biotinylation and SUMOylation. Phosphorylation of serine at position 10 on histone H3 (H3S10ph) during interphase is a sign for chromosome relaxation and gene expression. During metaphase it correlates with chromosome condensation (for review see (Prigent and Dimitrov, 2003)). The mono-ubiquitination of H2B (H2BK123ub) is important for the methylation of H3K4me2,3 and H3K79me (for review see (Nightingale et al., 2006)). Polyubiquitination is a general sign for proteasome-mediated proteolysis (for review see (Pickart and Cohen, 2004)). The other modifications are less well studied.

2.5 Chromatin immunoprecipitation (ChIP)

Complex inductive signaling networks bring about epigenetic alterations in the chromatin environment, resulting ultimately in the change of gene expression. These events are part of cellular determination and differentiation processes. A method to investigate the chromatin environment during development is the chromatin immunoprecipitation (ChIP). This technique allows studying the association of proteins to a specific genomic region *in vivo*. The assay involves the fixation of chromatin proteins to DNA, fragmentation of the chromatin, immunoprecipitation, purification and quantification of the enriched DNA (see Figure 11).

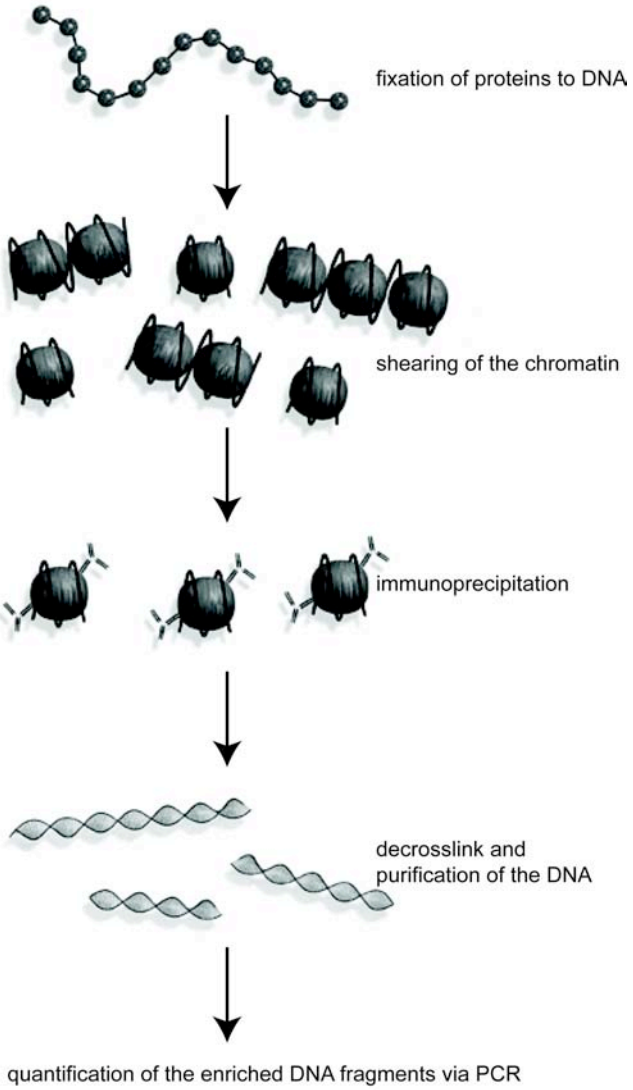

Figure 11: Flowchart of the ChIP procedure

Modified flowchart from www.upstate.com.

The fixation of proteins to DNA with formaldehyde can be traced back to the late 1960ies, when the distribution of newly synthesized histones together with newly replicated DNA was studied with isopycnic CsCl gradient centrifugation (Brutlag et al., 1969; Ilyin and Georgiev, 1969). About five years later, the technique was extended to map histone-histone interactions within nucleosomes (Jackson, 1978; Van Lente et al., 1975). In the 1980's, two groups independently combined the *in vivo* crosslinking and the immunoprecipitation of the chromatin fragments (Gilmour and Lis, 1984; Gilmour et al., 1991; Solomon et

al., 1988; Solomon and Varshavsky, 1985). In these early ChIP assays, the enriched DNA was detected via Southern blot analysis. In the mid 1990's, the extract preparation was simplified and the DNA analysis with Southern Blot was replaced by PCR (Braunstein et al., 1993; Dedon et al., 1991; Hecht et al., 1996; Strahl-Bolsinger et al., 1997). From these pioneering work onwards, the ChIP assay was used for a variety of objectives concerning histone modification, transcription factor binding etc. Multiple modifications of the protocol for several species were published. A good and reviewed protocol collection is provided at the epigenome network of excellence (ENOE) homepage (http://www.epigenome-noe.net). For about seven years, the ChIP technology has been combined with microarray technology to identify genome wide location patterns of proteins (for example (Iyer et al., 2001; Ren et al., 2000)).

Very few ChIPs using antibodies against endogenous proteins have been published for early *Xenopus* embryos (Morgan et al., 2004; Park et al., 2005; Stancheva et al., 2003). The *in vivo* ChIP in developing *Xenopus laevis* embryos is challenging for several reasons: First, the expression domains of important developmental regulators like the organizer gene *siamois* are rather small. Secondly, the younger the embryos are the less cells they have and thus the less desired protein-DNA interactions they contain. Thirdly, no inbred lines of the *Xenopus laevis* exist and therefore, the populations are very heterogenic. However, in order to understand the underlying epigenetic alterations of determination and differentiation processes, the chromatin immunoprecipitation assay with developing vertebrate embryos is an important tool. Therefore, it was very important to establish a reliable protocol for ChIP in early *Xenopus laevis* embryos.

2.6 Objectives

How transcription factors gain access to their target sites *in vivo* in the correct spatio-temporal manner is an important biological issue for the understanding of gene regulation. The accessibility of a putative binding site on the DNA template depends on one hand on the biochemical activities of transacting factors, on the other hand on the local chromatin environment. Chromatin immunoprecipitation (ChIP) examines the *in vivo* association of proteins with specific DNA sequences in the genome.

My methodological goal was to establish a reliable ChIP protocol for early *Xenopus laevis* embryos and ideally, for animal cap explants as well. Furthermore, I aimed to generate antibodies as tool for the ChIP. To understand the influence of inducing signaling events on the chromatin environment of target genes, I analyzed three different scenarios:

1. The temporal and spatial changes of the chromatin environment at the locus of the muscle determination factor *myoD.*
2. The influence of the canonical Wnt signaling pathway on the association of Wnt signaling components to Wnt target genes.
3. The association of the chromatin remodeling ATPase CHD4 to the *sip1* locus.

3 Materials and Methods

3.1 Reagents

3.1.1 Fine chemicals

The subsequent fine- and bio-chemicals were ordered at the following companies:
Fluka, Merck, Sigma, USB.
Agar (Difco); Agarose (Gibco/BRL); Ampicillin, Streptomycin, Bacto trypton, Yeast extract (Difco); Chicken serum, lamb serum (Gibco/BRL); Human choriongonadotrophin (Sigma); Levamisol (Vector Laboratories).

3.1.2 Enzymes and proteins

The following enzymes were ordered at the companies put in brackets:
Alkaline phosphatase (Roche); BSA fraction V, Chymostatin, Leupeptin, Pepstatin (Sigma); DNase I (Stratagene); Klenow enzyme (Roche); MMTV reverse transcriptase (Gibco/BRL); Restriction endonuclease with 10x restriction buffer system (New England Bio Labs, Roche, Fermentas); RNaseA (Sigma); RNasin (Promega); T3, T7 and SP6 RNA polymerase with 5x incubation buffer (Promega); Taq DNA polymerase with 10x PCR buffer (NEB), Advantage 2 Polymerase Mix (BD Bioscience Clontech), Proteinase K (Sigma); RNase free DNase I (Promega); Pre-stained protein molecular weight standard (Sigma), Precision Plus Protein Prestained Standard (Biorad)

3.2 Laboratory Equipment

The subsequent laboratory equipments were used. The companies are put in brackets.
CCD camera: ProGres C14 (Zeiss)
Centrifuges: Eppendorf centrifuge 5417C (Eppendorf); Omnifuge 2.0 RS (Haereus); Sorvall RC-5B (Du Pont), Micro 22R (Hettich Zentrifugen), Optima LE-80K Ultracentrifuge (Beckman Coultier), PicoFuge (Stratagene)
Developer: Curix-60 (Agfa)
FRENCH® Pressure Cells and Press (Thermo Spectronic)

Glass injection needles: Glass 1BBL W/FIL 1.0 mm (World Precision Instrument).
Injector Pli-100 (Digitimer Ltd.).
Incubator: Driblock DB1 and DB20 (Teche).
Microneedle Puller P-87 (Sutter Instrument).
Micromanipulator: Mm-33 (Science Products).
Microscopes: Stereomicroscopes Stemi SV6, Stemi SV11 (Zeiss), MZFCIII (Leica), Axiophot (Zeiss), Axiovert 200M (Zeiss)
Microsurgery: Gastromaster (Xenotek Engineering).
Nylon membrane: Hybond™ N (Amersham).
Software: Photoshop CS2 (Adobe); Illustrator CS2 (Adobe); MacVector 7.1 (Oxford Molecular Group); Office 2004 for Mac (Microsoft), Endnote 9.0 (Thomson), ABI Prism Primer Express (Applied Biosystems), ABI Prism 7000 SDS Software (Applied Biosystems)
Spectrophotometer: GeneQuant II (Pharmacia Biotech), Nanodrop ND-1000 (PeqLab)
Thermocycler: Primus 96 plus (MWG) used for semi-quantitative PCR, ABI Prism 7000 SDS (Applied Biosystems) used for real-time PCR
Sonicators: Branson Digital Sonifier 250-D; Bioruptor™ (Diagenode)

3.3 Antibodies

3.3.1 Primary Antibodies

3.3.1.1 Primary Antibodies, commercially available or published

Acetyl Histone H4 (Upstate); Chicken myosin heavy chain MF20 (ICC 1:100) (Bader et al., 1982); c-Myc 9E10 (WB 1:100) (Evan et al., 1985); FLAG M2 (WB 1:1000) (Sigma); H3 dimethyl K4 (Abcam); H3 dimethyl K9 (Abcam); H3 trimethyl K27 (Abcam); Histone H3 core region (Abcam); Rabbit anti-Rat IgG (Dianova); SRF G-20 (Santa Cruz Biotechnology), Mouse anti-Rat IgM (Biozol)

3.3.1.2 Rat monoclonal antibodies

The antibodies were generated in collaboration with Dr. Elisabeth Kremmer, GSF München (see chapter 4.1).
Antigen xMyoDb as a recombinant GST fusion protein:
MYO 7F11: subtype: IgG2a, epitope: C-terminus (transactivation domain) (Western blot analysis (WB) negative, positive in immnoprecipitation (IP) and chromatin

immunoprecipitation (ChIP), immunocytochemistry (ICC) not tested, immnofluorescence (IF) not tested)

MYO 5A9: subtype IgG2a, epitope: C-terminus (transactivation domain), WB negative, IP + ChIP positive, ICC not tested, IF not tested)

MYO 6C8: subtype IgG2b, epitope: C-terminus (transactivation domain), (WB: 1:10, positive in IP + ChIP, ICC negative, IF not tested)

Antigen Lef1 Dom A+B as a recombinant GST fusion protein (see Figure 13):

LEF 3D4: subtype IgG1, (WB 1:10, positive in IP + ChIP, ICC undiluted, IF undiluted)

LEF 5F12: subtype IgG1, (WB 1:10, positive in IP + ChIP, ICC not tested, IF not tested)

LEF 1F12: subtype IgG2b, (WB negative, positive in IP + ChIP, ICC not tested, IF not tested)

LEF 5B10: subtype IgG2a, (WB negative, IP + ChIP negative, ICC not tested, IP not tested)

Antigen xTCF3 Dom A+B as a peptide (LDSPSTAGLKDARSPSPA) (see Figure 13):

TCF3 6B6: subtype IgG1, (WB negative, IP+ ChIP negative, ICC negative, IF not tested)

TCF3 3E5: subtype IgG2b, (WB negative, IP+ ChIP negative, ICC negative, IF negative)

The peptide was selected and synthesized by Peptide Specialty Laboratories GmbH (Heidelberg).

Antigen xTCF1c Dom A+B as a peptide (IPHSGNKDMDIYER) (see Figure 13):

TCF1 5F2: subtype IgG2a, (WB negative, IP positive, ChIP not tested, ICC not tested, IF not tested)

TCF1 7E3: subtype IgG2c, (WB negative, IP + ChIP positive, ICC not tested, IF not tested)

TCF1 2F4: subtype IgG2b, (WB 1:10, positive in IP + ChIP, ICC undiluted, IF undiluted)

TCF1 1D12: subtype IgG1, (WB negative, positive in IP + ChIP, ICC not tested, IF not tested)

The peptide was selected and synthesized by Peptide Specialty Laboratories GmbH (Heidelberg).

Antigen xβ-catenin as a peptide of last 15aa of the C-terminus (Schneider et al., 1996):

PGDS 1B1: subtype IgG2b, (WB 1:10, positive in IP + ChIP, ICC not tested, IF undiluted)

PGDS 7D12: subtype IgG2a, (WB 1:10, positive in IP + ChIP, ICC not tested, IF not tested)

The peptide was synthesized by Peptide Specialty Laboratories GmbH (Heidelberg).

Antigen xBrg1 (Singhal, 2005):

XB 3F1: subtype IgG1 (WB 1:10, positive in IP + ChIP, ICC + IF not tested)

Antigen xChd4 as GST-fusion protein of the N-terminus (aa1-aa357) (Linder et al., 2007; Singhal, 2005):

CH4-N 3A11: subtype IgG2a (WB negative, positive in IP + ChIP, ICC negative)

CH4-N 5H4: subtype IgG1 (WB negative, positive in IP + ChIP, ICC negative)
CH4-N 5A2: subtype IgG2a (WB negative, positive in IP + ChIP, ICC negative)
Antigen xChd4 as GST-fusion protein of the C-terminus (aa 1513- aa 1891) (Linder et al., 2007):
CH4-C 7C9: subtype IgM (WB negative, positive in ChIP, ICC positive)
CH4-C 7E8: subtype IgM (WB negative, positive in ChIP, ICC positive)

3.3.2 Secondary Antibodies

3.3.2.1 Immunocytochemistry

Sheep anti-mouse IgG coupled with alkaline peroxidase (1:1000, Chemicon); Anti-Rabbit IgG (Fc) coupled with alkaline peroxidase (Promega); Alkaline Phosphatase-conjugated AffiniPure Goat-Anti-Rat IgG + IgM (H+L) (1:10000) (Dianova).

3.3.2.2 Immunofluorescence

Alexa Fluor® 488 rabbit anti-rat (IgG (H+L) (1:100) (MoBiTec)

3.3.2.3 In Situ Hybridization

Sheep anti-Digoxigenin Fab fragment coupled with alkaline phosphatase (Roche);

3.3.2.4 Western Blot analysis

Peroxidase-conjugated AffiniPure Goat-Anti Mouse IgG (H+L) (1:10000) (Dianova), Peroxidase-conjugated AffiniPure Goat-Anti Rat IgG + IgM (H+L)(1:5000) (Dianova), Peroxidase-conjugated AffiniPure Goat-Anti-Rabbit IgG (H+L) (1:10000) (Dianova),

3.4 Nucleic acids

3.4.1 Solutions

Real-time PCR reaction 2xMastermix: TaqMan Universal PCR Mastermix (Applied Biosystems)

3.4.2 Size standard

1kb ladder: GeneRuler™ 1kb DNA ladder (Fermentas). The DNA ladder yields the following 14 discrete fragments (in base pairs): 10000, 8000, 6000, 5000, 4000, 3500, 3000, 2500, 2000, 1500, 1000, 750, 500, 250.

100bp ladder: GeneRuler™ 100bp DNA ladder plus (Fermentas). The DNA ladder yields the following 14 discrete fragments (in base pairs): 3000, 2000, 1500, 1200, 1031, 900, 800, 700, 600, 500, 400, 300, 200, 100.

3.4.3 Oligonucleotides

Oligonucleotides were synthesized by either MWG Biotec or Biomers. Fluorescence-labeled oligonucleotides were synthesized by MWG Biotech or Applied Biosystems. MGBNFQ-Probes were ordered from Applied Biosystems, TAMRA quenched TaqMan-Probes from MWG Biotech.

3.4.3.1 Oligonucleotides for RT-PCR

Random Hexamer:
RR13: 5' - NNNNNC -3 ' (N = G, A, T or C)

Xenopus Histone H4 (Niehrs et. al, 1994):
Forward: 5' - CGGGATAACATTCAGGGTATCACT -3 '
Reverse: 5 ' - ATCCATGGCGGTAACTGTCTTCCT -3

Xenopus GAPDHb (Genbank accession No: AF549496)
Forward: 5'- TGAGCGGTAAAGTTCAAGTCGTC -3'
Reverse: 5'- CACTACATACTCGGCACCAGCATC -3'

Xenopus TH/bZIP (Furlow, D[1], personal communication)
Forward: 5'- CGTGTCATTGCCCTTCTTGA -3'
Reverse: 5'- TCATGTTCTGGCACTCGGTC -3'

3.4.3.2 Oligonucleotides for cloning

Primer no. 1: xLef1 FLAG XhoI F
5'- CCGCTCGAGCGGATGCCTCAGCTCTCTGGAGC -3'

Primer no. 2: xLef1 FLAG XhoI R
5'- GCTCTAGAGCCGATGTAGGCAGCTGTCATT -3'

Primer no. 3: xTCF1 FLAG XhoI F
5'- CCGCTCGAGACCATGCCCCAAATGAACAGCG -3'

[1] J. David Furlow, Ph.D., University of California, Davis, CA 95616-8519

Primer no. 4: xTCF1 FLAG XbaI R
5'- GCTCTAGAGCCTCTGCATGGGCCGCACC -3'

Primer no. 5: xTCF3 FLAG XhoI F
5'- CCGCTCGAGCGGATGCCTCAGCTCAACAGCGGC -3'

Primer no. 6: xTCF3 FLAG XbaI R
5'- GCTCTAGAGCCGTCACTGGATCTGGTCACTAG -3'

Primer no. 7: xTCF4a FLAG EcoRI F
5'- GGAATTCGATGCCGCAGTTGAATGGCG -3'

Primer no. 8: xTCF4a FLAG XhoI R
5'- CCGCTCGAGCGGGATAAGCTTCCATCTGAAGAGGGC -3'

Primer No. 9: MyoD AB EcoRI F
5'- CGGAATTCCGAGCTGTTGCCCCCACCACT -3'

Primer No. 10: MyoD AB SalI R
5'- ACGCGTCGACCTATAAGACGTGATAGATGG -3'

Primer No. 11: Tcf1 dom a+b EcoRI F
5'- GGAATTCCGCCTCACATCCCCG -3'

Primer No. 12: Tcf1 dom a+b XhoI R
5'- CCGCTCGAGCTCTTTTTCTCTCTTTGGCTC -3'

3.4.3.3 Oligonucleotides for real-time PCR

Amplicons were designed with the Primer Express program (Applied Biosystems).

Egr1 Promoter:

Forward: 5'- CCAGCACCTCATCAGCACTTT- 3'

Reverse: 5' -CGGCAGCTTAGGCCATGTAA- 3'

Probe: 5'-6FAM-CTTTCCGGATCAGCTCCCTCTCCCTTT-TAMRA-3'

Myf5 Tcf:

Forward: 5'- CATCGAATAGGCTACTACGACCTTCTAC - 3'

Reverse: 5'- CGAATGGTCTAACAGTCAAACGATT - 3'

Probe: 5'-6FAM- TCGAATGATTCGAACTAAA-MGBNFQ -3'

MyoDb 5'Region:

Forward: 5'- TGGAGGACACTCGGCACC - 3'

Reverse: 5'-CACAGCACAGTGCTGGCC - 3'

Probe: 5'-6FAM-TGAGAACTGCTGATCAATCCCATGTCGTA-TAMRA-3'

MyoDb Maintenance Enhancer (ME):

Forward: 5'- AGTTGGCTGGTGAAGGTCTCC - 3'

Reverse: 5'– TTAACGCGGCACCTTCCT- 3'

Probe: 5'-6FAM-AGCAGCCTTGTCAGCAGGCCTCACTTC-TAMRA-3'

MyoDb Induction Enhancer (IE):

Forward: 5'- ACTAACCATTCACAGAGCGACTGA - 3'

Reverse: 5'- TTACAGCCCCACCCCCA - 3'

Probe: 5'-6FAM-CTATATTCGCAAACCTAGCAGCATCCACAG-TAMRA-3'

MyoDb Promoter (P):

Forward: 5'- CCCTCCTAAAAGTGCAGCCATA - 3'

Reverse: 5'- GCCCACGCACAGTCACCTT - 3'

Probe: 5'- 6FAM- CTCTCACCCTCTCAGGG-MGBNFQ -3'

MyoDb Exon1 (E1):

Forward: 5'- AGGAAGGCCGCCACTATGA - 3'

Reverse: 5'- GTTGCGCAGGATCTCCACTT - 3'

Probe: 5'-6FAM-TTTGAGACCCTGAAGCGATACACCTCAACTAAC -TAMRA-3'

MyoDb Exon3 (E3):

Forward: 5'- AAACCTTCATTCCCTTTGTTCC - 3'

Reverse: 5'- CCGCTCTACGATGCTGGA - 3'

Probe: 5'- VIC-TCCCAAGTCTCGAGTCTG -MGBNFQ -3'

TH/bZIP:

Forward: 5'- GACATGTTGATAGGCTGTGCATTC - 3'

Reverse: 5'- GAAAATGTGCCAGCCTTTCC - 3'

Probe: 5'- 6FAM- TCTCAACTCCTGAACGGCACTCGCT -TAMRA-3'

GAPDH:

Forward: 5'- TTACACTGCCACCCAGAAGACA - 3'

Reverse: 5'- ATGTTCTGACCGGCACCTCTT - 3'

Probe: 5'- VIC-CCCATCAGGGAAGCT- MGBNFQ-3'

Siamois Promoter:

Forward: 5'- CATATGCACCCTGAAAGAATTGG - 3'

Reverse: 5'- GGGCAAGATCAAGGGAAACA - 3'

Probe: 5'-6FAM-TGTCATCAGAATCATCAAAGGACCTCCCTT-TAMRA-3'

xU5 (*sip1* locus):

Forward: 5'- CATAAGGCTTTACAGTATCTCCAGGA - 3'

Reverse: 5'- TGGGAGGAGGAATCAAAGGG - 3'

Probe: 5'-6FAM- CCTCACCTACTCTCCTTCTTCCATGCTTCTTG -TAMRA-3'

xE1 (*sip1* locus):

Forward: 5'- GCCGAGTCCATGCGAACT - 3'

Reverse: 5'- GGCCATCCGCCATGATC - 3'

Probe: 5'-6FAM-CCATCTGATCCCACTCTTATCAATGAAGCAAGAAGCAA – TAMRA-3'

xE2 (*sip1* locus):

Forward: 5'- CATGCTCAACCACGAGACTTCT - 3'

Reverse: 5'- TCAATTCATCTTCCTCTTCGTCTCT - 3'

Probe: 5'-6FAM- CCCAAGCCAACCAAGCACTATTGCC -TAMRA-3'

3.4.4 Plasmids

Unless stated otherwise, the plasmids were constructed and cloned in our lab.

3.4.4.1 Vectors for cloning

pBS (Stratagene)
pCS2+ (Rupp et al., 1994)
pCS2+MT6 (Rupp et al., 1994)
pCS2+ FLAG: FLAG tag cloned into pCS2+ between XbaI and SnaBI
pET-M30 (Novagen)
pGEX 4T3 (Pharmacia)
pGEM-T (Promega)

3.4.4.2 Plasmids for in vitro transcription

pXLef1: *Xenopus* Lef1 cDNA cloned into pCS2+ with XhoI. For *in vitro* transcription linearize with NotI, transcribe with RNA-Polymerase SP6, kindly provided by Gradl, D[2].

pLef1-FLAG: *Xenopus* Lef1 cDNA subcloned via PCR (primer no 1 & 2) of pXLef1 with XhoI and XbaI into pCS2+FLAG. For *in vitro* transcription linearize with NotI, transcribe with RNA-Polymerase SP6.

pMT-Lef1-FLAG: *Xenopus* Lef1 cDNA subcloned of pLef1-FLAG with XhoI and NotI into pCS2+MT6. For *in vitro* transcription linearize with NotI, transcribe with RNA-Polymerase SP6.

pMT-Tcf1-FLAG: *Xenopus* Tcf1c cDNA subcloned of pTcf1-FLAG with XhoI and NotI into pCS2+MT6. For *in vitro* transcription linearize with NotI, transcribe with RNA-Polymerase SP6.

pMT-Tcf3-FLAG: *Xenopus* Tcf3 cDNA subcloned of pTcf3-FLAG with XhoI and NotI into pCS2+MT6. For *in vitro* transcription linearize with NotI, transcribe with RNA-Polymerase SP6.

pMT-Tcf4a-FLAG: *Xenopus* Tcf4a cDNA subcloned of pTcf4a-FLAG with EcoRI and NotI into pCS2+MT6. For *in vitro* transcription linearize with NotI, transcribe with RNA-Polymerase SP6.

pRR65: Xenopus xMyoDb cloned into pCS2+.

pRR107: Xenopus xMyoDb cloned into pCS2+MT6.

pTCF1-FLAG: *Xenopus* Tcf4a cDNA subcloned of EST BU916421 via PCR (primer no. 3 & 4) with XhoI and XbaI into pCS2+FLAG. For *in vitro* transcription linearize with NotI, transcribe with RNA-Polymerase SP6.

pTcf3-FLAG: *Xenopus* Tcf3 cDNA subcloned via PCR (primer no. 5 & 6) of pTcf3 (Pukrop et al., 2001) with XhoI and XbaI into pCS2+FLAG. For *in vitro* transcription linearize with NotI, transcribe with RNA-Polymerase SP6.

pTcf4a-FLAG: *Xenopus* Tcf4a cDNA subcloned via PCR (primer no. 7 & 8) of pxTCF4a with EcoRI and XhoI into pCS2+FLAG. For *in vitro* transcription linearize with NotI, transcribe with RNA-Polymerase SP6.

pxTcf4a: *Xenopus* Tcf4a cDNA cloned into pCS2+ with EcoRI and XhoI. For *in vitro* transcription linearize with NotI, transcribe with RNA-Polymerase SP6. Kindly provided by Gradl, D[2].

pTH/bZIP cDNA in pBS KS- (Stratagene) (Brown et al., 1996).

[2] Dr. Dietmar Gradl, Universitiät Karlsruhe, Zoologisches Institut II, Kaiserstr. 11, 76131 Karlsruhe

pUE16: Deletion of C-terminus (aa 153-289) of *Xenopus* MyoD cloned into pCS2+MT6.

pUE24: Deletion of N-terminus (aa 2-123) of *Xenopus* MyoD cloned into pCS2+MT6.

pUE28: bHLH domain (aa 63-153) of *Xenopus* MyoD cloned into pCS2+MT6.

3.4.4.3 Plasmids for dig-labeled RNA in situ hybridization probes

pRR 104: XMyoDb cloned into pCS2+ via EcoRI/XbaI (Rupp et al., 1994).

3.4.4.4 Plasmids for recombinant GST-Fusion-Proteins

pET-M30XTCF3DomAandB: *Xenopus* Tcf3 cDNA Domain A and B cloned into pET-M30, kindly provided by Gradl, D^2.

pET-M30XLef-1A,B: *Xenopus* Lef1 cDNA Domain A and B cloned into pET-M30, kindly provided by Gradl, D^2.

pGEX-MyoD: *Xenopus* MyoDb cDNA subcloned of pRR3 (Rupp et al., 1994) by PCR (primer no. 9 & 10) with EcoRI and NotII into pGEX 4T3.

pGEX-Tcf1 Dom A+B: *Xenopus* Tcf1c cDNA domain A+B subcloned of pTcf1-FLAG by PCR (primer 11& 12) with EcoRI and NotI into pGEX 4T3.

3.4.4.5 Plasmids for real-time PCR tests

pMD-6,0/4,7GFP2: xMyoDb locus from -6000 until +4710 (Otto, 2000).

3.4.5 Handling of bacteria

Preparations of competent cells and transformation have been performed according to standard methods (Sambrook et al., 1989).

3.4.6 Bacteria strains

Table 1: Summary of *Escherichia coli* strains

Strain	Genotype	Company
BL21(DE3)	*B F- dcm ompT hsdS(rB- mB-) gal (DE3)*	Novagene
XL1Blue	*F'::TN10 proA$^+$B$^+$lacI^q Δ(lacZ)M15/recA1 end A1 gyrA96(Nal^R) thi hadR17 ($r_K^-m_K^-$) glnV44 relA1 lac*	Stratagene

3.5 Molecular biological methods

3.5.1 Solutions

AB buffer: 80% TBSX, 15% heat-inactivated lamb serum, 5% *Xenopus* egg extract.

AP-Buffer: 100mM trichlorethane Tris/HCl 9.5; 100mM NaCl; 50mM $MgCl_2$

Bleaching solution: 1% H_2O_2; 5% Formamid; 0.5x SSC

DEPC-H_2O: ddH_2O with 0.1% Diethylpyrocarbonat (DEPC) agitated at 23°C over night and autoclaved afterwards.

10mM DIG NTP mixture: 10mM CTP, GTP, ATP, 6.5mM UTP and 3.5mM Dig-11-UTP.

Hybridizing solution: 5x SSC, 50% formamide, 1% Boehringer block, 0.1% Torula RNA, 0.01% Heparin, 0.1% Tween-20, 0.1% CHAPS, 5mM EDTA.

Lamb Serum: Heat-inactivated lamb serum (30 min with 56°C), stored at -20°C.

MEMFA: 0.1M 3-(N-Morpholino)-propanesulfonic acid (MOPS), 2mM EGTA, 1mM $MgSO_4$, 3.7% formaldehyde pH 7.4

Paraformaldehyde: 4% paraformaldehyde in PBSw

PBS: 137mM NaCl, 2.7mM KCl, 8mM Na_2HPO_4, 1.7mM KH_2PO_4 pH 7.2

PBSw: 1xPBS, 0.1% Tween-20

PCI: 50% phenol, 48% chloroform, 2% isoamyl alcohol.

Proteinase K: 10µg/ml Proteinase K in PBSw

20xSSC: 3M NaCl, 0.3M sodium citrate (pH 7.0 at 23°C).

TBS: 50mM trichloroethylene (Tris)/HCl, 150mM of NaCl (pH 7.5 at 23°C).

TBSX: 1xTBS, 0.1% Triton X-100 (pH 7.5 at 23°C).

TE: 1mM EDTA, 10mM of Tris/HCl (pH 8.0 at 23°C).

TBE: 100mM Tris/HCl, 83mM borate, 0.1mM EDTA (pH 8.6 at 23°C).

Xenopus egg extract for *in situ* hybridization: dejelly unfertilized eggs with 2% cysteine, wash 3 times, add 1 volume of PBS, then lysed by 10 strokes of a Dounce homogenisators, and centrifuged (7500xg, Sorvall Rc-5b, rotors SS-34, 10000rpm, 4°C, 10min). The supernatant was transferred into a fresh centrifuge tube and recentrifuged twice under the same conditions. The supernatant was aliquoted and stored at -20°C.

3.5.2 Isolation of nucleic acids

3.5.2.1 Mini-preparation with Qiagen kit

Plasmid DNA mini-preparations were carried out using Qiagen mini-preparation kits.

3.5.2.2 Isolation of RNA

The embryos or explants were collected at the proper developmental stage in 1.5ml Eppendorf tubes, five animal caps or five whole embryos in one tube. As much buffer as possible was removed, 30µl per explant or 100µl per embryo of Trizol (GibcoBRL) was added and vortexed for 30sec at room temperature. If not used immediately, Trizol samples were stored at -80°C. The cell debris were removed by centrifugation for 10min at 12000xg and 4°C. 2µl per 10µl of chloroform was added, vortexed, and centrifuged 5min at 4°C with maximal speed. The upper phase was transferred into a new tube. The RNA was precipitated with 0.5 volume equivalents isopropanol, incubated for 10min at RT, followed by a centrifugation at 4°C for 20min. The pellet was washed with 70% ethanol and dried at room temperature for 20min. The RNA was dissolved in DEPC-treated H_2O and stored at -80°C.

3.5.3 Analysis and manipulation of nucleic acids

3.5.3.1 Cloning methods

The cloning of DNA has been performed according to standard methods (Sambrook et al., 1989).

3.5.3.2 Gel electrophoresis of nucleic acids

DNA or *in vitro* synthesized RNA was isolated in horizontal agarose gel. Depending upon fragment size, one to two percent TBE agarose gels were used. After electrophoresis the gels were photographed. 1kb or 100bp DNA ladder was used as size standard.

3.5.3.3 Isolation of DNA fragments from agarose gel

In order to isolate DNA fragments after electrophoresis from agarose gel, the appropriate bands were cut out under long-wave UV light. The DNA was extracted from the gel with Qiagen gel-extraction kit.

3.5.4 Polymerase chain reaction (PCR)

3.5.4.1 PCR amplification of DNA fragments for cloning

The reaction was accomplished in a total volume of 50µl. The reaction mixture contained 100ng template DNA, 25pmol each primer, 0.5mM dNTPs, 1U Advantage Taq Polymerase (Invitrogen) or Taq polymerase (NEB) and 1x of

the supplied buffer. The program was 95ºC 30 sec, xºC 30sec (annealing temperature depended on the primers used), 68°C/72ºC 1min/kb, 30 cycles. The PCR products were digested with the suitable endonuclease and separated on agarose gel. Subsequently, the desired DNA fragment was isolated.

3.5.4.2 RT-PCR assay

In the RT-PCR assay, 1µg mRNA was reverse-transcribed with RevertAid™ M-MuLV Reverse Transcriptase (Fermentas) and random hexamers according to the manufacturer's protocol to generate cDNA. The cDNA samples were normalized by PCR amplification of housekeeping genes, such as H4 (Histone H4), and then the desired target cDNA species were amplified using specific primers. PCRs were carried out in the exponential phase of amplification and PCR samples were loaded side by side in the agarose gel to compare their intensity.

3.5.4.3 Real-time PCR

For the real-time PCR 96-Well Optical Reaction Plates (Applied Biosystems) were used. PCR-Reaction of 25µl were pipetted the following: Mastermix Probe: 1.25µl Probe 5µM, 2.25µl Primer F 10µM, 2.25µl Primer R 10µM; Mastermix Template: 12.5µl 2x TaqMan Universal PCR Mastermix, DNA + ddH_2O to 6,75µl. PCR reaction was performed according to the manufacturer's protocol, but with 45 cycles.

3.5.5 *In vitro* transcription

3.5.5.1 In vitro transcription for microinjection

Capped mRNAs for microinjection were *in vitro* transcribed with RNA polymerase. Reactions were set up as following: in a total volume of 50µl, 4µg linearized plasmid DNA, 1x of the supplied transcription buffer, 0.5mM dNTPs, 2.5mM RNA cap structure analogue, 10mM DTT, 20U RNAsin and 40U Sp6 or 60U T3 or T7 RNA Polymerase. The reaction was incubated for 4 hours at 37°C. Subsequently, the template DNA was digested with 10U RNase free DNaseI for 30min at 37°C. The RNA was purified with the RNeasy Spin Kit (Qiagen). The concentration of the RNA was determined by NanoDrop ND-1000 spectrophotometer (Peqlab).

3.5.5.2 In vitro transcription of dig labeled RNA probes

Plasmids were linearized and antisense RNA was generated by *in vitro* transcription. The reactions were set up in a total volume of 50µl as following: 4µg linearized plasmid DNA, 1x of the supplied transcription buffer, 0.1mM Dig-NTPs, 20U RNAsin and 20U SP6 or T3 or T7 RNA Polymerase. The reactions were incubated at 37°C for 4h and purified with the RNeasy Kit (Qiagen).

3.5.6 RNA *in situ* hybridization

The embryos were fixed in fresh MEMFA for 1.5-2 hours and washed afterwards with PBS 3x5min. The dehydration of the embryos was performed over a period of one hour by replacing the PBS subsequently with 100% ethanol. The lipid membranes were dissolved overnight at -20°C in 100% ethanol. The embryos were rehydrated through a 75, 50, 25% ethanol series in PBSw. Each ethanol step was incubated for 5min at room temperature. Afterwards 3 washes with for 5min with PBSw were performed. The solution was then changed to Proteinase K in PBSw and incubated for 20min at 17°C, followed by a short rinse with PBSw. Again two washes for 5min each were performed with PBSw. After the Proteinase K digest the embryos were refixed with paraformaldehyde for 20min. A short rinse with PBSw was performed followed by subsequent washing in PBSw for 5x5min. The PBSw was replaced with hybridization solution (50% PBSw: 50% hybridization solution; 100% hybridization 3min each step). 0.5ml of fresh hybridization solution was added to each vial and incubated at 65°C for 1h to inactivate endogenous phosphatases. The embryos were then prehybridized at 60°C for 2-6h. To 100µl of hybridization solution 30-50ng of RNA probe was added and incubated at 95°C for 2-5min, cooled immediately afterward on ice and added to the embryos in prehybridization solution. The RNA probe was hybridized to the mRNA over night at 60°C. To remove excessive RNA probe, the embryos are washed the following after the hybridization: 2xSSC; 0.1% CHAPS short rinse; 2xSSC;0.1% CHAPS for 20min; short rinse with 0.2xSSC;0.1% CHAPS; 2x for 30min at 60°C in 0.2xSSC;0.1% CHAPS. Prior to the antibody binding the embryos were transferred into TBSX (short Rinse in 50% TBS: 50% 0.2xSSC; 0.1% CHAPS), washed in TBS for 5min and rinsed in TBSx. To block unspecific antibody binding sites, the embryos were incubated in antibody buffer (0.5ml per vial) for 2h at 4°C. In parallel, AP-conjugated anti-DIG antibody (1/5000 diluted) was preabsorbed against *Xenopus* proteins present in antibody

solution. 0.5ml of preabsorbed antibody solution was added to the embryos and incubated overnight at 4°C. After antibody binding, the embryos were briefly rinsed with TBSx and washed 6 times for 1h in TBSx. Embryos were shortly rinsed in AP buffer and equilibrated for 15min. AP-buffer was replaced with 0.5ml staining solution and incubated overnight until or to 3 days at 17°C in the dark. The staining reaction was stopped by washing twice in PBS for 10min. If the embryos were over-stained, some color was removed by washing the embryos in 75% ethanol in PBS for 20min. The stain was fixed in MEMFA for 90min. The embryos were bleached in bleaching solution on a light box for 2h. The bleach solution was washed off with PBS 3x5min. For long-term storage, the embryos were transferred to PBSw containing 0.2% Azid and kept at 4°C.

3.6 Embryological methods

3.6.1 Solutions

Cystein**:** 2% L-Cystein in 0.1xMBS (pH7.8 at 23°C, adjusted with 5M NaOH).

Human Chorionic Gonadotropin (HCG): 1000 I.U./ml HCG in ddH_2O.

MEMFA: 0.1M 3-(N-Morpholino)-propanesulfonic acid (MOPS), 2mM EGTA, 1mM $MgSO_4$; 3.7% formaldehyde (pH 7.4 at 23°C).

1xModified Barth's Saline (MBS): 5mM HEPES, 88mM NaCl, 1mM KCl, 0.7mM $CaCl_2$, 1mM $MgSO_4$, 2.5mM $NaHCO_3$ (pH 7.6 at 23°C). Add the $CaCl_2$ before use.

MBS/high salt: 1xMBS with 50mM NaCl

0.1xMBS/Gentamycin: 0.1xMBS, 10µg/ml Gentamycin

0.5xMBS/BSA: 0.5xMBS, 1mg/ml BSA, 10µg/ml Gentamycin

MBS/CS: 0.8xMBS high salt with 20% chicken serum, 200U Penicillin/ml, 200µg/ml streptomycin stored at -20°C

0.5xMBS/PIF: 0.5xMBS/BSA with activin supernatant diluted 1:10 (Sokol et al., 1990)

3.6.2 Experimental animals

Adult wild-type *Xenopus laevis* frogs (Xenopus Express) were used. The frogs were kept in tab water with a temperature of 17-19°C and a population density of 5l water per frog. The animals were fed three times per week with Pondsticks Premium brittle (Interquell GmbH, Wehringen).

3.6.3 Superovulation of female *Xenopus laevis*

Xenopus laevis females were stimulated to lay eggs by injection of 800 units of human chorionic gonadotropin (Sigma) into the dorsal lymph sac and incubated at 18-20°C over night. Egg lying started about 12-18h later.

3.6.4 Preparation of testis

A male frog was anaesthetized in 0.1% 3-Aminobenzoeacid-ethyl-ester in ddH_2O for 30min, cooled down in ice-cold water and killed by decapitation. The two testes were taken from the abdominal cavity by pulling out the yellow fat body, with which they are connected by connective tissues. Until use, the testes were stored in MBS/CS for maximal 7 days.

3.6.5 *In vitro* fertilization of eggs and culture of the embryos

For *in vitro* fertilization a piece of testis was minced in 1xMBS and mixed it with freshly laid eggs. Afterwards the embryos were cultured in 0.1xMBS at 16-23°C in 110mm Petri dish.

3.6.6 Removal of the egg jelly coat

One hour after fertilization or later, the egg jelly coat was removed in 2% cysteine solution pH 7.8 for about 5min with gentle agitation in a conical glass flask. Embryos were washed three times with 0.1xMBS and cultured further in 0.1xMBS at 16-23°C.

3.6.7 Injection of embryos

Injection needle was pulled from capillaries with the Microneedle Puller (setting: heat:800; pull:35; vel:140; time: 139; Sutter Instrument, model P-87). It was placed into the holder of the injection equipment (Medical System, model Pi-100). The tip of the injection needle was broken carefully with Dumont tweezers. The needle was filled with 1-2µl nucleotide acid containing solution shortly before the injection. The injection volume was adjusted by choosing the injection pressure (25-30psi) and/or the injection duration (30ms-1s). 5nl nucleotide solution was injected into each blastomere. Embryos were injected at two to eight cell stages into the animal hemisphere. After injection, the embryos were incubated in 0.1xMBS at 16-23°C until the desired developmental stages in a 60mm Petri dish covered with 1% agarose in 0.1xMBS. The saline was changed every day to increase the survival rates of the embryos.

3.6.8 Preparation of animal cap explants

For the preparation of explants, injected embryos were transferred into 3cm cell culture dishes covered with 1% agarose and filled with 0.5xMBS. Afterwards the animal caps were dissected with the Gastromaster (Xenotek Engineering, Belleville, IL, USA). Each animal cap was transferred into one well of a 96-well plate, which was covered with 50µl 1% Agarose and filled with 100µl 0.5xMBS/BSA or 0.5xMBS/PIF, respectively.

3.7 Histological methods

3.7.1 Solutions

AP buffer: 100mM Tris/HCl (pH 9.5), 50mM $MgCl_2$, 100mM NaCl, 0.1% Tween 20, 5mM Levamisole.

AP staining solution: 4.5µl NBT, 3.5µl BCIP in 1ml AP buffer.

A-PBS: 103mM NaCl, 2.7mM KCL, 0.15mM KH_2PO_4, 0.7mM NaH_2PO_4 pH7.5

A-PBS-T: APBS with 0.1% Tween20

Blocking buffer: PBT plus 10% heat inactivated serum

Citrate buffer: Stock A: 0.1M citrate monohydrate (10.5g for 500ml solution)
Stock B: 0.1M Trisodiumcitrate-dihydrate (14.7g for 500ml solution)
Working Sol.: 9ml A with 41ml B to 450 ml ddH_2O. pH should be 6.

DAPI: Hoechst dye (1mg/ml) 1:1000 in APBS-T

Dent's Fixative: 80% methanol, 20% dimethyl sulfoxide (DMSO)

Elvanol: 2.4g Moviol 4 (Hoechst, Frankfurt) were mixed with 6g glycerol and 6ml ddH_2O and stirred at least for 2h at room temperature. Then 2ml 0.2M Tris/HCl pH8.5 were added and incubated for 10min at 60°C. Afterwards 50mg/ml DABCO (1.4-Diazabicyclo(2.2.2)-Octane) were added and centrifuged for 30min at 17000xg. Aliquots of the supernatant were stored at -20°C.

MEMFA: 0.1M MOPS, 2mM EGTA, 1mM $MgSO_4$, 3.7% formaldehyde (pH7.4 at 23°C), prepare freshly.

PBS: 137mM NaCl, 2.7mM KCl, 8mM Na_2HPO_4, 1.7mM KH_2PO_4 (pH7.2 at 23°C).

PBT: PBS, 2mg/ml BSA, 0.1% Triton-X-100.

3.7.2 Immunocytochemistry

The vitelline membrane was removed from the embryos.

Subsequently, they were fixed in MEMFA for 1-2h at room temperature with rotation and rinsed afterwards with PBS. PBS was gradually replaced with methanol. The embryos were incubated in methanol at -20°C for at least over night. They were rehydrated by 80%, 50%, 0% methanol in PBS for 5min each, followed by a short 1x5min rinse with PBS and one rinse in PBT for 15min. The embryos were incubated in PBT plus 10% heat inactivated goat serum, blocking unspecific antibody binding sites at room temperature for 1h. The primary antibody was diluted in the blocking buffer and incubated over night at 4°C. Afterwards the embryos were washed 6 times with PBT for one hour. The secondary antibody coupled with alkaline phosphatase was diluted 1:1000 blocking buffer. The embryos were incubated in this secondary antibody solution over night at 4°C. Subsequently, the embryos were washed 6 times with PBT for on hour. Prior to the stain, incubating the embryos twice in AP buffer for 30min blocked the endogenous alkaline phosphatases due to the addition of Levamisol to the AP buffer. The embryos were stained in 1ml staining solution in the dark for 30 to 120min at room temperature. The staining reaction was stopped by rinsing the embryos in PBS. The stain was fixed in MEMFA over night. If necessary, the embryos were bleached with bleaching solution for 2h on a light box.

3.7.3 Immunofluorescence on Embryo Sections

The following protocol is based on Kunz et al. (Kunz et al., 2004) with modification for paraffin sections after Judy Wally (http://tgmouse.compmed.ucdavis.edu/HistoLab/ihc.htm). The embryos were fixed under rotation in MEMFA for one hour at room temperature. Afterwards, they were transferred into ice-cold Dent's Fixative over night at -20°C. Prior to embedding, the embryos were rehydrated for 30min in 100mM NaCl, 100mM Tris/HCl pH7.4. Embryos were again dehydrated with an ascending ethanol series of 50%, 70%, 80%, 96% and 100% for 2h each. The ethanol was replaced by incubating the embryos for two times two hours in Xylene. Then they were soaked in paraffin at 55°C for two times two hours. The embryos were orientated in moulds and the paraffin was hardened on a cooling plate. The embryos were sectioned to slices of 4µm and dried for 2h at 37°C. The paraffin was removed by the following steps: 2x10min Rotihistol (Roth), 2min 100% Ethanol, 2min 96% Ethanol, 2min 80% Ethanol, 1min 70% Ethanol, 1min 70% Ethanol, briefly in ddH_2O. After a short rinse with citrate buffer, the

antigen was refolded by boiling the slides in citrate buffer in the microwave for two times seven minutes with a 2min break. The sections were cooled down to room temperature for at least 20min. A short rinse with ddH_2O followed. Prior to immunostaining, unspecific antibody binding sites were blocked by incubation for one hour at room temperature in APBS-T with 20% heat inactivated lamb serum. The primary antibody was incubated over night at 4°C in APBS-T with 10% heat inactivated lamb serum. Subsequently, the slides were washed the following: 2x5min in APBS-T, 5min in APBS-T with 0.3M NaCl, 2x5min in APBS-T. The secondary antibody was again incubated over night at 4°C in APBS-T with 10% heat-inactivated lamb serum. Since the secondary antibody was labeled with a fluorescent dye the sections were kept in the dark from this step on. Afterwards the slides were washed the following: 2x5min in APBS-T, 5min in APBS-T with 0.3M NaCl. The DNA was stained for 10min with DAPI. The slides were washed for the last time for 5min in APBS-T. Afterwards they were dried and embedded in Elvanol. The cover slips were fixed with colorless nail polish. The sections were analyzed with fluorescence microscopy.

3.8 Protein analysis

3.8.1 Solutions

3x Lämmli buffer: 150mM Tris pH6.8, 300mM DTT, 4% SDS, 30% glycerol,

Blocked ProteinG-Sepharose Beads Fast Flow 4 (Amersham Pharmacia): 25µl beads in 25µl 20% BSA, 6.25µl 10µg/µl herring sperm DNA and 0.1% Tween20 blocked over night at room temperature.

Chemiluminescence reagents (ECL):
Luminol solution: 0.44g luminol in 10ml DMSO, freeze in 1ml aliquots, store at -20°C; p-coumaric acid: 0.15g in 10ml of DMSO, freeze in 0.44ml aliquots, store at -20°C;
solution 1 (100ml): 10ml 1M Tris/HCl pH 8.5, 1ml luminol, 0.44ml p-coumaric acid;
solution 2 (100ml): 10ml 1M HTris/Cl pH 8.5, 60µl 30% H_2O_2

GST-lysisbuffer: 1xHEMG, 0.5M NaCl, 0.1% NP-40, 1mM PMSF, 2.5µg/ml Leupeptin, 10µg/ml Aproptinin, 0.7µg/ml Pepstatin

GST-washbuffer I: 1xHEMG, 0.7M NaCl, 0.1% NP-40, 1mM PMSF, 2.5µg/ml Leupeptin, 10µg/ml Aproptinin, 0.7µg/ml Pepstatin
GST-washbuffer II: 1xHEMG, 0.7M NaCl, 0.01% NP-40, 1mM PMSF, 2.5µg/ml Leupeptin, 10µg/ml Aproptinin, 0.7µg/ml Pepstatin

GST- urea-elutionbuffer: 1xHEMG, 8M Urea

HEG buffer: 50mM Hepes pH7.6, 10% Glycerol, 1mM EDTA, 1mM DTT, 1% TritionX-100, 1mM PMSF, 2.5µg/ml Leupeptin, 10µg/ml Aproptinin, 0.7µg/ml Pepstatin

HEG150: HEG buffer with 150mM NaCl

HEG500: HEG buffer with 500mM NaCl

1x HEMG**:** 25mM Hepes pH7.6, 0.1mM EDTA pH8, 12.5mM $MgCl_2$, 10% Glycerol

LiCl-Solution: 10mM Tris pH8, 250mM LiCl, 0.1% NP40, 0.5% Na Desoxycholate, 1mM EDTA

Lysozyme solution: 0.5g/10ml GST-lysisbuffer

PBS-PI: 136mM NaCl, 2.7mM KCl, 1.5mM KH2PO4, 6.5mM Na_2HPO_4, pH7.4, 1mM PMSF, 2.5µg/ml Leupeptin, 10µg/ml Aproptinin, 0.7µg/ml Pepstatin

3.8.2 *In vitro* translation

In vitro translations of proteins were performed with the TNT® SP6 Quick Coupled Transcription/Translation System (Promega) according to the manufacturer's protocol.

3.8.3 Protein extract for SDS-PAGE with StrataClean™ resin

The embryos were lysed in HEG500 buffer through pipetting up and down a 200µl tip. 50-100µl HEG500 were used per embryo. The lysate was incubated on ice for 20min and afterwards cleared via centrifugation at 4°C for 10min at 14000rpm. The supernatant was transferred into a new tube. 10µl StrataClean™ resin (Stratagene) were added per 10 embryos, vortexed for 1min and incubated on ice for 10min. The StrataClean™ resin was pelleted by a short spin in the PicoFuge, the supernatant was discarded, and 3xLämmli buffer was added and boiled for 5min. An equivalent of 1 to 10 embryos was loaded per slot on a SDS-PAGE gel.

3.8.4 Protein extract for SDS-PAGE with StrataClean™ resin and sonication

The embryos were lysed in HEG500 through pipetting up and down a 200µl tip. 50-100µl HEG500 were used per embryo. The lysate was incubated on

ice for 60min, sonicated 3x30sec with setting High in the Bioruptor (Diagenode) and cleared via centrifugation at 4°C for 10min at 14000rpm. The supernatant was transferred into a new tube. 10µl StrataClean™ resin (Stratagene) were added per 10 embryos, vortexed for 1min and incubated on ice for 10min. The StrataClean™ resin was pelleted by a short spin, the supernatant was discarded, and 3xLämmli Buffer was added and boiled for 5min. An equivalent of 1 to 10 embryos was loaded per slot on a SDS-PAGE gel.

3.8.5 SDS-PAGE and Western Blot Analysis

SDS-PAGE (SDS-polyacrylamide gel electrophoresis) and Western blot analysis were carried out according to standard protocols (Sambrook et al., 1989), and signals were detected by enhanced chemiluminescence solution in a relation of 1:1. The signals were exposed to X-ray film (Kodak) and developed according to the manufacturer's protocol.

3.8.6 Immunoprecipitation (IP)

25µl blocked ProteinG-Sepharose Beads were reabsorbed in 0.5ml antibody supernatant under rotation for one hour at room temperature to bind the antibodies to the beads. The embryos were lysed in 50-100µl HEG500 per embryo with a yellow tip and incubated on ice for 20min. The lysate was cleared via centrifugation at 4°C for 10min at 14000rpm. The supernatant was transferred into a new tube. The lysate was split into the desired samples. One sample equivalent was put aside as the input sample. 25µl blocked antibody incubated ProteinG-sepharose suspension were added into the samples and incubated overnight with rotation at 4°C. The sepharose was pelleted by a gentle centrifugation at 4000xg for about 10sec. The supernatant was carefully removed and discarded. The beads were washed with a rotation lasting 15min at 4°C with the buffers as follows: 2xHEG150, 2xHEG500. After the last step, as much washing buffer as possible was removed carefully. The beads were boiled in 20µl 3xLämmli buffer for 5min. The entire IP samples including input dilutions were loaded on an SDS-PAGE.

3.8.7 ChIP-type Immunoprecipitation (ChIP-type IP)

100 embryos were fixed in 10ml 1% formaldehyde (270µl of 37% stock solution) in 0.1xMBS 30 min at 37°C in tube on a roller. The reaction was

quenched by adding 500µl 2.5M glycine to a final concentration of 125mM. The embryos were washed twice with ice-cold PBS-PI. HEG150 was added to 4ml total volume and applied to the minicell of the FRENCH Press (2 times at 1100psi). The lysate was centrifuged for 10min at 14.000rpm at 4°C. The supernatant was transferred to a new tube. 25µl blocked ProteinG-sepharose suspension was added to 1ml of lysate and incubated for 1h with rotation at 4°C. The ProteinG-sepharose was pelleted for 1min at 2000rpm. The supernatant was transferred to a new tube. The samples were split as desired. One volume was put aside as the input sample. The input sample was precipitated with 2 volume equivalents ice-cold acetone, kept at -20°C for 30min and pelleted for 30min with 20,000xg at 4°C. The pellet was air-dried and resuspended in 3xLämmli buffer. The antibody and 25µl blocked ProteinG-sepharose suspension were added and incubated with rotation overnight at 4°C. For the ChIP-type IP with rat monoclonal antibodies, 25µl ProteinG-sepharose were preabsorbed with antibody out of 0.5ml of antibody supernatant for 1h at room temperature. After binding of the crosslinked chromatin to the antibody and ProteinG-sepharose, the ProteinG-sepharose/Protein/DNA-complex was pelleted by centrifugation for 1min at 2000rpm. The supernatant with the unbound, non-specific chromatin was removed carefully. The ProteinG-sepharose/Protein/DNA-complex was washed with 15min rotation at 4°C with the 500µl of buffers: HEG150 one wash, HEG500 two washes, LiCl solution two washes. After the last washing step as much washing buffer as possible was removed carefully. The beads were boiled in 20µl 3xLämmli buffer for 20min. The total of 20µl IP sample plus input dilutions were loaded on an SDS-PAGE gel.

3.8.8 Purification of GST-tagged, recombinant proteins

The expression vectors were transformed into *Escherichia coli* strain BL21. A starter culture was grown over night at 37°C. The starter culture was diluted 1:100 and grown until at 37°C to an OD_{595} of 0.6. A 1ml aliquot was taken out for the uninduced state. The protein expression was induced with 1mM IPTG for 1-2h at 37°C. Another 1ml aliquot was taken out for the induced state. The cells were harvested at 4,000xg for 20min and the supernatant was discarded. The pellet was resuspended in 15ml GST-lysis buffer per 1l culture volume. 200µl lysozyme solution were added per 1l culture volume and rotated for 30min at 4°C. Afterwards the lysate was frozen in liquid N_2 and thawn at 37°C for three

times. To shear the genomic DNA, the lysate was sonicated 3x30sec with amplitude of 50% with a microtip. Warming up was avoided by putting the tube on ice. The lysate was cleared via centrifugation for 30min at 15.000rpm, 4°C. Samples from supernatant and pellet were frozen away for the purification analysis on a SDS-PAGE. Prior to the GST purification, the glutathione sepharose beads were washed with 5-10 bed volumes of GST-lysis buffer. 300µl beads were added to 20ml of crude lysate and rotated for one hour at 4°C to allow binding of GST-fusion protein to glutathione beads. Afterwards the beads were washed three times with 5ml GST-washbuffer I and three times with 5ml GST-washbuffer II for 15min at 4°C. The GST-fusion protein was eluted off the beads with GST-urea-elutionbuffer for 2h at RT. A second elution was performed overnight at RT. Again aliquots of washing steps, elution steps and beads was analyzed by SDS-PAGE.

3.9 Chromatin Analysis

3.9.1 Solutions

Buffer A1**:** 60mM KCl, 15mM NaCl, 4mM MgCl2, 15mM HEPES (pH7.6), 0.5% Triton X-100, 0.5mM DTT, 10mM sodium butyrate, 1mM PMSF, 2.5µg/ml Leupeptin, 10µg/ml Aproptinin, 0.7µg/ml Pepstatin

Dialysis buffer: 5% Glyercol, 10mM Tris pH8, 1mM EDTA, 0,5mM EGTA

HEG buffer: 50mM Hepes pH7.6, 10% Glycerol, 1mM EDTA, 1mM DTT, 1% TritionX-100, 1mM PMSF, 2.5µg/ml Leupeptin, 10µg/ml Aproptinin, 0.7µg/ml Pepstatin

HEG150: HEG buffer with 150mM NaCl

HEG150S: HEG150 + 1%SDS

HEG500: HEG buffer with 500mM NaCl

LiCl-Solution: 10mM Tris pH8, 250mM LiCl, 0.1% NP40, 0.5% Na Desoxycholate, 1mM EDTA

Lysis buffer: 140mM NaCl, 15mM HEPES pH 7.6, 1mM EDTA, 0.5mM EGTA, 0.5mM DTT, 0.1% sodium deoxycholate, 10mM sodium butyrate, 1mM PMSF, 2.5µg/ml Leupeptin, 10µg/ml Aproptinin, 0.7µg/ml Pepstatin
1xMBS (1xModified Barth's Saline): 5mM HEPES, 88mM NaCl, 1mM KCl, 0.7mM $CaCl_2$, 1mM $MgSO_4$, 2.5mM $NaHCO_3$ (pH7.6 at 23°C), add the $CaCl_2$ before use

PBS: 136mM NaCl, 2.7mM KCl, 1.5mM KH_2PO_4, 6.5mM Na_2HPO_4, pH7.4

PBS-PI: 136mM NaCl, 2.7mM KCl, 1.5mM KH_2PO_4, 6.5mM Na_2HPO_4, pH7.4, 1mM PMSF, 2.5µg/ml Leupeptin, 10µg/ml Aproptinin, 0.7µg/ml Pepstatin

PCI: Phenol:Chloroform:Isoamyl alcohol 25:24:1 saturated with 10mM Tris pH8.0, 1mM EDTA (Sigma)

PFA: para-formaldehyde, 37% - 320µl aliquots. For 30ml of solution: 11.1g para-formaldehyde in 20ml ddH_2O heated in a water bath with magnetic stirring. 400µl 1M KOH was added. When the para-formaldehyde was dissolved, volume was brought to 30ml. 320µl aliquots were frozen by plunging in liquid nitrogen. Aliquots were stored at -80°C. Prior to use, they were thawn at 65°C water bath. Each aliquot was used only once.

ProteinG- or A-sepharose-suspension: Block ProteinG or A-Sepharose beads (Fast Flow 4, Amersham Pharmacia) in 1 volume 20% BSA and ¼ volume 2.5µg/µl Herring sperm DNA over night at room temperature

Proteinase K: 10mg/ml

RNase: 1mg/ml in ddH_2O

Sarcosine: 10% solution N-lauroylsarcosine in ddH_2O

TE: 10mM Tris-HCl pH7.4, 1mM EDTA pH 8.0

3.9.2 In Situ Chromatin Immunoprecipitation (ChIP)

The In-Situ ChIP protocol was modified for *Xenopus laevis* embryos after Hörz and colleagues (Reinke and Horz, 2003). 100 embryos were fixed in 10ml 1% formaldehyde (270µl of 37% stock solution, Sigma) in 0.1xMBS 30min at 37°C in tube on a roller. The reaction was quenched by adding 500µl 2.5M glycine to a final concentration of 125mM. The embryos were washed twice with ice-cold PBS-PI. HEG150 was added to 4ml total volume and applied to the minicell of the FRENCH Press (2 times at 1100psi). The lysate was centrifuged for 10min at 14.000rpm at 4°C. The supernatant was transferred to a new tube. 50µl blocked ProteinG-sepharose suspension was added to 2ml of lysate and incubated for 1h with rotation at 4°C. The ProteinG-sepharose was pelleted for 1min at 2000rpm. The supernatant was transferred to a new tube. The samples were split as desired. The antibody and 50µl blocked ProteinG-sepharose suspension were added and incubated with rotation overnight at 4°C. For the ChIP with rat monoclonal, 50µl ProteinG-sepharose were preabsorbed with antibody out of 2ml of antibody supernatant for 1h at room temperature. After binding of the fixed chromatin to the antibody and

ProteinG-sepharose, the ProteinG-sepharose/Protein/DNA-complexes was pelleted by centrifugation for 1min at 2000rpm. The supernatant that contained unbound, non-specific DNA was removed carefully. The ProteinG-sepharose/Protein/DNA-complex were washed with 15min rotation at 4°C with the 500µl of buffers: HEG150 one wash, HEG500 two washes, LiCl solution two washes, HEG150 two washes. About 100µl HEG150 was left on the bead after the last wash. 1/20 volume equivalent of 20% SDS was added and incubated 2h at 4°C with rotation. The elution was repeated. The eluates were combined and adjusted to a sample volume of 200µl with HEG150S. The combined eluates were incubated to reverse Protein-DNA-crosslink by heating at 65ºC overnight. The samples were cooled down to room temperature. 1µl RNase was added to the samples and incubated for 30min at 37°C. Afterwards 10µl Proteinase K were added and incubated 2h at 37°C. The samples were adjusted to a volume of 400µl with 0.1xTE pH 8.0. The DNA was recovered by PCI extraction. The DNA was precipitated with 1/25 volume equivalent 5M NaCl, 1µl Glycogen, 1 volume equivalent isopropanol for 1h at -20°C and centrifuged for 40min at 4°C at 14000rpm. The DNA pellet was washed twice with 70% ethanol and dissolved in 50µl ddH_2O.

3.9.3 Douncer ChIP

The Douncer ChIP protocol was modified for *Xenopus* after Orlando and colleagues (Chanas et al., 2004). 200 embryos were homogenized in 10ml of buffer A1 + 1%PFA (320µl of 37% solution) at 17°C in a Douncer with a type “small” pestle (3 strokes). The lysate was transferred to 15ml Flacon tube and incubated for 15min at 17°C (total time starting from beginning of homogenization). 1.8ml glycine solution was added, mixed and incubated for 5min at 17°C. Afterwards the tubes were placed on ice. The lysates were centrifuged for 5min, 3500rpm at 4°C. The supernatant was discarded. The pellet was resuspended in 3ml of buffer A1 and centrifuged for 5min, 3500rpm at 4°C. This washing step was repeated three times. Afterwards the pellet was washed once in 3ml of lysis buffer and pelleted again by centrifugation for 5min 3500rpm at 4°C. The cross-linked material was resuspended in 2ml lysis buffer containing 0.1% SDS and 0.5% Sarcosine and incubated for 10min at 4°C on a rotating wheel. To shear the eluted chromatin, the lysate was sonicated using the Bioruptor eleven times at level High for 30sec in a 15ml tube with 30sec break in

between. After the sonication the solution was again rotated for 10min and centrifuge for 5min, 3500rpm at 4°C. The supernatant was transferred to a new tube. The pellet was again resuspended in 2ml lysis buffer containing 0.1% SDS and 0.5% Sarcosine and incubated for 10min at 4°C on a rotating wheel. The lysate was centrifuged again for 5min, 3500rpm at 4°C. The supernatants were combined and cleared twice via centrifugation at 14000rpm for 10min. The chromatin lysate was frozen in liquid N_2 and stored at -80°C until use.

For immunoprecipitation with monoclonal rat antibodies, 50µl blocked ProteinA-sepharose beads were pre-coupled for 60-90min with 50µg rabbit anti-rat antibodies or mouse anti-rat IgM at room temperature in PBS. Coupled beads were washed with PBS and transferred to the appropriate mount of monoclonal supernatant.

For preclearing 50µl blocked ProteinA-sepharose suspension were added to 1ml of lysate and incubate 1h with rotation at 4°C. The sepharose was pelleted for 1min at 2000rpm. Beads were discarded and the supernatant taken. The samples were split as desired. The antibody and 50µl blocked ProteinA-sepharose suspension were added and incubated with rotation overnight at 4°C. After binding of the fixed chromatin to the antibody and ProteinA-sepharose, the ProteinA-sepharose/Protein/DNA-complexes were pelleted by centrifugation for 1min at 2000rpm. The supernatant that contained unbound, non-specific DNA was removed carefully. The ProteinA-sepharose/Protein/DNA-complex were washed with 15min rotation at 4°C with the 500µl of buffers: lysis buffer with 0.1%SDS four washes, lysis buffer with 500mM NaCl and 0.1%SDS one wash, TE two washes. 250µl elution buffer were added to pelleted ProteinA-sepharose/Protein/DNA-complex, vortexed briefly and rotated at room temp 15min. The beads were pelleted for 1min at 2000rpm room temperature. The supernatant was kept and the elution was repeated.

The supernatants of the two elutions were pooled. 20µl 5M NaCl were added and DNA/proteins complexes were decrosslinked at 65°C over night. Also the input sample was adjusted to 1% SDS and 250mM NaCl. The sample eluates were cooled down to room temperature, 1µl RNase was added and incubated for 30min at 37°C. 5µl Proteinase K were added and incubated at 37°C for 2h. The DNA was recovered by Phenol-Chloroform extraction. The DNA was precipitated with 1/25 volume 5M NaCl, 1µl Glycogen, 1 volume isopropanol for 1h at -20°C

and centrifuged for 40min at 4°C at 14000rpm. The DNA pellet was washed twice with 70% ethanol and dissolved in 50µl ddH_2O.

3.9.4 Cesium chloride isopycnic centrifugation

50 embryo equivalents (eeq) of the Douncer ChIP lysate were used to test the correct degree of protein/DNA crosslink. 2.272g CsCl were dissolved into the lysate and filled up with lysis buffer to an end volume of 4ml. In order to establish the gradient, the samples were centrifuged for 36-48h, 195.000xg at 20°C. The gradient was collected in 0.5ml fraction from the bottom to the top. The density of each fraction was measured with a refractometer. Properly crosslinked protein-DNA complexes have a density of 1.39g/cm^3 (Orlando et al., 1997). The fractions were dialyzed against the dialysis buffer with a 12-14K MWCO membrane over night at 4°C. 1µl RNase was added to each sample and incubated for 30min at 37°C. 1.5µl 20%SDS and 2.5µl Proteinase K were added and incubated for 1h at 55°C. The crosslink was removed over night at 65°C. The DNA was recovered by PCI extraction. The DNA was precipitated with 1/25 volume 5M NaCl, 1µl Glycogen, 1 volume isopropanol for 1h at -20°C and centrifuged for 40min at 4°C at 14000rpm. The DNA pellet was washed with 70% ethanol and dissolved in 20µl ddH_2O. The DNA was visualized by agarose gel electrophoresis.

3.9.5 Quantification of enriched DNA through ChIP with real-time-PCR

3.9.5.1 ΔΔCt Method

Requirement: slope of standard curves = -3,32 to -3,34

Correlation R ≥0,99

- Average of Ct values
- Ct probe - Ct internal control = ΔCt
- ΔCt probe - ΔCt calibrator = ΔΔCt
- $2^{-\Delta\Delta Ct}$

3.9.5.2 Quantification via standard curves

- Average of Ct values
- Calculation of relative DNA amounts via standard curve
- Normalization to input

4 Results

4.1 Generation of tools for ChIP analyses

Antibodies that are applicable in chromatin immunoprecipitation (ChIP) analyses are a prerequisite for successful experiments. I chose to use monoclonal antibody, because they have a high specificity and selectivity for their antigen. Furthermore, immortal hybridoma cell lines, which secrete the monoclonal antibodies into the cell culture medium, are a constant source for the antibodies. The antibodies were raised in cooperation with the laboratory of Elisabeth Kremmer (GSF München). I cloned and purified the GST-fusion proteins (see 3.8.8). Positive primary hybridoma cell supernatants were prescreened by the Kremmer laboratory concerning their specificity to bind the antigen, but not to the GST-fusion part. Using Western blot and immunoprecipitation (IP) analyses, positive clones were further analyzed for their specific detection of *in vitro* translated antigens in our lab. Subsequently, the Kremmer laboratory stabilized the positive tested hybridoma clones. Clones were then tested in IPs and ChIP-IPs for their specificity and affinity to their antigen (see 3.8.6 and 3.8.7).

4.1.1 Antibodies against MyoD

The up-regulation of *myoD* expression requires autocatalysis (Steinbach et al., 1998), yet direct binding of the MyoD protein to its own locus has not been shown so far. In order to perform ChIP, antibodies against MyoD were required. Hopwood and colleagues described a monoclonal antibody for the specific detection of the transactivation domain (TD) of MyoD (see Figure 12B, right side) (Hopwood et al., 1992). Since this antibody was no longer available, new antibodies were raised against MyoD. Three stabilized αMyoD monoclonal antibodies MYO 7F11, MYO 5A9, and MYO 6C8 were characterized by Western blot analysis in whole embryo lysates of morula (NF6) and tailbud stage embryos (NF22) (see 3.8.3, Figure 12A). Since the *myoD* expression is activated at the early gastrula stage (Hopwood et al., 1989), all three antibodies detected MyoD in tailbud stages (NF22), but not in the morula stages (NF6). Although the theoretical molecular weight of MyoD is 32kDa, it showed a decreased mobility upon SDS-PAGE analysis as described previously (Hopwood et al., 1992). In

contrast to the monoclonal antibodies MYO 7F11 and MYO 5A9, which additionally recognized multiple unspecific bands, the MYO 6C8 antibody detected a single band of correct molecular weight in the appropriate embryonic stage. In Figure 12B, the antigen epitopes of MyoD were mapped. All three antibodies recognize an epitope located in the N-terminus of the protein. They could not detect the other two MyoD deletion constructs, which lack the bHLH or the C-terminal domain of MyoD. Based on this, the transactivation domain (TD) appears to be the preferred antigenic domain. Interestingly, also the published antibody recognized the MyoD protein in this domain (Hopwood et al., 1992). After Western blot analysis, the antibodies were tested for their ability to immunoprecipitate MyoD from embryonic extracts, which were treated under ChIP conditions (Figure 12C). The endogenous MyoD levels are low, the protein migrates at the same size as the IgG heavy-chain, and therefore it is not detectable in the IP assay. For that reason, 4-cell stage embryos were injected 4 times into the animal pole of all four blastomeres with 400pg of Myc-tagged MyoD RNA. These embryos were cultured until late blastula/early gastrula stage and treated further according to the ChIP-type protocol (see 3.8.7). Untreated embryos were used as a control. The IPs were analyzed by immunoblotting with an antibody directed against the Myc-epitope. Whereas MYO 7F11 and MYO 5A9 precipitated only ~12.5% of the injected Myc-tagged MyoD, the IP with MYO 6C8 resulted in approximately 50% precipitated input protein.

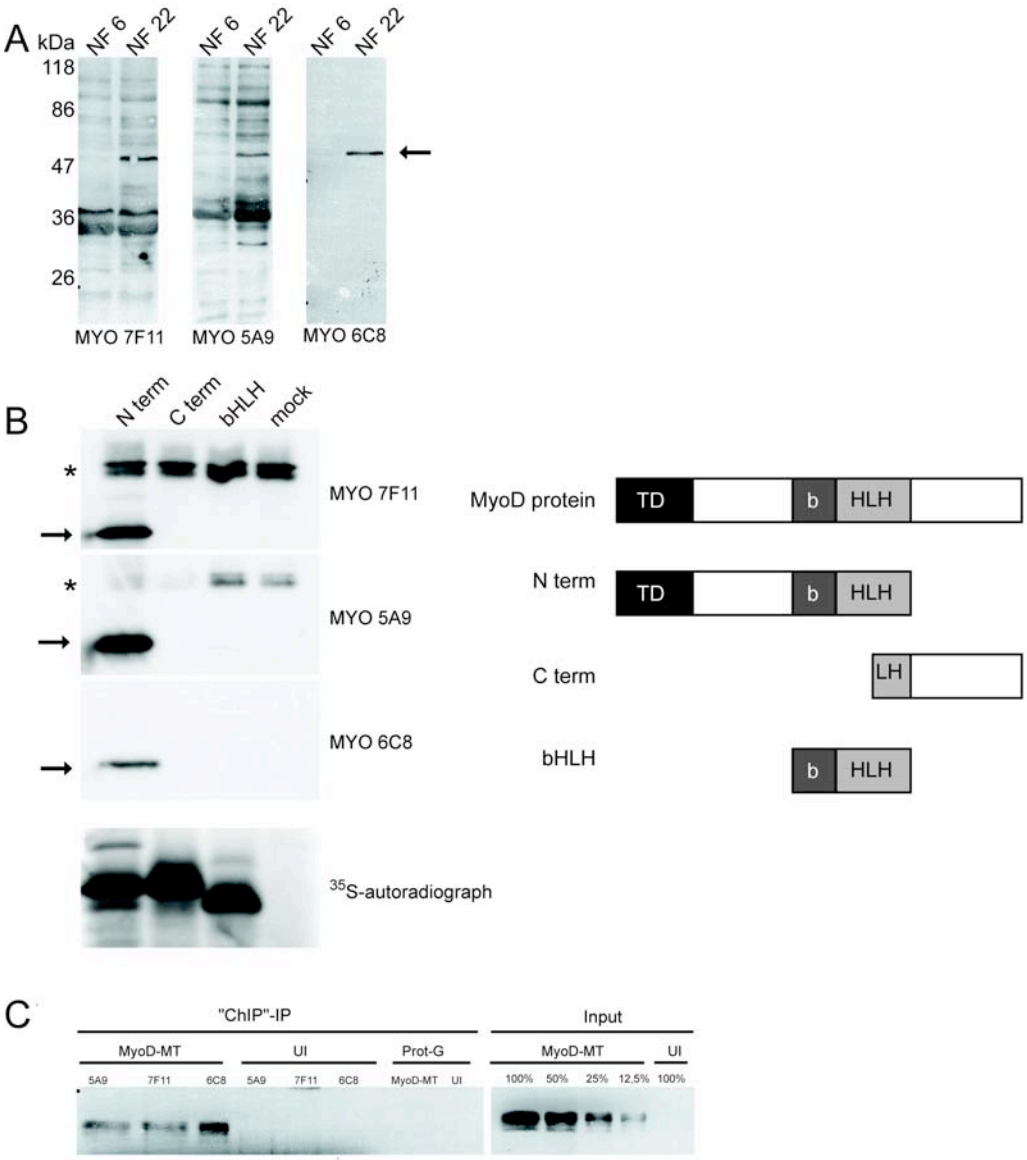

Figure 12: Characterization of monoclonal antibodies against MyoD

A) Western blot analysis of MyoD with rat monoclonal antibodies MYO 7F11, MYO 5A9 and MYO 6C8. In each lane protein lysates of 10 embryo-equivalent (eeq) of morula (NF6) and tailbud stage embryos (NF22) were loaded. The lysates were treated according to the protein extraction protocol of Strataclean resin. The arrow marks the MyoD band. **B**) Left side: Determination of the antibody epitope of MYO 7F11, MYO 5A9, and MYO 6C8 in *in vitro* translated, ^{35}S-labelled MyoD truncations. N term: N-terminus and bHLH domain of MyoD (encoded on plasmid pUE16), C-term: C-terminus of MyoD (encoded on plasmid pUE24), bHLH: basic helix-loop-helix domain of MyoD (encoded on plasmid pUE28), mock: no DNA added. The arrow marks the MyoD band. The asterisk labels unspecific bands. Bottom panel: autoradiograph of radiolabeled *in vitro* translated proteins serves as translation and loading control. Right side: Cartoons representing MyoD truncations. **C**) "ChIP-type" IP with MYO 5A9, MYO 7F11, and MYO 6C8. 4 eeq of Myc-tagged MyoD-MT (pRR107 mRNA injected) or UI (uninjected) lysates were applied to the IP. Prot-G showed the background that sticks to the ProteinG-sepharose beads. Input dilutions of 100%, 50%, 25%, and 12.5% were loaded on the SDS-PAGE to

estimate the precipitation efficiency of the IP. Immunoblotting was performed using αMyc antibody 9E10.

Based on these results, MYO 6C8 was identified as the antibody most suitable for Western blot analyses, IPs and ChIP experiments.

4.1.2 Antibodies against Lef1, Tcf1 and Tcf3

No *Xenopus*-specific Lef/Tcf antibodies were available, which enable the characterization of the Lef/Tcf1 transcription factors, when and where they are bound to their binding sites of the model promoters *myf5* and *siamois,* Therefore, antibodies were raised against Tcf1, Lef1 and Tcf3. The focus of this study was on maternal and early zygotic Wnt signaling until the gastrula stage. Therefore, we raised no antibodies against Tcf4, because Tcf4 is not expressed until the neurula stage (Konig et al., 2000; Kunz et al., 2004). Figure 13A shows a schematic overview of the Lef/Tcf transcription factors and their conserved domains. To reduce or exclude cross-reactivity, the antibodies were directed against the most divergent domain between the β-catenin binding domain and the HMG box (see Figure 13B).

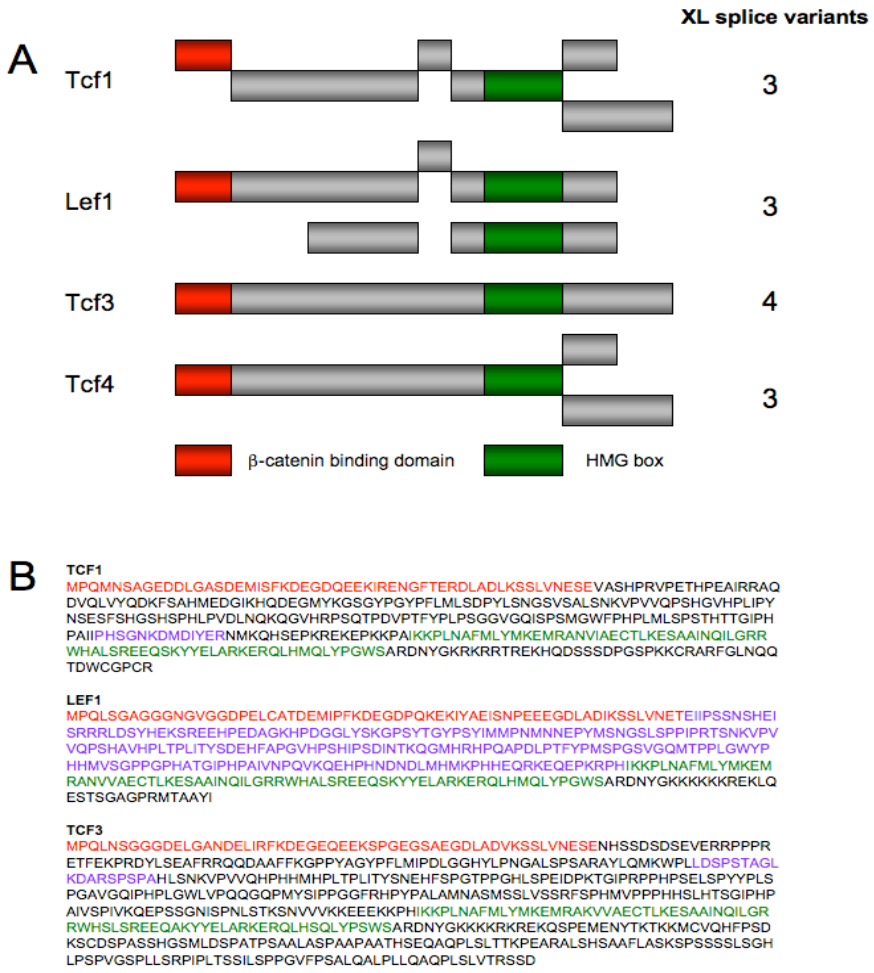

Figure 13: Lef/Tcf protein family and antigens for monoclonal antibodies

A) Schematic representation of Tcf splice variants (modified after (van Noort and Clevers, 2002)). Red box marks the β-catenin binding domain, green box the HMG box, a DNA binding motif. On the right the numbers of splice variants in *Xenopus laevis* are listed. **B)** Amino acid sequence of xTcf1, xLef1 and xTcf3. Red letters mark the β-catenin binding domain, green letter mark the HMG box and purple letters the antigen peptides (Tcf1, Tcf3) or GST-fusion-protein (Lef1).

We obtained five monoclonal antibody against Lef1 LEF 1F12, LEF 3D4, LEF 5B10, LEF 5F12, LEF 3F2, against Tcf1 four monoclonal antibodies Tcf1 7E3, Tcf1 5F2, Tcf1 1D12, Tcf1 2F4 and against Tcf3 two monoclonal antibodies Tcf3 6B6 and Tcf3 3E5. These antibodies were tested for their ability to immunoprecipitate their respective antigen. *In vitro* translated, ^{35}S-labeled Lef1 protein was used to test the IP performance of the αLef1 antibodies supernatants LEF 1F12, LEF 3D4, LEF 5B10, LEF 5F12 and LEF 3F2 (Figure 14A). LEF 3D4 and LEF 5B10 precipitated over 50% of the Lef1 protein, LEF 1F12 and LEF 5F12 around 50% and LEF 3F2 around 25%. Since the

endogenous proteins migrate approximately at the same molecular weight as the heavy chain of the IgG signal, overexpressed Myc-tagged Tcf1 and Tcf3 proteins were used to test the IP performance *in vivo.* The Myc-tag increases the molecular weight of about 10kDa. Therefore the Myc-tagged Lef/Tcf proteins can be distinguished from the endogenous protein and the IgG heavy chain signal. 250pg of MT-Tcf1-FLAG or MT-Tcf3-FLAG mRNA was injected 4x in to the animal pole of all four blastomeres of 4-cell stage embryos. These embryos were cultured until late blastula/early gastrula stage. Uninjected embryos were used as a control. The IPs were analyzed by immunoblotting against the Myc-epitope. Tcf1 1D12 and 2F4 precipitated more than 50% of the injected Myc-tagged Tcf1 protein. Tcf1 7E3 and 5F2 precipitated in addition to the Tcf1 an unspecific protein. Tcf3 3E5 precipitated also over 50% of the overexpressed protein, but Tcf3 6B6 precipitated barely anything of the overexpressed Tcf3 protein.

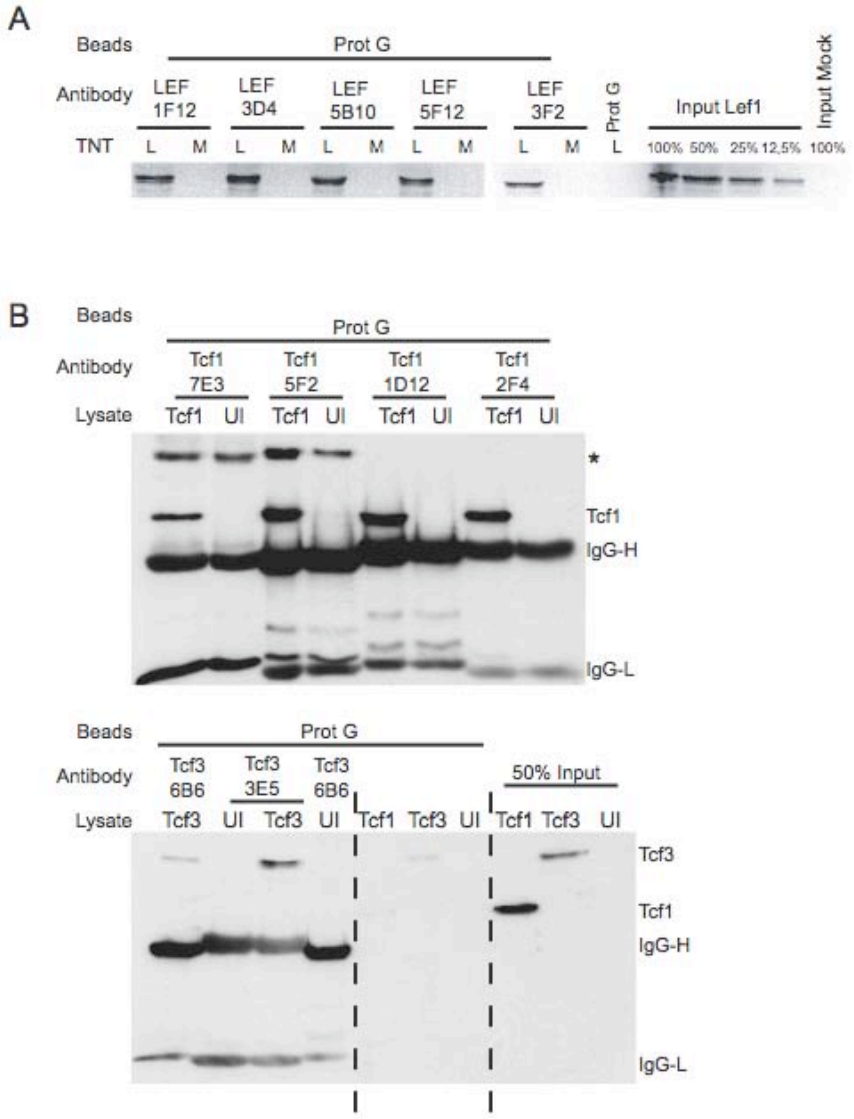

Figure 14: Screening of monoclonal antibodies against xLef1, xTcf1 and xTcf3 for immunoprecipitation

A) IP of *in vitro* translated, ^{35}S-labeled Lef1 protein (L, encoded by plasmid pLef1-FLAG) or mock translation (M, no DNA) with the indicated antibodies. As a background control for the IP served the ProteinG-sepharose (Prot G) without antibody. In order to estimate the IP efficiency, input dilutions were loaded on the gel. The figure shows an autoradiograph. **B)** IP with the indicated antibodies. 250pg of MT-Tcf1-FLAG mRNA for αTcf1 antibodies or 250pg of MT-Tcf3-FLAG mRNA for αTcf3 antibodies were injected 4x into the animal pole. 2eeq of the injected (Tcf1 or Tcf3) and UI (uninjected) lysates were applied to the IP. Prot-G showed the background. 50% of the input was loaded in the SDS-PAGE. The immunoblotting was performed with αMyc antibody 9E10. The asterisk marks an unspecific band. IgG-H: heavy chain of IgG, IgG-L: light chain of IgG.

The calculated theoretical molecular weight of Lef1 is 42kDa, which corresponds to band a detected in Figure 15A. An equivalent band at the same molecular weight was detected by LEF 1F12, LEF 3D4 and LEF 5B10. In addition

LEF 1F12 and LEF 5B10 recognized a second moiety (band b, Figure 15A). This signal is likely to be the *Xenopus* version of Lef1-S (molecular weight of murine Lef1-S: 31.8kDa). Lef1-S is a short, dominant negative version of the Lef1 protein, which lacks the β-catenin binding domain. This short variant does not originate from differential splicing, but from differential promoter usage (Hovanes et al., 2001). In Figure 15B, the ability of the αTcf1 antibodies (Tcf1 7E3, Tcf1 5F2, Tcf1 1D12, Tcf1 7E3) to recognize their antigen by immunoblotting was tested on whole embryo lysate of gastrula stages (NF11) (see 3.8.4) in comparison to *in vitro* translated Tcf1c-Flag protein (see 3.8.2). Only Tcf1 2F4 recognized a protein of approximately 55kDa (Figure 15B band 1). But this signal did not correspond to the molecular weight signal of Tcf1c-Flag (Figure 15B, band 2). This observation could be due to splice variants of Tcf1, which have been already described in (Van de Wetering et al., 1996). Therefore, we performed developmental Western blot analysis to identify other splice variants in lysate from various stages (see 3.8.3): 2-cell stage, blastula stage (NF8), gastrula stage (NF11), neurula stage (NF18), and tailbud stage (NF26). Hoppler and colleagues described for *Xenopus* two of the five Tcf1 splice variants (Roel et al., 2003), originally identified for human Tcf1 by Clevers and colleagues (Van de Wetering et al., 1996). The Western blot analysis in Figure 15C suggested that five splice variants exist in all tested stage during *Xenopus* development. The appearance of the splice variants in Figure 15C in comparison to Figure 15B is due to the fact that different embryo lysis protocols were used (see 3.8.3 vs. 3.8.4); the embryo lysis protocol used in Figure 15C includes an additional sonication step. In addition to these splice variants, it was shown that maternal Tcf1 is more abundant in the ventral half of very early embryos as in the 4-cell stage (also see Appendix Figure 1). β-catenin served as a loading control, which is distributed equally during this stage (Fagotto and Gumbiner, 1994). Unfortunately, the endogenous Tcf3 protein was not detectable with any of the αTcf3 antibodies.

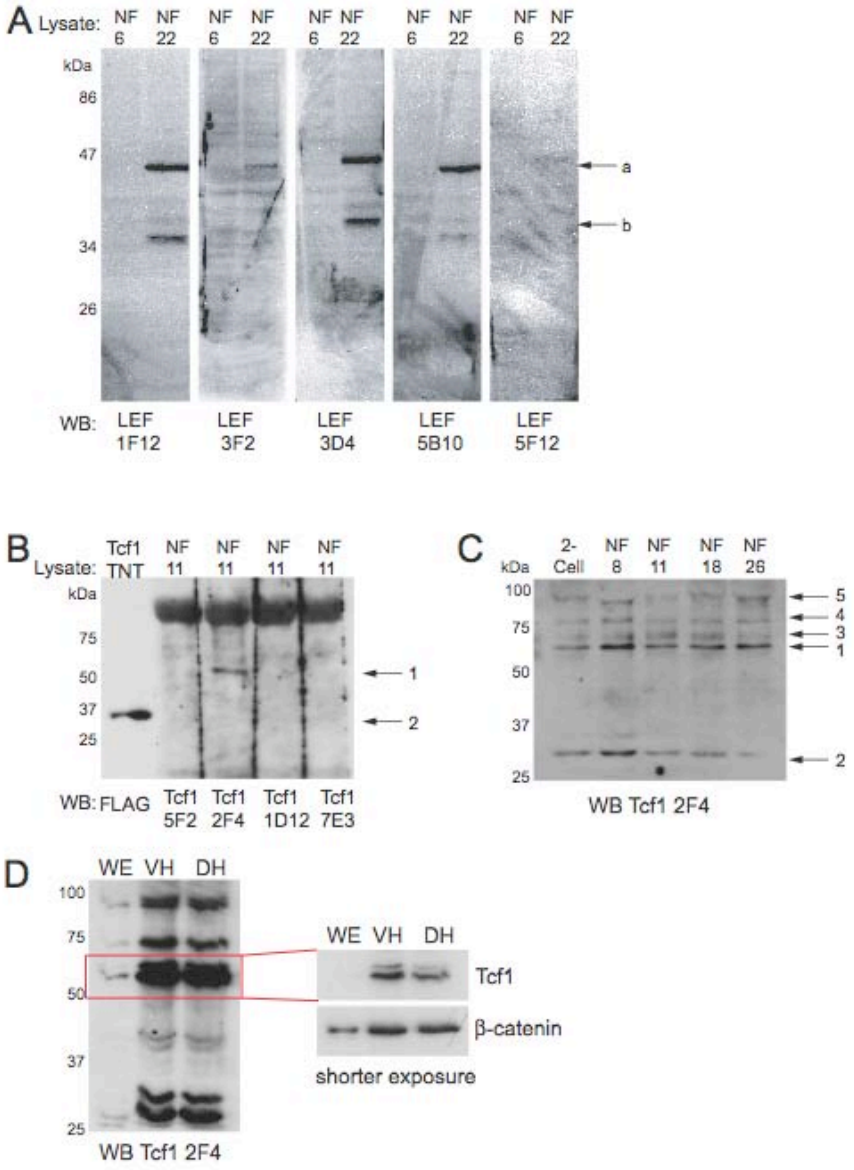

Figure 15: Screening of monoclonal antibodies against Lef1 and Tcf1 for Western blot analysis

A) Western Blot analysis of endogenous Lef1 protein with the indicated monoclonal supernatants. 2eeq were loaded per lane of morula (NF6) or tailbud stage embryos (NF22) (see 3.8.3). Arrows a and b mark putative variants of Lef1 and Lef1-S, respectively. **B)** Immunoblotting of endogenous xTcf1 protein with rat monoclonal supernatants Tcf1 5F2, Tcf1 2F4, Tcf1 1D12 and Tcf1 7E3. 1eeq was loaded per lane of gastrula stage embryos (NF11) (see 3.8.4). Arrows 1 and 2 mark putative splice variants of Tcf1. **C)** Developmental Western blot analysis with one eeq of the following stages: 2-cell stage, blastula stage (NF8), gastrula stage (NF11), neurula stage (NF18) and tailbud stage (NF26). The immunoblotting was prepared against Tcf1 with Tcf1 2F4. Arrows 1-5 mark different splice variants of Tcf1. The lysates were performed after the protein extraction protocol with Strataclean resin. **D)** Distribution of Tcf1 in a 4-cell stage embryo. WE: 1eeq of a whole embryo, VH: 1eeq ventral half, DH: 1eeq dorsal half. The immunoblotting was performed against Tcf1 with Tcf1 2F4. The blow up of the shorter

exposure shows immunoblotting with Tcf1 2F4 and β-catenin antibody PGDS 1B1. The lysates were prepared according to the protein extraction protocol with Strataclean resin.

Based on these results, αLef1 antibodies LEF 1F12, 3D4 and 5B10 were identified to be suitable for Western blot analyses, IPs and ChIP-IPs, Tcf1 2F4 in ChIP-IPs and Western blot analyses, Tcf1 1D12 in ChIP-IPs and Tcf3 3E5 in ChIP-IPs.

4.1.2.1 Specificity of the antibodies

The antibodies of the Lef/Tcf protein family members were directed against the most divergent domains between the β-catenin binding domain and the HMG box (see Figure 13). Nevertheless, these regions still share a sequence similarity of about 40%. Therefore, the antibodies were tested for cross-reactivity. In Figure 16, the antibodies LEF 3D4, LEF 5F12, Tcf1 1D12, Tcf1 2F4, Tcf3 3E5 were analyzed by IP with *in vitro* translated, ^{35}S-labeled Lef1, Tcf1, Tcf3 and Tcf4a alone or as a mixture. LEF 3D4 and LEF 5F12 were specific for Lef1, Tcf1 1D12 and Tcf1 2F4 for Tcf1. The αLef antibodies enriched the smaller band of the *in vitro* translated Lef1 double band. The αTcf3 antibody Tcf3 3E5 did not precipitate its antigen Tcf3.

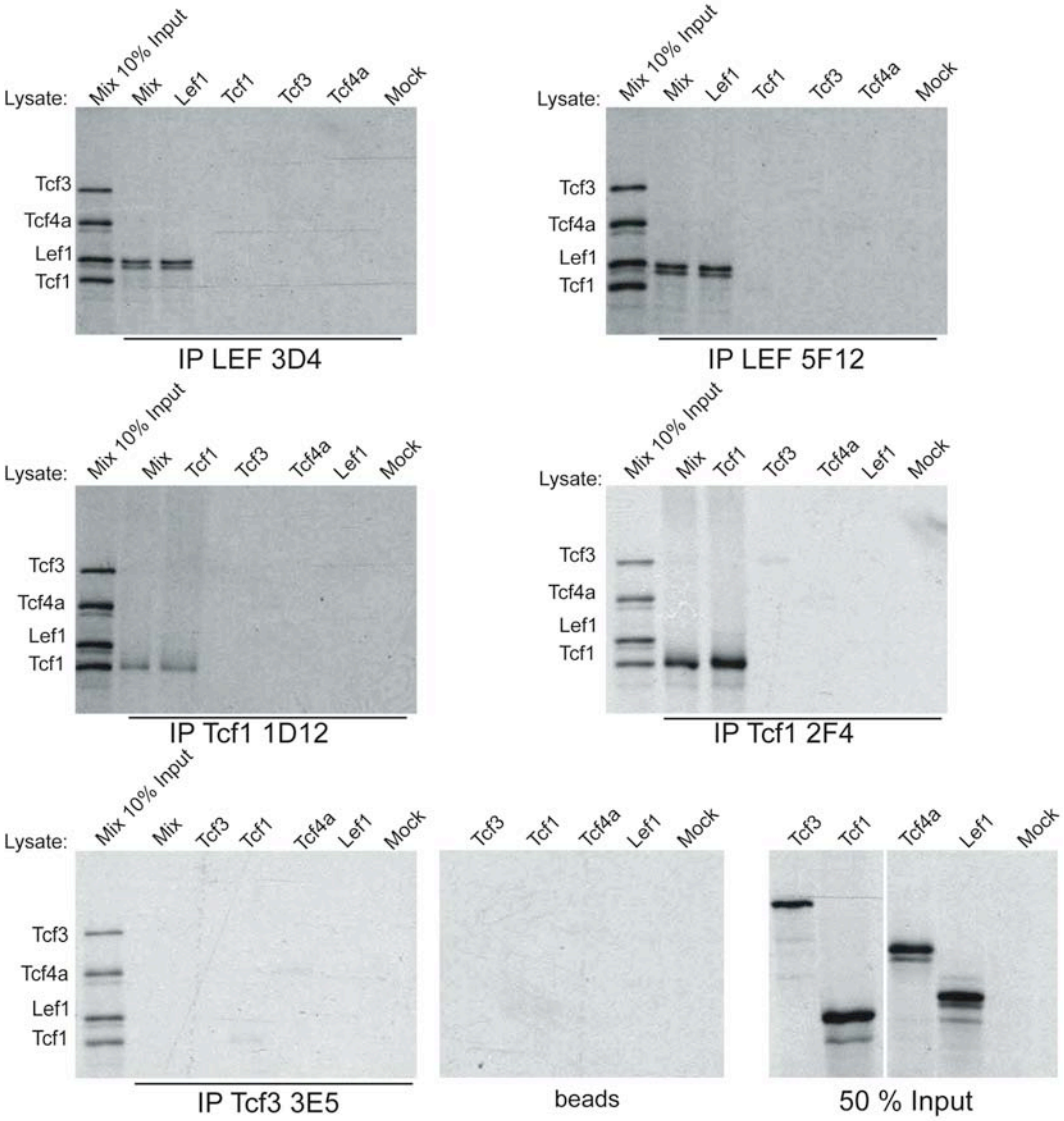

Figure 16: Lef/Tcf antibodies precipitate their specific *in vitro* translated antigen, but no other members of the protein family

2µl *of in vitro* translated, ^{35}S labeled Lef1 (encoded by plasmid pLef1-FLAG), Tcf1 (encoded by plasmid pTcf1-FLAG), Tcf3 (encoded by plasmid pTcf3-FLAG), Tcf4a (encoded by plasmid pTcf4a-FLAG) and mock control (no DNA) were supplied individually or as a mix of all 5 TNT reactions IPs with the indicated antibodies; Protein-G sepharose beads alone served as a control (beads). In addition to the 50% input, on each gel 10% of the input of the mixed *in vitro* translation reactions was loaded in the first lane of all gels to make it easier to discriminate between the four Lef/Tcfs. The figure shows an autoradiograph of the ^{35}S-labeling with an exposure time of 24h.

The antibodies LEF 3D4, LEF 5F12, and Tcf1 2F4 precipitated also *in vivo* specifically their over-expressed antigen out from a mixture of all four Lef/Tcf protein family members (Figure 17). Tcf1 1D12 also precipitated its specific

antigen Tcf1, but less efficiently than Tcf1 2F4. Therefore, the subsequent experiments were performed with Tcf1 2F4 solely. Tcf3 3E5 was again not able to precipitate Tcf3 or any of the other Lef/Tcfs.

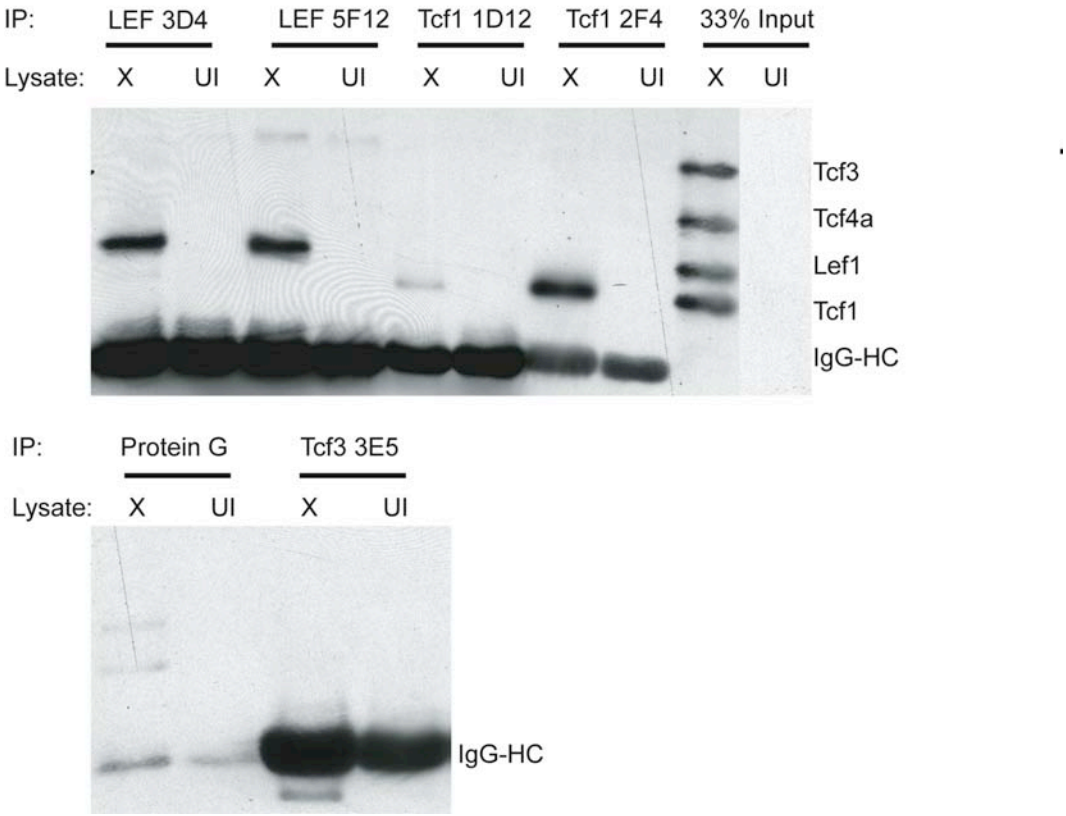

Figure 17: Lef1 and Tcf1 antibodies precipitate specifically their overexpressed antigen *in vivo*

250pg each of *in vitro* transcribed MT-Tcf1-FLAG mRNA, MT-Lef1-FLAG mRNA, MT-Tcf3-FLAG mRNA and MT-Tcf4a-FLAG mRNA were injected into 4 cell stage embryos and cultured until the blastula stage (NF9). Four eeq Tcf-Mix injected embryo lysate (X) or untreated embryos (UI) were used for the IPs with the indicated antibodies. ProteinG-sepharose beads (Protein G) served as a background control. 33% of the inputs were also loaded on SDS-PAGE. The immunoblotting was performed with αMyc antibody 9E10. IgG-HC: IgG heavy chain.

In addition to the IP specificity in non-crosslinked embryo lysates, also the IP specificities of the antibodies under formaldehyde-fixed ChIP conditions were investigated. Lysates of formaldehyde-fixed, Tcf-mix injected or uninjected embryos were applied to the ChIP-type IP. The αLef1 antibodies LEF 3D4 and LEF 5F12 precipitated predominantly Lef1. Unanticipated, they also precipitated the other three Tcf proteins Tcf1, Tcf3 and Tcf4a under ChIP conditions

(Figure 18). The αTcf1 antibody Tcf1 2F4 enriched primarily Tcf1 but also the other three Tcf family members Lef1, Tcf3 and Tcf4a. The αTcf3 antibody Tcf3 3E5 was able precipitated all 4 Lef/Tcfs, but did not preferentially bind to Tcf3. In order to exclude a DNA-dependent co-precipitation of the Lef/Tcfs, the IPs were performed with and without the presence of DNaseI. This revealed, that the co-precipitation of the Lef/Tcf protein occurred in a DNaseI-treatment independent manner.

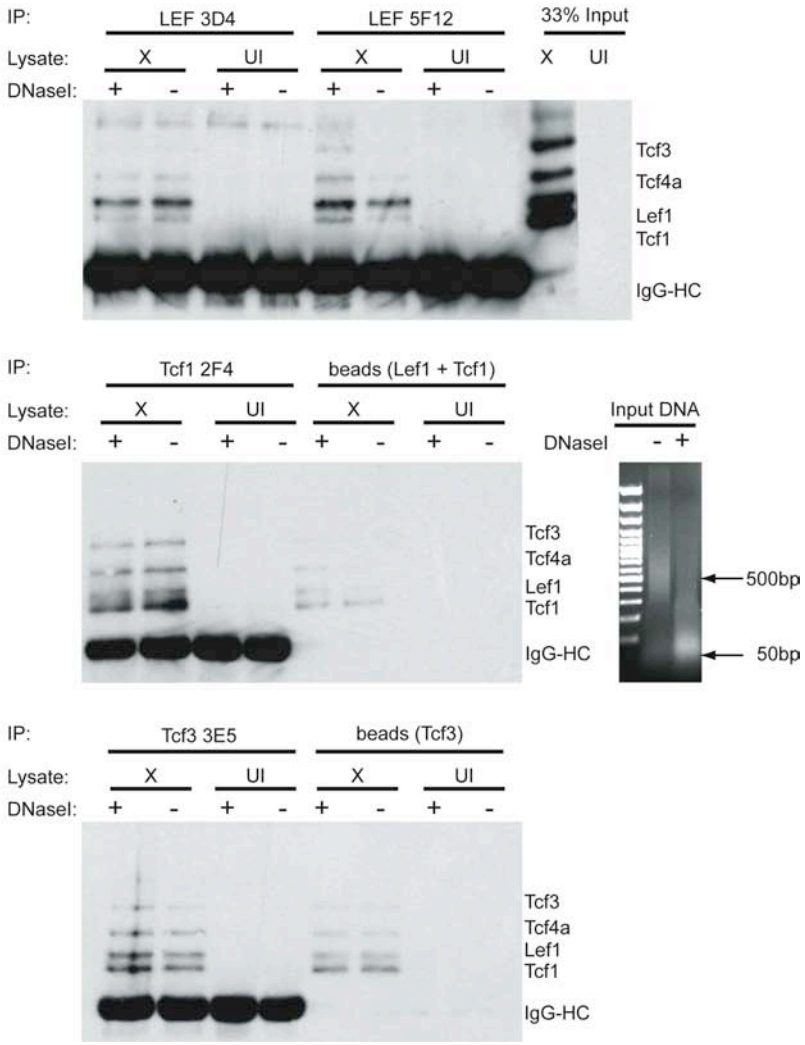

Figure 18: Lef/Tcf antibodies precipitate all four over-expressed Lef/Tcf family members upon formaldehyde fixation under ChIP conditions

250pg each of *in vitro* transcribed MT-Tcf1-FLAG mRNA, MT-Lef1-FLAG mRNA, MT-Tcf3-FLAG mRNA and MT-Tcf4a-FLAG mRNA were injected into 4-cell stage embryos, cultured until the blastula stage (NF9) and fixed for ChIP-type IP (see 3.7.7). 3eeq Tcf-Mix injected embryo lysate (X) or untreated embryos (UI) were used for the "ChIP"-type IPs with LEF 3D4, LEF 5F12, Tcf1 2F4 and Tcf3 3E5. ProteinG-sepharose was blocked for Lef1 and Tcf1 IPs in the presence of 0.05% Tween20 (beads Lef1+Tcf1), for Tcf3 without Tween20 (beads Tcf3). The proteins were bound to the antibodies with or

with out the presence of 10U DNaseI (Roche). 33% of the inputs were loaded on the SDS-PAGE. The immunoblotting was performed with αMyc antibody 9E10. IgG-HC: IgG heavy chain. For the analysis of DNaseI treatment, the chromatin was decrosslinked; the DNA was purified and analyzed on a 1% agarose gel.

A direct interaction of Lef/Tcf protein was not reported so far, although Lef/Tcf binding sites frequently appear as multimers on promoter elements like the *siamois* promoter (Brannon et al., 1997). Still, it is possible that Lef/Tcf proteins interact in someway directly or indirectly. The co-precipitation under formaldehyde-fixed conditions was further analyzed with the bimolecular fluorescence complementation technique (BiFC) (Hu et al., 2002). However, all attempts to demonstrate an interaction between Lef/Tcf proteins *in vivo* were fruitless, although the positive controls bJun fused to the N-terminal part of YFP and bFos fused to the C-terminal part of YFP showed the YFP fluorescent signal.

From these results, I conclude that the αLef1 LEF 3D4 and LEF 5F12 and αTcf1 Tcf1 2F4 are highly specific and do not cross-react with the other Lef/Tcf family members. The Tcf3 antibody Tcf3 3E5 was not able to precipitate its antigen under native conditions. Unexpected, the αTcf1, αLef1 and αTcf3 antibodies precipitated their own antigen. This precipitation is very specific under unfixed condition. The co-precipitation their family members under formaldehyde-fixed ChIP conditions in a DNaseI-treatment independent manner suggests that they are some uncharacterized parts of multimeric complexes, although they do not interact directly.

4.1.2.2 Lef/Tcf protein expression pattern

The mRNA expression pattern of the Lef/Tcf transcription factors is analyzed for *Xenopus* embryos (Kunz et al., 2004; Molenaar et al., 1998; Roel et al., 2003). The influence of these factors on the patterning of the *Xenopus* embryo is also very well studied via loss- and gain-of-function experiments (for example (Houston et al., 2002; Liu et al., 2005; Roel et al., 2002; Standley et al., 2006)). However, the protein expression patterns of Lef1 and Tcf1 were not yet described for *Xenopus* embryos due to the lack of antibodies. Therefore, the protein expression pattern was analyzed by immunocytochemistry (ICC, see 3.7.2) and immunofluorescence analysis (IF, see 3.7.3) on paraffin sections.

Lef1 mRNA is detectable from late blastula stage (NF9) on (Molenaar et al., 1998). However, the protein was not detected until neurula with ICC or IF (Appendix Figure 1). This might be due to low protein levels or low detection

sensitivity of the antibody in these assays. The ICC and IF analyses showed that Lef1 is expressed tissue-specifically. In neurula stage embryos, a stain in the dorso-anterior region is visible (Appendix Figure 6). From this stage on, the protein expression pattern is consistent with the published mRNA pattern (Molenaar et al., 1998). In the tailbud stage, the protein is detectable in the brain, retina, neural crest and dermis (Appendix Figure 7 and 8).

The maternal Tcf1 protein is more abundant on the ventral side of the embryo until blastula stage (Appendix Figure 1). During gastrula stage, it starts to accumulate on the dorsal portion of the ectoderm (Appendix Figure 2). From neurula stage on the protein is ubiquitously expressed (Appendix Figure 2-5). With the exception of the protein localization at the blastula stage, the observed protein expression pattern matches that of the mRNA described by Roel *et al.* (Roel et al., 2003).

From this analysis, I conclude that the generated antibodies against Lef1 and Tcf1 are not only suitable for IP and ChIP experiments, but are appropriate to study the *in vivo* protein localization by ICC and IF.

4.2 ChIP Analyses

4.2.1 SRF localizes to the *myoD* maintenance enhancer in activin-induced animal cap explants

In order to understand its complex regulation, the locus of the *myoD* gene was analyzed with a transgenic reporter gene approach. This study revealed two important regulatory elements. One element – the maintenance enhancer (ME) – is required to stabilize the *myoD* transcription subsequent to its induction during the gastrula stage. A functional serum response factor (SRF) binding site is located in this ME element (Xiao, 2003). The direct binding of SRF to this site was verified by ChIP with somite explants containing majorly *myoD* expressing cells and pre-gastrula stage animal cap explants with *myoD* non-expressing cells (Nentwich, 2003). With this ChIP analysis, I aimed to show the association of SRF to the *myoD* maintenance enhancer in an activation-dependent manner, which was not shown by Oliver Nentwich (Nentwich, 2003). Therefore, the ChIP against SRF on the *myoD* locus was used to establish a more sophisticated method in our lab. The protocol differs in three crucial steps: First of all, I established the SRF ChIP with whole embryos of

mid-gastrula stage (NF11), which have just induced the *myoD* expression in the preinvoluted mesoderm, and late neurula stage embryos (NF18), which have maintained the *myoD* expression in paraxial mesoderm (also see Figure 31). Subsequently, I extended my analysis by using induced and non-induced animal cap explants of neurula stage embryos (see Figure 19) to investigate, if the SRF binding to the *myoD* locus is induction-dependent. Secondly, I perform the lysis and the chromatin shearing as a single step by applying the explants to the FRENCH Press. Oliver Nentwich lysed his explants prior to the chromatin fragmentation, which he performed by sonication with a Branson sonifier microtip. Thirdly, I performed quantitative real-time PCR analysis of the enriched DNA fragments of amplicons located along almost the entire *myoD* locus. Oliver Nentwich performed his analysis with semi-quantitative PCR analysis; moreover, he used only two PCR amplicons located at the maintenance enhancer and in the 3' untranslated region of the *myoD* gene.

The flowchart in Figure 25 shows the experimental workflow of the subsequent ChIP analysis (modified after (Reinke and Horz, 2003)): Selection and fixation of the animal cap explants, lysis of the embryos with subsequent shearing of the chromatin with the FRENCH Press, IP, purification of the DNA and quantification of the enriched DNA with real-time PCR. For simplicity reasons, this ChIP protocol was called In Situ ChIP. The establishment of these steps was discussed in detail in the subsequent chapters.

4.2.1.1 Titration of activin containing cell culture supernatant for mesoderm and muscle induction of animal caps

In order to distinguish between *myoD* expressing and non-expressing cells of the same embryonic stage, we made use of the animal caps assay (Green et al., 1992). In this assay, the blastocoel roofs of blastula stage embryos are excised with the Gastromaster (Figure 19A). The animal cap explants are cultured further with or without the presence of mesodermal inducer. Animal caps, which are cultured in medium containing the TGFβ ligand activin, formed tissues of the mesodermal lineage in a dosage-dependent manner (Figure 19A) (Sokol et al., 1990). Non-induced animal cap explants stayed in the ectodermal lineage and developed to atypical epidermis (Ariizumi and Asashima, 2001). In Figure 19B, different dilutions of the activin containing medium were titrated to induce muscle tissue. The 1:10 dilution in 0.5xMBS/BSA showed the best

enrichment of muscle-induced cells, identified by the protein stain of the structural muscle protein Myosin (MF20) (Figure 20B5). The *in situ* hybridization in Figure 20C showed expression of *myoD* mRNA in the activin treated animal caps. Although less cells show *myoD* expression than MF20 staining, the induction of muscle differentiation with the 1:10 activin medium dilution was confirmed (Figure 20C8). This difference is due to variations of the induction.

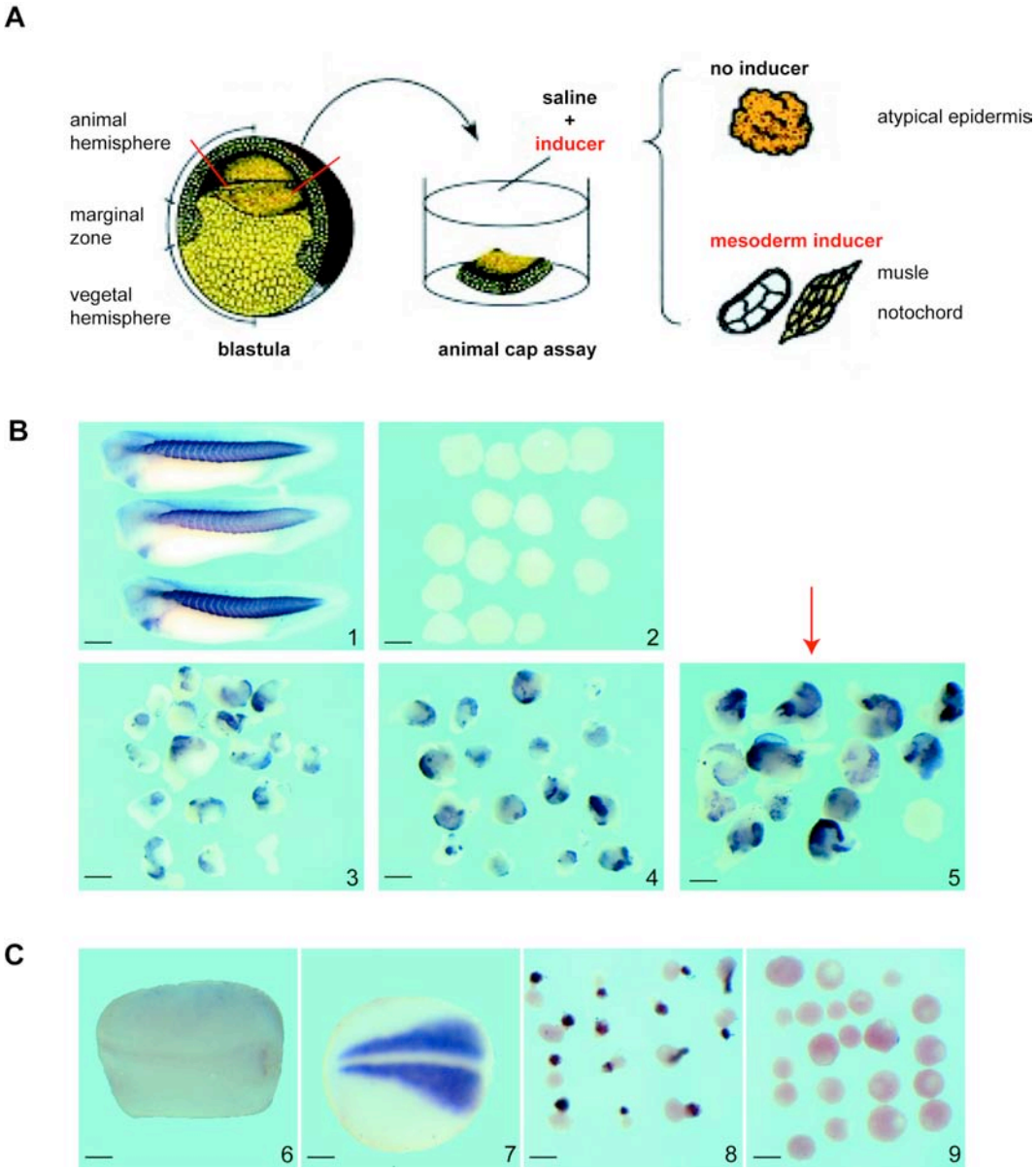

Figure 19: Titration of activin containing medium for muscle induction in animal caps

A) Schematic representation of the animal cap assay. Animal cap explants are excised in the blastula stage (NF9), cultured in saline with or without mesodermal inducer until the required stage, which is here in C the neurula stage (NF18) and in B the tailbud stage (NF30) (modified after (Ariizumi and Asashima, 2001)). **B)** Titration of activin containing

medium analyzed with ICC against MF20 (myosin heavy chain, a structural muscle component) to examine the muscle induction. 1: sibling embryos of tailbud stage (NF30) as a staging and staining control. 2: animal caps cultured without inducer. 3: animal caps cultured with activin containing medium diluted 1:2 in 0.5xMBS/BSA. 4: activin containing medium diluted 1:4. 5: activin containing medium diluted 1:10. Red arrow marks the 1:10 dilution, which was used for subsequent muscle induction of animal caps. **C)** MyoD *in situ* hybridization of neurula stage animal caps (NF18) treated with activin containing medium diluted 1:10 in 0.5xMBS/BSA (8) or without inducer (9) were performed to investigate the activation of *myoD*. 6: sibling embryos as negative control with MyoD probe. 7: sibling embryo as positive control with MyoD probe. Scale bar in A: 770µm, B-E and H,I: 800µm, F,G: 300µm.

4.2.1.2 Optimizing the chromatin shearing conditions

Having established the induction conditions for the animal cap explants, the fragmentation of the chromatin was the next crucial step, which had to be calibrated. It is an important step, because it determines the resolution of the ChIP. If the chromatin fragments are too large, amplicons, which are in close proximity, cannot be distinguished. If the fragments are too small, they are undetectable by PCR. Moreover, applying too much energy in order to generate smaller chromatin fragments might damage antigens such as modifications of histone tails. Following the protocol after (Reinke and Horz, 2003), the chromatin was sheared by the FRENCH Press. Exerting high pressure followed by abrupt relaxation leads to the shearing of the chromatin. Appling the lysate two times to the FRENCH Press was adequate to shear the chromatin to a size of 500-1000bp (Figure 20).

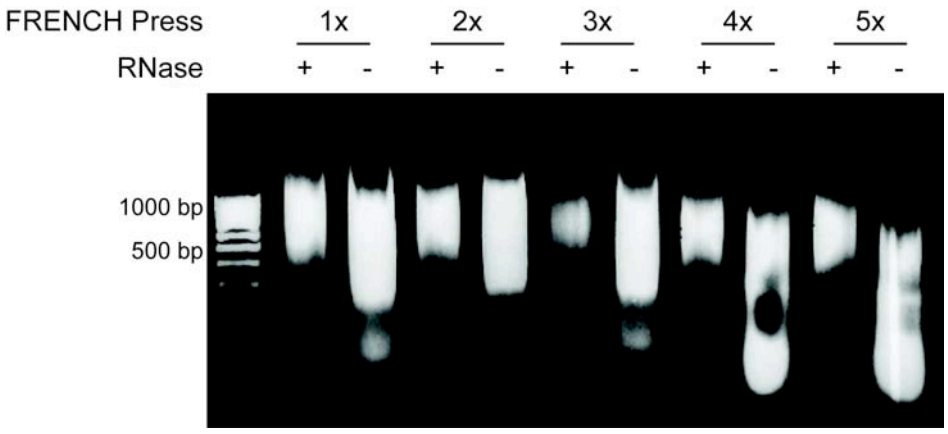

Figure 20: Testing of chromatin shearing conditions with the FRENCH Press Minicell set up

200 neurula stage embryos were formaldehyde-fixed (In Situ ChIP protocol), lysed in 4ml HEG150 and subjected to the Minicell of the FRENCH Press for up to 5x. After each round, a 100µl aliquot was put aside. The DNA of these aliquots was purified. Half of the DNA was treated with RNase. The shearing of the DNA was analyzed on a 1% agarose

gel. Already after two rounds of treatment, the DNA was sheared to an average size of 500-1000bp. As the size standard served the 100bp ladder.

4.2.1.3 Quantification of the precipitated DNA via TaqMan technology-based real-time PCR

The precipitated DNA was quantified with real-time polymerase chain reaction (PCR). The advantage of this PCR method is that the data are collected in the exponential amplification phase. Thus, the dynamic range of the detection is increased compared to quantitative PCR, which measures at the end-point of the PCR reaction. The increase in DNA is measured by a fluorescent dye. Two different ways of detection are available. One stain is SYBR Green, a fluorescent dye that intercalates sequence-unspecifically into double-stranded DNA and becomes thereby fluorescent. The other staining technique is a fluorescent-labeled oligonucleotide used by the TaqMan probe that binds within the PCR amplicons after the denaturing step. Upon DNA polymerase elongation, the fluorescent-labeled oligonucleotide is chopped up. This decouples the fluorescent and quenching dyes and thus fluorescence increases in each cycle, proportional to the amount of probe cleavage. I decided to use the TaqMan detection system, because the probe hybridizes to its target sequence and thus increases the specificity of the PCR detection. Unlike with SYBR Green staining, the PCR products generated by non-specific amplification due to mis-priming or primer-dimer artifacts do not generate a signal.

The fluorescent signal is recorded and plotted as an amplification curve over 45 PCR cycles. The baseline reflects the background fluorescence. It is set, according to the manufacturer's protocol suggestion, from cycle 3 until the two cycles before the fluorescent signal is detectable. In order to measure DNA amplification in the exponential range of the PCR reaction, a threshold has to be determined. Therefore, a standard curve with serial dilution 1:10 of mock ChIP DNA over a range of five orders of magnitude (Figure 21A) was performed with real-time PCR. (Mock ChIP DNA is DNA purified under ChIP conditions, but without immunoprecipitation.) The threshold was set at the level, where the standard curve was approximating the optimal slope. The optimal PCR reaction leads to a doubling of the amplified DNA. The standard curve is plotted as log10 by the PCR program (Figure 21B). As a consequence, the optimal slope is -3.322 ($2^{3.322}$=10). Figure 21 shows as an example the standard curve of the amplicon MyoD ME (SRF) (also see Figure 22A). The PCR amplification is therefore

determined by the threshold and is measured by the Ct value. The Ct value displays the cycle number, when the fluorescent signal of the PCR reaction crosses the threshold.

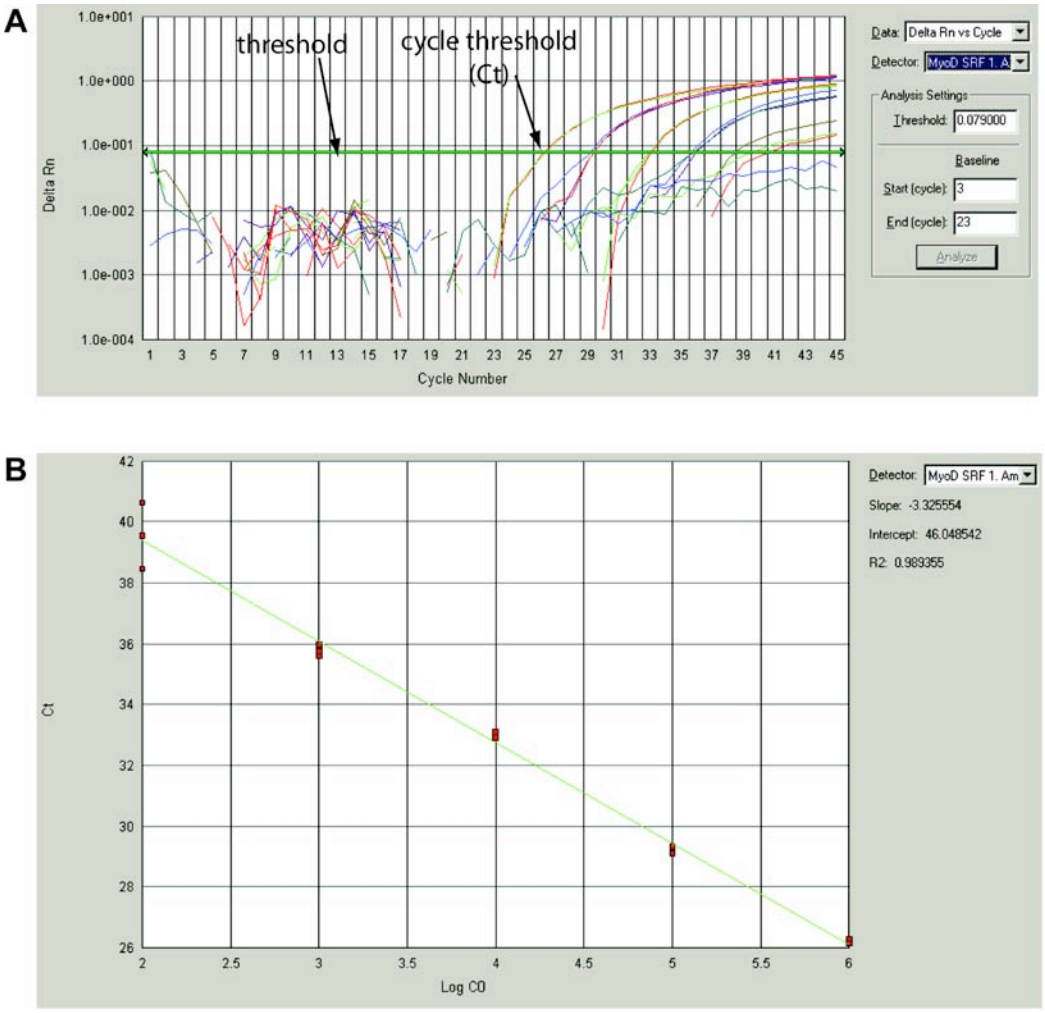

Figure 21: Standard curve on mock ChIP DNA with real-time PCR

A) Screen shot of amplification curves from individual PCR reactions. Green bar: threshold level of the MyoD SRF (ME) amplicon, DNA amounts used: five 1:10 dilution, starting concentration 300ng = 46,875 genomic copies (1 genomic copy = 12.8pg). Each dilution is accomplished in three replicates. **B)** Log10 of Standard curve of the input dilutions with determinants for the standard curve of the MyoD SRF (ME) amplicon. The slope gives the number of slope of the standard curve. The intercept is the value, at which the ordinate is crossed. R2 shows the correlations of three PCR replicates.

Table 2 shows a summary of the standard curves of all used PCR amplicons for the αSRF ChIP. From the slopes of these standard curves are close to the optimum of -3,322, the slopes differ less than 0.1 and the correlation of the PCR reaction replicates is at 0.99. Therefore, the standard curves fulfill the prerequisite for the ΔΔCt quantification method (see above).

Amplicon	Baseline	Threshold	Slope	Intercept	Correlation of PCR triplicates R2
Egr1	3 – 22	0.15	-3.325187	43.853996	0.98
MyoD ME (SRF)	3 - 23	0.079	-3.327664	45.038616	0.99
MyoD IE	3 - 23	0.245	-3.327779	47.399097	0.99
MyoD P	3 - 23	0.052	-3.369062	47.300529	0.99
MyoD E3	3 - 21	0.052	-3.270968	42.98996	0.99
xGAPDH MGB	3 - 27	0.2	-3.325291	47.638584	0.99

Table 2: Standard curves of the different real-time PCR amplicons

After the determination of the standard curves, the quality of the mock ChIP DNA was investigated. In Figure 22A, equal copy number of plasmid DNA (encoded by plasmid pMD-6,0/+4,7GFP2) and mock ChIP DNA were compared with each other. The difference of nine cycles reflects an approximate discrepancy of 10,000-fold. It was analyzed, whether this large difference was a reflection of the chemical damage in the ChIP DNA sample, or whether it was due to some inhibitor of the PCR reaction. Mixing plasmid DNA and mock ChIP DNA showed no considerable retardation of the PCR amplification in comparison to the plasmid DNA alone. The experiment in Figure 22B demonstrated that the PCR reaction is inhibited in *cis* at the level of the DNA. If the inhibition was in *trans*, this should be reflected by a gap of nine cycles compared to plasmid DNA alone.

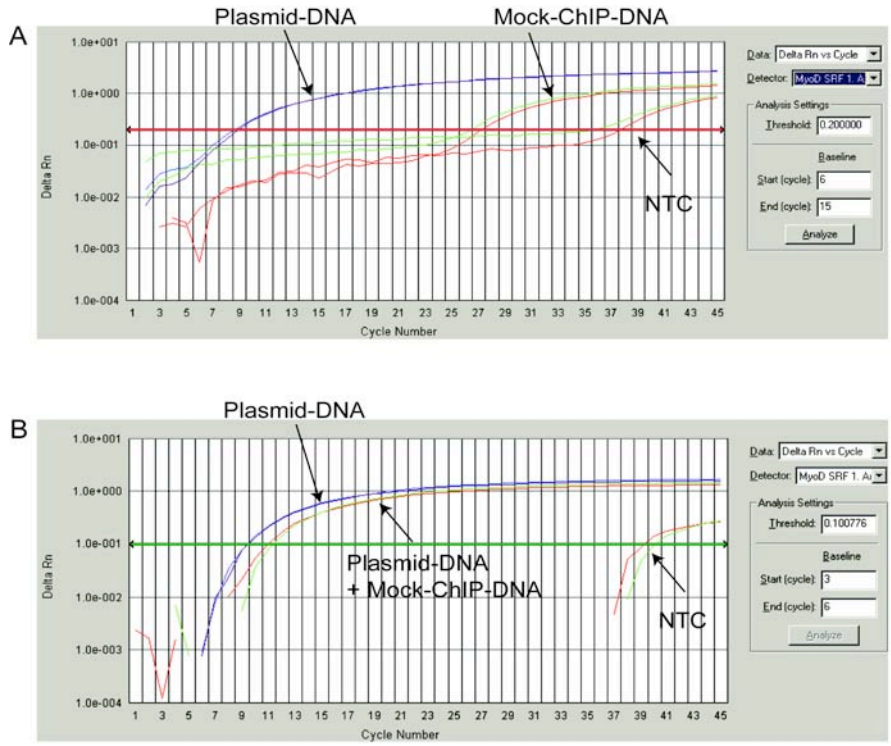

Figure 22: Comparison of the amplification efficiency of plasmid DNA compared to mock ChIP DNA

A) About 870000 copies of the plasmid pMD-6,0/+4,7GFP2, encoding the *myoD* locus and about 870000 genome copies of the mock ChIP DNA were tested with real-time PCR on the MyoD SRF amplicon, NTC: no template control **B)** Plasmid-DNA 870.000 copies, Plasmid-DNA 870.000 copies + mock ChIP DNA 870.000 copies. NTC: no template control

For the quantification of the ChIP results, the ΔΔCt method was chosen. It involves two steps of normalization. In a first step, the ΔCt value is calculated by subtraction of the Ct value of the internal standard from the Ct value of the target gene. In a second step, the ΔΔCt value is determined by subtraction of the ΔCt value of calibrator from the ΔCt value of the probe. The results is then calculated by using the formula $2^{-(\Delta\Delta Ct)}$. For the ΔΔCt calculation to be valid, the amplification efficiencies of the target and the endogenous reference must be approximately equal. The slopes should be close to -3.32 and should not differ by more than 0.1. This was fulfilled by the standard curves used for the ChIP analysis (see Table 2).

4.2.1.4 SRF is bound to the MyoD maintenance enhancer in activin-treated animal cap explants

Following the determination of the shearing conditions, at first ChIP experiments with the αSRF antibody with gastrula-stage embryos (NF11) compared with neurula stage embryos were performed (data not shown). These preliminary experiments confirmed Oliver Nentwich's data that SRF is bound to the maintenance enhancer in neurula stage embryos (NF18). Subsequently, the ChIP analysis with the αSRF antibody was extended and performed with activin treated and untreated animal cap explants of neurula stage (NF18) (Figure 23) to prove that SRF is exclusively bound to the *myoD* maintenance enhancer on the active locus. Figure 23A depicts a schematic chart of the used amplicons. As the internal control, the housekeeping gene GAPDH was chosen, which is expressed in all analyzed stages (see Figure 29). The promoter amplicon at the *egr1* locus served as a positive control, because the immediate early gene *egr1* is constitutively bound by the SRF protein independently form its transcriptional status (Nentwich, 2003; Panitz et al., 1998). Four amplicons were investigated on the *myoD* locus. The MyoD probe at the maintenance enhancer (ME) and at the third exon (E3) were placed across putative SRF binding sites (CArG box) with the consensus sequence $CC(A/T)_6GG$ (Latinkic et al., 2002). Two other probes located at the induction enhancer (IE) and the promoter (P) are not in close proximity to any SRF binding sites. The amplicons are at least 500bp apart from each other. With an average size of 500bp of the chromatin fragments, they are distinguishable from each other. Therefore, they served as negative controls in *cis*. In Figure 23B, I showed that the SRF protein is bound in an activation-dependent manner to the maintenance enhancer of *myoD*, which is demonstrated by the 5-fold increase in SRF binding upon *myoD* induction. In addition, I also showed a binding of SRF to a site at the end of the 2nd intron. The binding of SRF to this site was not observed before. Further analyses will be needed to investigate its function. In contrast to Oliver Nentwich's data (Nentwich, 2003) our data suggest an increase in SRF binding to the Egr1 promoter. This is dependent on the activation upon activin treatment in animal caps of neurula stage (NF18) (2-fold increase).

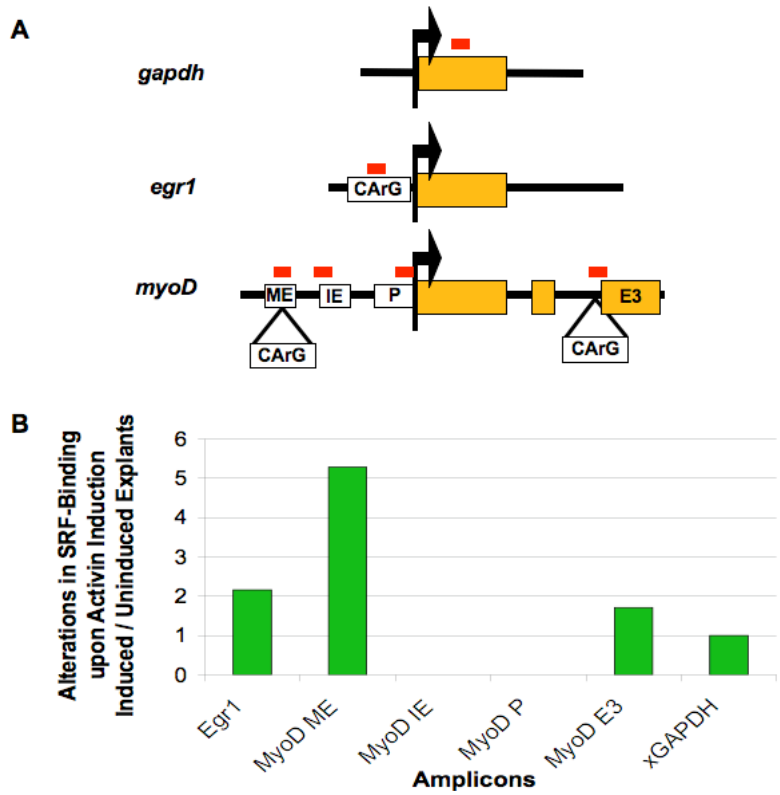

Figure 23: SRF is bound to the MyoD maintenance enhancer in activin-treated animal caps

A) Schematic chart of the TaqMan amplicons. The chart is not drawn to scale, for scale see Figure 28. CArG: SRF binding site. Orange boxes: coding sequence, exons. Red bar: TaqMan probe. ME: maintenance enhancer. IE: induction enhancer. P: promoter. E3: exon 3. **B)** shows a representative αSRF ChIP experiment with activin treated and untreated animal caps in neurula stage (NF18) plotted as the alteration in SRF binding upon activin induction. 100 animal caps were used per IP. Amplicons were normalized to GAPDH. As the calibrator, the IP of the untreated animal caps was used.

Taking my ChIP experiments with whole embryos and animal cap explants into account, I demonstrated that SRF is bound to the maintenance enhancer exclusively on the activated locus. In addition, I showed that SRF is also bound to the 3rd exon of the *myoD* locus in an activation-dependent manner.

4.2.2 αLef/Tcf ChIP at the *siamois* and *myf5* loci was irreproducible

The canonical Wnt/β-catenin signaling cascade is one of the most important pathways during development. The Wnt signal is transmitted by β-catenin, which enters the nucleus upon Wnt stimulation, binds to Lef/Tcf transcription factors and thus activates target gene expression (Wang and

Wynshaw-Boris, 2004). During *Xenopus laevis* development it is crucial for the axis determination, where it induces its target the organizer gene *siamois*. The promoter of *siamois* contains five Lef/Tcf binding sites, three at the promoter possess activating and two repressing functions (see Figure 5B) (Brannon et al., 1997). Furthermore, the canonical Wnt signaling exerts repressive function. In the organizer region, it prevents the expression of the muscle determining transcription factor *myf5.* This locus exhibits two distal Lef/Tcf binding sites, which are involved in the repression of the gene (Yang et al., 2002). Since the same signaling cascade can have different functions in regards to gene expression, I aimed to study, if Tcf1 and/or Lef1 in concert with Brg1 and β-catenin are bound to the Lef/Tcf binding sites of the model promoters *myf5* and *siamois* (also see 4.1.2). Additional TaqMan probes were generated, which are located upon the Lef/Tcf sites of the Myf5 locus and at the *Siamois* promoter (Figure 24, Table 3).

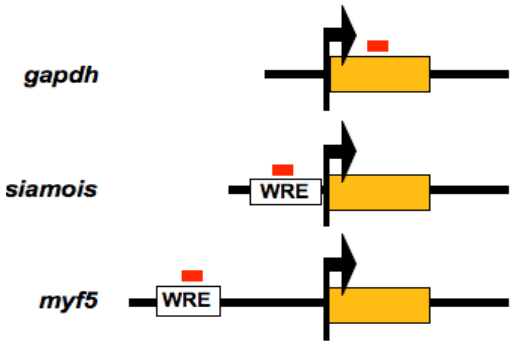

Figure 24: Schematic chart of the TaqMan amplicons used for the αLef/Tcf ChIP

The chart shows an overview of the used TaqMan amplicons, it is not drawn to scale WRE: Lef/Tcf binding site. Orange boxes: coding sequence, exons. Red bar: TaqMan probe.

Amplicon	Baseline	Threshold	Slope	Intercept	Correlation of PCR triplicates R2
Siamois promoter	3 – 23	0.2	-3.340479	48.376823	0.99
Myf5 Tcf	3 - 25	0.05	-3.249039	44.888489	0.99

Table 3: Additional amplicons for αLef/Tcf ChIP

In this ChIP assay, blastula stage embryos (NF9), in which the *siamois* gene is actively transcribed in the organizer region, were compared to early tailbud stage embryos (NF24) (calibrator) that do not express *siamois*. The analysis was performed three times with the αLef antibodies LEF 3D4 and 5F12 and αTcf1 Tcf1 1D12 and 2F4. Siamois promoter, Myf5 Tcf and GAPDH (internal control) amplicons were analyzed. Unfortunately, the ChIPs were inconsistent and not reproducible with respect to specific enrichments of Lef1 or Tcf1 at the *siamois* and *myf5* loci (data not shown). In addition, ChIPs with αβ-catenin PGDS 7D12 and αBrg1 XB 3F1 antibodies (Singhal, 2005) on the *siamois* locus with the same set up as for the αLef/Tcf ChIPs were also irreproducible with regard to the specific enrichments (data not shown).

The failure of these ChIPs might have multiple reasons. One critical determinant is the abundance of the expected antigen-DNA interaction. Early *Xenopus laevis* embryos contain only few cells, but are very rich in maternal proteins stored as yolk. This stored pool of the antigen might interfere in the IP with the antigen bound to the DNA and thus decrease the IP efficiency. Tcf1, β-catenin and Brg1 are high abundant and maternally expressed proteins, which are also stored in the yolk pool. Due to this reason, I changed the protocol. I made this effort, to rule out the above-mentioned technical problem.

4.2.3 The switch to the Douncer ChIP protocol helps to remove excessive proteins

The portion of the maternally stored proteins might interfere in the IP with the chromatin-associated antigens. This is especially critical in young embryos like in the blastula stage, in which the embryos contain only about 15,000 cells (see Table 5). The ChIP procedure was changed to a modified protocol after Orlando and colleagues (Chanas et al., 2004). For simplicity reasons, the protocol will be called Douncer ChIP (see 3.9.3). Two major differences of this protocol compared to the In Situ ChIP are introduced in terms of the preparation of the chromatin lysate (Figure 25).

The first major change is that the chromatin in the Douncer ChIP is fixed during mechanical lysis of the embryos with a douncer. Thereby, the chromatin remains in the crude pellet. This pellet is washed several times. Subsequently, the chromatin is eluted from the pellet by addition of the detergents SDS and N-lauroylsarcosine. With these washing and elution steps

the chromatin becomes purified to a certain extend and non-chromatin-associated proteins are washed out. In the In Situ ChIP though, the chromatin is fixed in the intact cells. In doing so, the generated cell lysate containing the chromatin is rather crude. This crude lysate of the early *Xenopus* embryos is very likely to contain a lot of antigen maternally stored in the yolk, which could interfere with the IP of the antigen in the chromatin fraction.

The second important protocol difference is the shearing of the chromatin. The chromatin of the In Situ ChIP is sheared with the Minicell of the FRENCH Press. This Minicell can hold up to 4ml of lysate, but there are always about 250µl of liquid, which remains in the minicell. After 2 rounds with the FRENCH Press this leads at least to a loss of 25% of the lysate. The Bioruptor, a sonication waterbath, circumvents this large loss of lysate material, since the shearing takes place in the test tube and does not need to be transferred.

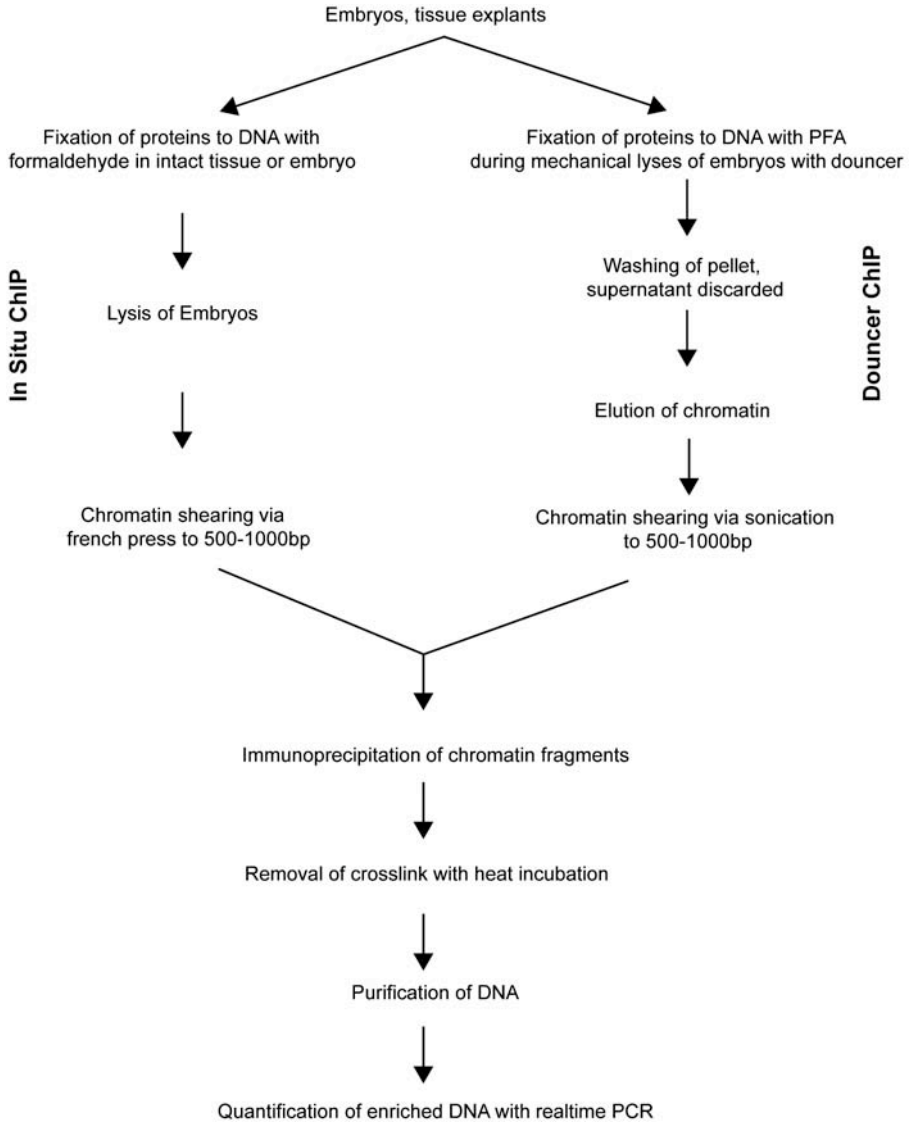

Figure 25: Comparison of ChIP methods

Flowchart of the different ChIP protocols In Situ ChIP and Douncer ChIP

In the subsequent chapters, the establishment of the various steps including the quality control of the chromatin of the Douncer ChIP will be discussed. For the detailed procedure see chapter 3.9.3.

4.2.3.1 Titration of the chromatin lysate condition

In order to determine the fixation conditions, initially 2% and 4% para-formaldehyde (PFA) were used to fix the chromatin under conditions of the Douncer ChIP. Subsequently, the crosslink of the chromatin was analyzed with a CsCl isopycnic centrifugation (see 3.9.4) (Orlando et al., 1997). Although the cross-linked chromatin peak was correlated with the correct density of 1.39g/cm^3,

it was not properly sheared (Figure 26A). For my ChIP analyses, the optimal DNA fragment size is between 500 and 1000bp due to the spacing of the amplicons (see Figure 28). The DNA fragments of this chromatin are much larger. This was due to over-fixation of the chromatin (Orlando et al., 1997). Therefore, also the concentration of 1% PFA was tested. This is in contrast to Chanas et al., 2004, who fixed their chromatin of *Drosophila* embryos with 1.8% PFA. The chromatin, which was fixed with 1% PFA, was sheared reproducible to the expected DNA size of around 500bp (Figure 26B).

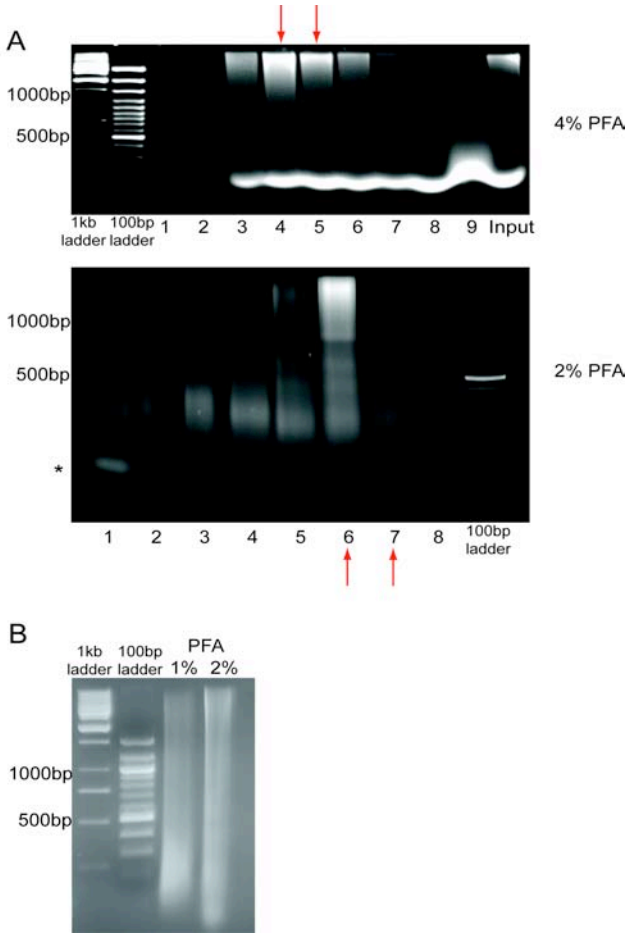

Figure 26: Titration of the PFA concentration

A) 200 gastrula stage embryos (NF11) fixed with either 2% PFA or 4% PFA and were sonicated 3x30sec in the Bioruptor in 0.5ml lysis buffer. 50eeq were analyzed by CsCl isopycnic centrifugation. The figure shows half of the DNA of each centrifugation fraction from bottom (lane 1) to the top of the tube (lane 8) on 1% agarose gels. The red arrows mark the fraction with the proper density of the crosslinked chromatin. The asterisk marks free DNA in fraction 1 of the CsCl isopycnic centrifugation with 2% PFA. The low bright band in the upper gel shows unspecific background. **B)** 200 gastrula stage embryos (NF11) fixed with either 1% or 2% PFA were sonicated 3x30 sec in the Bioruptor in 0.5ml lysis buffer. The DNA was de-crosslinked and purified. A small portion was visualized on a 1% agarose gel.

Although the chromatin of gastrula stage embryos could be sheared to the required size around 500bp, the chromatin of neurula stage embryos and older could not be fragmented. This might be due to the higher chromatin density of the older embryos. Therefore, the lysis buffer volume was increased to 2ml. In Figure 27, the settings for the shearing in a volume of 2ml were tested. Sonication of 11 times 30sec in the Bioruptor sheared the chromatin of the proper density reproducible to the correct size of around 500bp. Since the majority of the chromatin peaked at around 500bp, the sonication was not carried further in order to avoid destruction of histone tails or other chromatin-associated factors.

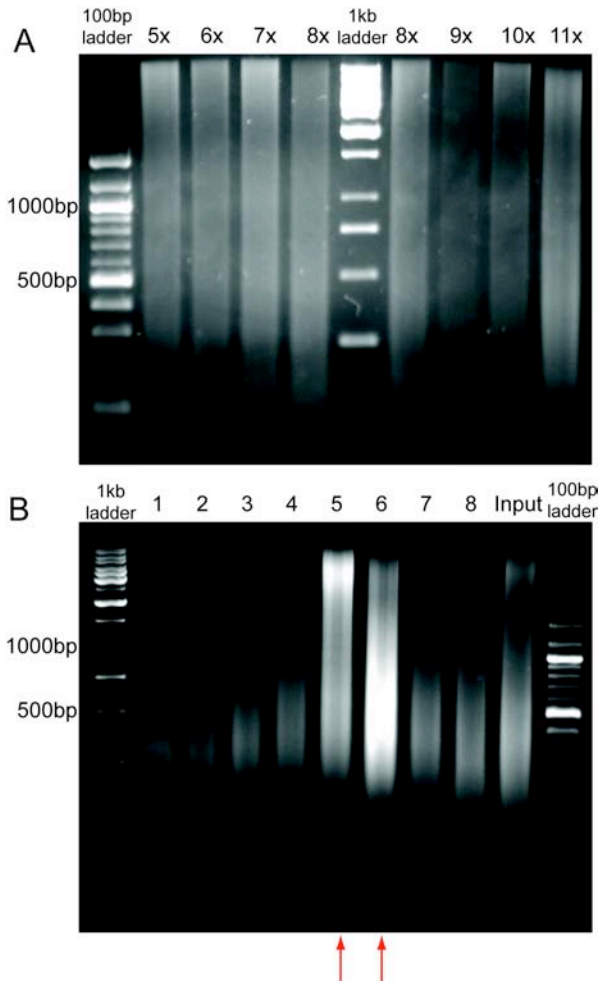

Figure 27: Sonication conditions

A) 200 neurula stage embryos (NF18) fixed with 1% PFA were sonicated 5-8x 30sec and 8-11x 30sec in a second experiment in the Bioruptor in 2ml lysis buffer. The DNA was de-crosslinked, purified and visualized with a 1% agarose gel. **B)** 200 neurula stage embryos (NF18) fixed with 1% PFA and sonicated 11x30sec in the Bioruptor in 2ml lysis buffer. 50eeq were analyzed by CsCl isopycnic centrifugation. The figure shows the DNA of each centrifugation fraction on 1% agarose gels. The red arrows mark the fraction with correct density of the crosslinked chromatin.

Based on these results, I have established the following settings: 200 embryos are fixed with 1% PFA. After the elution in 2ml lysis buffer, the lysate is sonified 11x30sec with the Bioruptor in order to shear the chromatin to a fragment size of 500bp.

4.2.3.2 TaqMan amplicons and method of quantification

For the subsequent ChIP analysis of the *myoD* locus against the various histone modifications and MyoD (see 4.2.4), eight amplicons were analyzed. Six of the eight amplicons were derived from the *myoD* locus (Figure 28). Aside from the previously used amplicons MyoD ME, MyoD IE, MyoD P and MyoD E3 (see Figure 23), two additional probes were designed. The probe MyoD 5'Region is located about 1,3kb 5' of the maintenance enhancer element, while the locus and the amplicon MyoD E1 at the 3' portion of the first exon. The probes at the *myoD* locus have a distance of 400bp up to 1500bp to each other (Figure 28). Since the chromatin was sheared to an average size of 500bp (see Figure 27), this should allow discrimination by PCR.

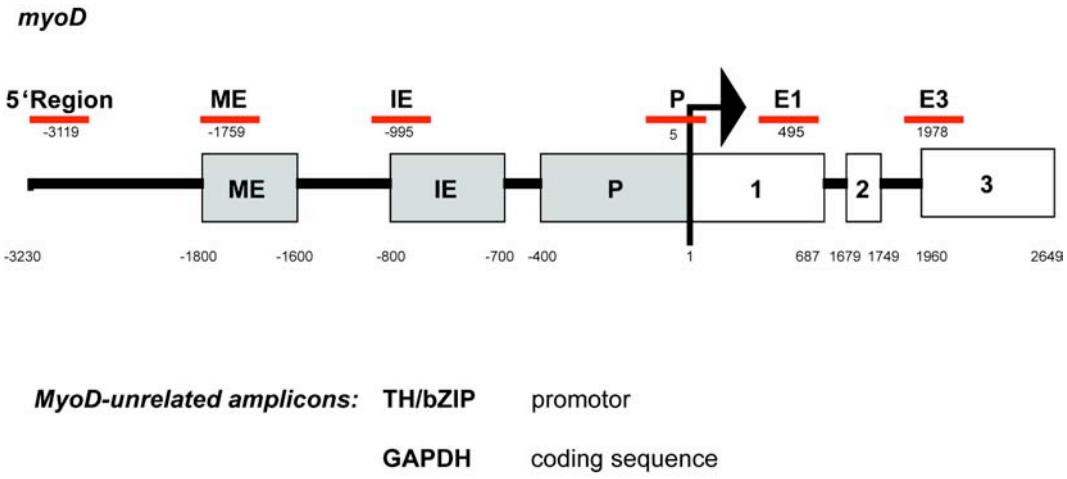

Figure 28: Amplicons derived from the *myoD* locus and unrelated control amplicons

Schematic diagram of the *myoD* locus and the TaqMan amplicons. The TaqMan amplicons are depicted as red bars. The numbers underneath are the center of the amplicons. The amplicons have an average length of about 100bp. The grey boxes outline the enhancer and promoter elements on the *myoD* locus. The white boxes mark the exons. The numbers underneath the boxes are the starting and end point of the elements/exons. ME: maintenance enhancer; IE: induction enhancer; P: promoter; 1: exon1; 2: exon 2; 3: exon3.

The probes GAPDH and TH/bZIP are unrelated to the *myoD* locus. They are not only unrelated to the *myoD* locus in terms of the physical proximity to the *myoD* locus, also their expression pattern is distinct. The housekeeping gene *gapdh* is transcribed ubiquitously throughout the analyzed stages blastula (NF9), gastrula (NF11), neurula (NF18), tailbud (NF26) and activin treated or untreated animal caps (Figure 29). TH/bZIP is a gene that is activated by thyroid hormone during metamorphosis (Brown et al., 1996) (also see chapter 2.1). It was reported to be inactive during embryogenesis. This was verified for the analyzed embryonic stages under investigation by RT/PCR (Figure 29). As described previously in chapter 4.2.1.4, the probe GAPDH is located in the coding region of the *GAPDH* gene, whereas the PCR amplicon TH/bZIP was placed at the promoter.

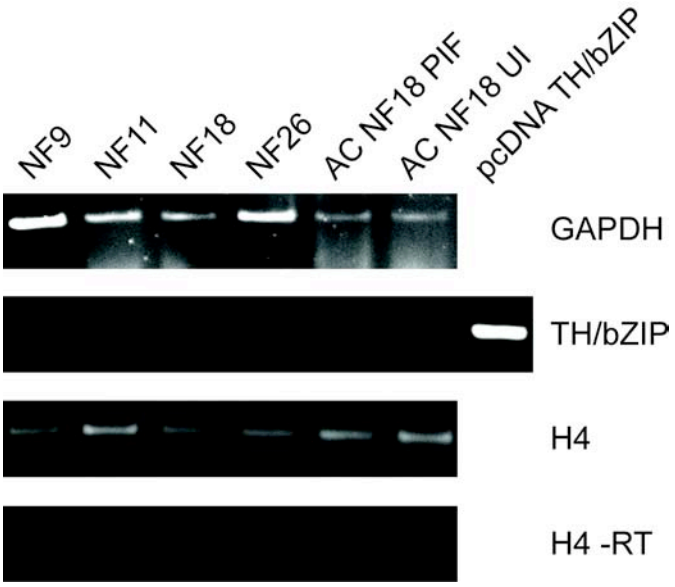

Figure 29: GAPDH and TH/bZIP mRNA expression profile during early *Xenopus* development

RT-PCR of the *myoD*-unrelated amplicons GAPDH and TH/bZIP of the different stages used in the Histone ChIP (see 3.9.4.2). Blastula stage embryos (NF9), gastrula stage embryos (NF11), neurula stage embryos (NF18), tailbud stage embryos (NF26), neurula stage, activin-treated animal caps AC NF18 PIF, neurula stage, untreated animal caps AC NF18 UI, plasmid pcDNATH/bZIP as positive control for TH/bZIP RT-PCR. Histone H4 serves the control for equal mRNA loading of the different samples. –RT is the control for genomic DNA contaminations of the samples.

Amplicon	Baseline	Thres hold	Slope	Intercept	Correlation of PCR triplicates R2
GAPDH	3 - 20	0.1	-3.320723	32.753403	0.99
MyoD 5'Region	3 - 22	0.089	-3.345328	36.610786	0.97
MyoD ME	3 - 22	0.3	-3.286521	36.05439	0.98
MyoD IE	3 - 22	0.235	-3.323773	35.379673	0.96
MyoD P	3 - 23	0.05	-3.450624	35.82766	0.99
MyoD E1	3 - 22	0.2	-3.108521	33.538055	0.98
MyoD E3	3 - 20	0.1	-2.847332	33.888596	0.99
TH/bZIP	3 - 20	0.21	-3.320156	32.8461	0.98

Table 4: Amplicons for Histone ChIP with Douncer protocol

The ΔΔCt method to quantify ChIP has the advantage that it compares biological differences of two different samples. In doing so, the comparison expels the possibility to quantify a ChIP precipitation without a calibrator (other IP sample). Furthermore, it neglects differences of chromatin preparations. They can vary in their quality with regards to the DNA performance in the real-time PCR. This detriment can be circumvented by normalization to the input (mock ChIP DNA). Therefore, the method of quantification was changed to the following method:

1. Average of Ct value (PCR duplicates): Av Ct
2. Calculation of relative DNA amounts via standard curve: $y=10^{((\text{Av Ct} - \text{Intercept})/\text{slope})}$
3. Normalization to input: y / Input DNA amount
4. Average of 3-4 independent IPs plus standard deviation

4.2.3.3 Determination of the amount of antibody

In Figure 30, the amount of commercially available antibody used for the histone ChIPs was determined. 1µg, 2µg, 4µg and 10µg of αH3K4me2 antibody were tested. The signal of 4µg showed maximal enrichment at the MyoD P amplicon, which is in agreement with published data as the histone modification H3K4me2 is usually enriched at the promoter of actively transcribed genes (Sims and Reinberg, 2006). This enrichment was not further improved by using 10µg of the antibody. As a compromise, 4µg were used of the commercially available ChIP antibodies.

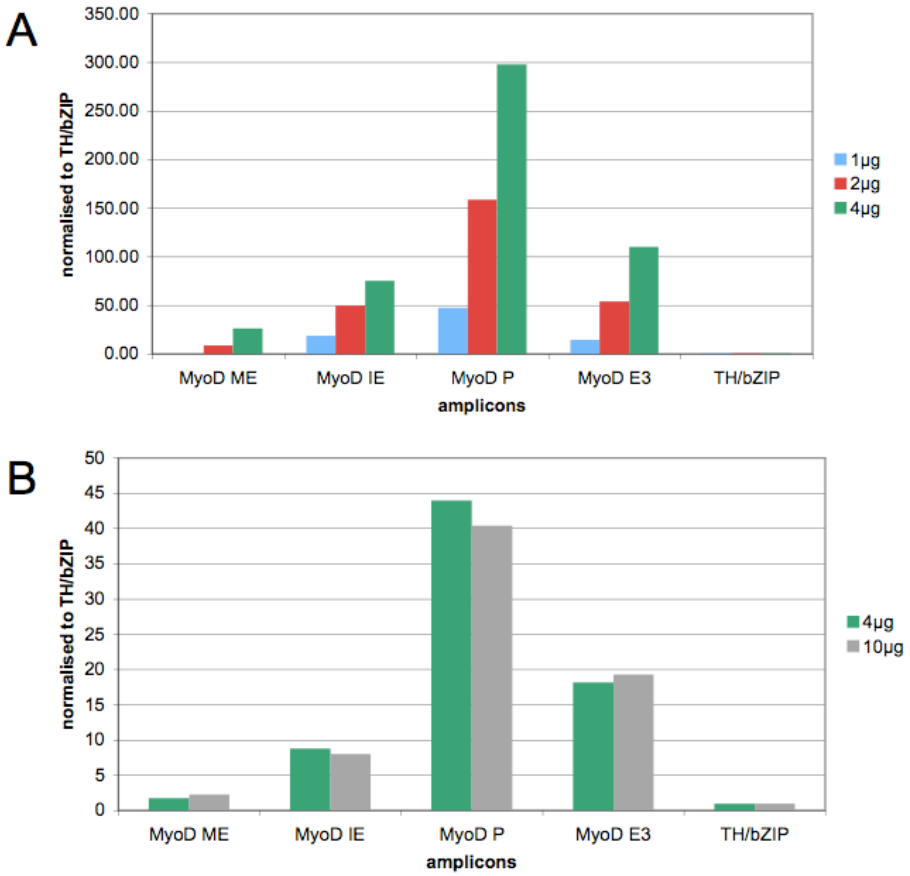

Figure 30: Titration of the antibody amount

65eeq of neurula stage embryos (NF16) were used for ChIP with different antibody concentrations of αH3K4me2. **A)** 1µg, 2µg and 4µg. **B)** 4µg and 10µg. These ChIP experiments are quantified differently to chapter 4.2.4: 1., Average Ct. 2., DNA amount via standard curve 3., subtraction of IgG background, 4., normalization to Input, 5., normalization to TH/bZIP. Analyzed amplicons were MyoD ME, MyoD IE, MyoD P, MyoD E3 and TH/bZIP (see Figure 30 and Table 4). The graphs display a single experiment each.

4.2.4 Chromatin profiling of the *myoD* locus

After the establishment the Douncer ChIP protocol, I proceeded with ChIP analyses of the *myoD* locus. The timing events of the *cis* regulatory elements of *myoD* are well studied. In addition to the functional SRF site at the maintenance enhancer, a transgenic reporter gene approach determined two important regulator elements within the induction enhancer: LS5, which is important for the induction, and LS9, which is necessary to prevent to early induction of *myoD* (Xiao, 2003). Nevertheless, a direct inducer was not identified so far. Factors that are involved in transcriptional silencing of the *myoD* locus are better understood. The accumulation of somatic H1 protein was shown to be

rate-limiting for the induction competence of the *myoD* expression (Steinbach et al., 1997). This observation suggests for a contribution of chromatin in the regulation of the *myoD* locus. For example, alterations of histone modifications might enable the induction or the repression of the gene. Therefore, a time course ChIP analysis of the *myoD* locus was performed with antibodies against histone modifications, which mark actively transcribed, committed or silenced loci. Commercially available antibodies were used to analyze the histone modification profile of the *myoD* locus. The histone proteins and the modifications of their N-terminal tails are highly conserved among all eukaryotes (Alberts et al., 2004). Therefore, the antibodies cross-react across species (see www.abcam.com or www.upstate.com). As a mark for actively transcribed genes, antibodies against pan-acetylated histone H4 (H4ac) and dimethylated lysine 4 on histone H3 (H3K4me2) were used (see Figure 9). For hallmarks of silent gene loci I used antibodies against di-methylated lysine 9 on histone H3 (H3K9me2) and tri-methylation of lysine 27 on histone H3. In order to quantitate the local nucleosomal density, ChIPs against histone H3 were performed.

Up to now, SRF is the only direct, positive regulator of the *myoD* transcription (see chapter 4.2.1.4). The only candidate for the direct *myoD* induction is the MyoD protein itself, because the up-regulation of *myoD* expression from the basal expression to the proper induction requires autocatalysis (Steinbach et al., 1998). For that reasons, additional time-course ChIP experiments were performed with the αMyoD antibody MYO 6C8 to investigate, if the MyoD protein is at all bound to its own locus.

With this ChIP approach I aimed to understand which and when histone modification marks appear during muscle cell determination and differentiation. Therefore, the following time-points of *myoD* transcription were analyzed (see Figure 31): In blastula stage embryos (NF9), *myoD* expression is not significantly induced yet, although a basal, ubiquitous *myoD* expression exists. The *myoD* expression is induced in prospective myoblasts in the gastrula stage (NF11). Neurula stage embryos (NF18) show stable *myoD* expression in presumptive myoblasts. In tailbud stage embryos (NF30), *myoD* expression begins to be down-regulated in postmitotic, differentiating myocytes. In order to distinguish between *myoD* expressing and non-expressing cells, the animal cap explants were used. In untreated, neurula stage animal cap explants, *myoD* is stably repressed in all cells (see Figure 19). In activin-treated, neurula stage

animal cap explants (NF18), stable *myoD* expression is enriched the explanted cells (see Figure 19).

Figure 31 describes the potential histone modifications at the *myoD* locus. In the blastula, when *myoD* is basally and ubiquitously expressed, the histone modification H3K4me2 might be detectable, since it can also be found on committed but not yet activated promoters (Sims and Reinberg, 2006). After the induction of *myoD* in the gastrula stage, the embryo consists of a mixed population of *myoD*-expressing and non-expressing cells. Therefore, both typically active and inactive marks should be precipitated from the *myoD* locus. In the maintenance or stably silent phase of the *myoD* transcription, both silence and activation marks in the neurula and tailbud stages were expected to be detectable.

embryonic stage	**Blastula NF9**	**Gastrula NF11**	**Neurula NF18**	**Tailbud NF30**
ISH				
***myoD* expression**	basal and ubiquitous pre-induction	high in preinvoluted mesoderm post-induction	high in paraxial mesoderm	high in myocytes
histone modification	H3K4me2 ? ?	H4ac ? H3K4me2 ? H3K9me2 ? H3K27me3 ?	H4ac H3K4me2 H3K9me2 H3K27me3	H4ac H3K4me2 H3K9me2 H3K27me3

Figure 31: Overview the analyzed embryonic stages

Top row indicates the embryonic stages analyzed by ChIP. Second row shows the mRNA expression pattern of *myoD* with *in situ* Hybridization (ISH) (see 3.5.6). Third row describes the *myoD* expression pattern. Fourth row shows the potential histone marks, marks for active transcription in green, for repressed transcription in red. The histone modifications are listed after the Brno nomenclature (Turner, 2005)

To have enough desired antigen-chromatin associations, $1x10^6$ to $1x10^7$ cells are used for the ChIPs in general (see e.g. ChIP protocol collection at www.epigenome-noe.net). Since it is not possible to determine the exact cell number of an embryo, the amount of chromatin per IP was applied as embryo equivalents (see Table 5). In order to judge the quantities I used for my experiments, I had to determine the cell count. From the input samples, the

average DNA amounts were determined. With this value, it was possible to calculate the cell numbers per embryo with the knowledge that a *Xenopus laevis* nucleus contains 12.8pg DNA. By multiplication with the number of eeq per IP, I calculated the number of cells per IP. It is important to note that this number includes the total cell number of *myoD*-expressing and non-expressing cells. Due to technical reasons, it was not feasible to collect more than 100 eeq per IP reaction (≈ $1{,}6x10^6$ cells), because for one replicate with the 6 antibodies plus IgG background control and input sample, 800eeq were necessary. Since the ChIPs were repeated four times, we collected 3200eeq of blastula embryos. The same amount was used for gastrula stage embryos (NF11) (≈ $4x10^6$ cells). For neurula and tailbud stage embryos, 40eeq (≈ $4x10^6$ cells) or 30eeq (≈ $1x10^7$ cells) per IP were used. For the two replicates of the animal cap assay, 3200 animal cap explants were dissected and 100 animal cap equivalents (≈ $7x10^5$ cells) were used per IP sample. In summary, about 12,000 embryos and animal cap explants were collected for the subsequent ChIP data set.

Stage	Numbers of eeq per IP	Average DNA amount	Numbers of cells per IP	Number of cells per stage
Blastula (NF9)	100	21230	1,658,579	16,586
Gastrula (NF11)	100	61027	4,767,713	47,677
Neurula (NF18)	40	55064	4,301,863	107,547
Tailbud (NF30)	30	118801	9,281,320	309,377
AC UI (NF18)	100	9406	734,880	7,349
AC PIF (NF18)	100	11294	882,373	8,824

Table 5: Cell numbers used in the different stages.

The average DNA amount is the average of eight individual measured input DNAs of each stage/explant. A *Xenopus laevis* nucleus contains 12.8pg DNA (assumption of diploid organism, source: www.bio.nagoya-u.ac.jp:8000/compG01.html). This was used to calculate the cell numbers. AC UI (NF18):, untreated animal caps of neurula stage (NF18). AC PIF (NF18): activin-treated animal caps of neurula stage (NF18).

In Figure 30, the amount of antibody to use for the subsequent ChIP analyses was determined. Therefore, IPs with 4µg unspecific rabbit IgG were performed to investigate unspecific binding of the chromatin fragments to the ProteinA-sepharose beads. According to the manufacturer's protocol, they have a binding capacity of 10µg/µl. Therefore, the inserted 15µl ProteinA-sepharose beads are not saturated with 4µg of antibody. Consequently, it is important to determine whether some amplicons stick more to the beads than other. Figure 32

displays this background. If I compare the individual and average binding levels off each stage, I can conclude that none of the amplicons adhered to a greater extend to the beads than the other amplicons. For unknown reasons, the chromatin of gastrula embryos offered the lowest background (see Figure 32, last columns “average”). The rather large standard deviations reflect the variations of the individual IP reactions. The averages of the IgG background were used to investigate the signal-to-noise ratio of the subsequent ChIP analysis.

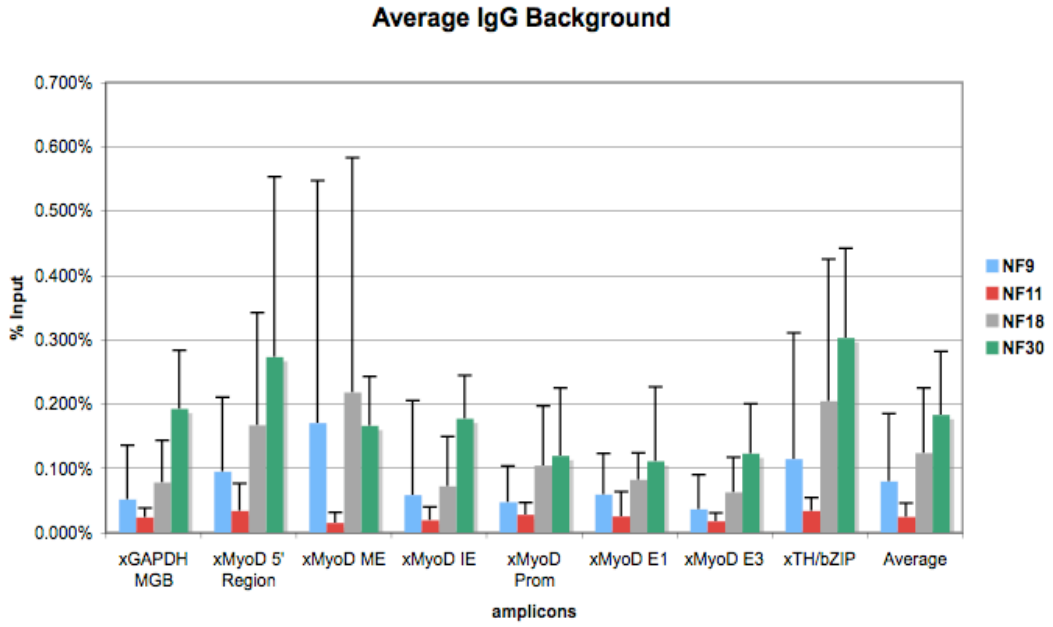

Figure 32: Average of IgG Background

This graph shows the average of the IPs with 4µg unspecific rabbit IgG for each stage and each sample. The DNA amounts were calculated via the standard curves. The background is then plotted as % Input. The last columns (average) give the average background of each stage as the average of all 8 analyzed amplicons.

Prior to the investigation of histone modifications, it is necessary to examine the nucleosomal density at the studied genomic loci. Figure 33 displays the results of the ChIP analysis with the antibody against total Histone H3. This ChIP indicates the relative nucleosomal density at the analyzed loci. This information is important to interpret the presence or absence of specific histone modifications. Figure 33B demonstrates the ration of αH3 ChIP signal over the average IgG background. This IP signal is at least 22-fold (tailbud stage embryos (NF30)) until up to 879-fold (gastrula stage embryos (NF11)) over IgG background. The precipitation efficiency of αH3 ChIPs, which is reflected by the %-Input value, is high compared to other antibodies like αH3K27me3 (see

Figure 37). Figure 33C represents the relative enrichments of the raw ChIP data of A in arbitrary units. From this graph, it is apparent that the H3 occupancy and thus the nucleosomal density at the maintenance enhancer (ME) is lower compared to the *myoD* gene body and the silent *TH/bZIP* promoter. In general, the relative density changes a lot during the analyzed stages. During the blastula stage, the chromatin appears to be more compacted. In gastrula stage, the nucleosome density seems to be rather low. This increases in neurula stages and decreases in the tailbud stage. The promoter region of the silent *TH/bZIP* locus appears to be nucleosome rich particularly in neurula, while the coding region of the actively transcribed housekeeping gene *GAPDH* harbors less nucleosomes. This corresponds to the findings that actively transcribed loci are loosely packed whereas the nucleosomal density is high in silenced loci (Nemeth and Langst, 2004). The large standard deviations are discussed in the following chapter 4.2.6. As a result, I concluded that the nucleosomal densities at the *myoD* locus and at the control loci differ dramatically over space and time. This might indicate that the chromatin of *Xenopus* embryos is very dynamic over time. However, it awaits further investigation.

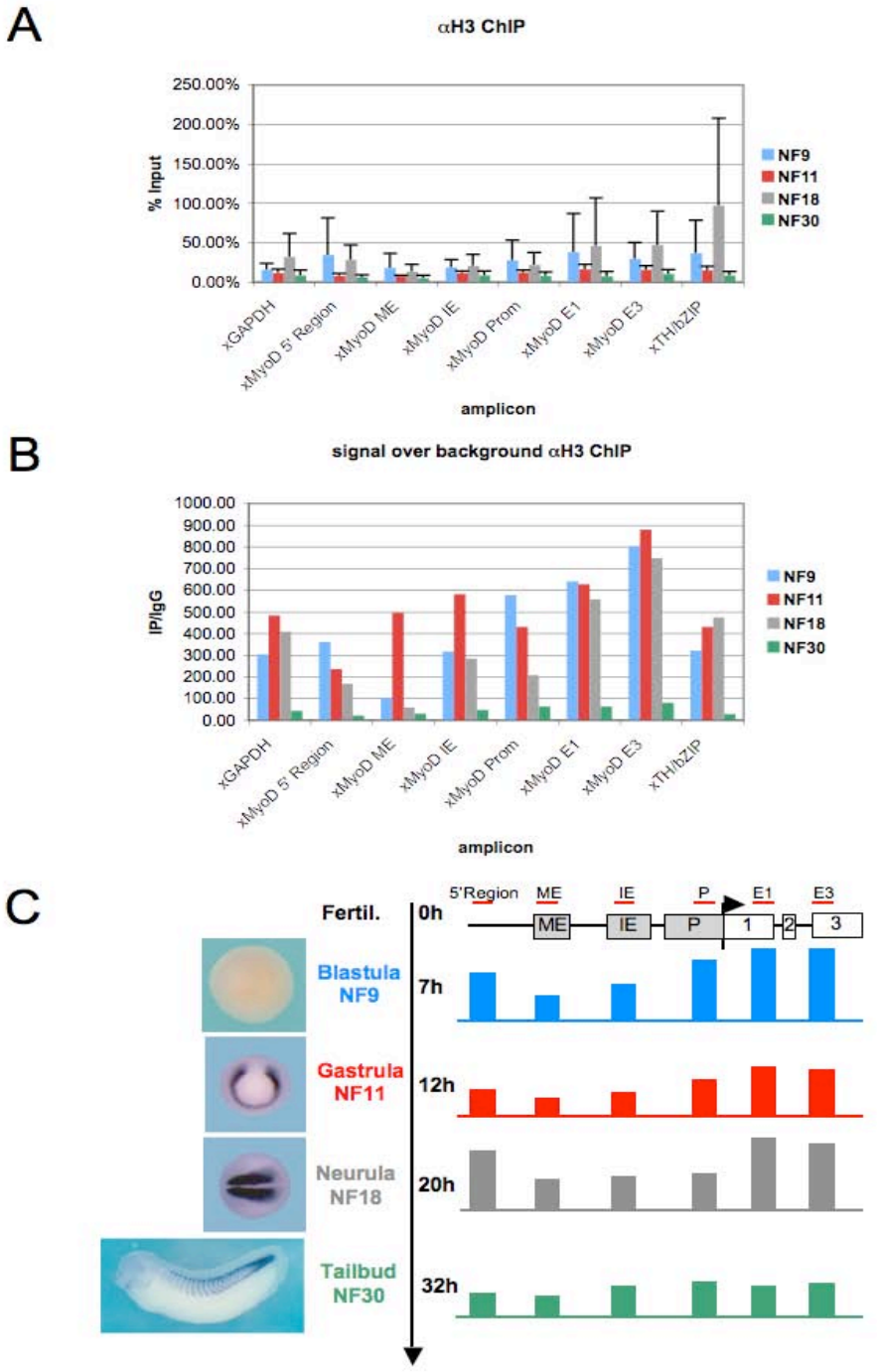

Figure 33: αHistone H3 ChIP shows relative nucleosomal densities

A) The chart of the αHistone H3 ChIP is plotted as % of Input. The analyzed stages and amplicons were described previously (see Figure 28 & 31). The standard deviations reflect 4 individual experiments. **B)** This chart shows the signal over background ratio. Division of average % Input (IP) by average % Input (IgG) calculates this ratio. **C)** A diagram of the graph in A of the αH3 ChIP results in arbitrary units. The y-axis gives a time scale of analyzed stage with pictures of a *myoD* mRNA *in situ* hybridization. The x-axis shows the *myoD* locus from 5' to the 3' end plus the amplicons as red bars.

Dimethylation of lysine 4 at histone H3 (H3K4me2) is put in place by SET domain proteins like the MLL protein family, SET1 or ASH1 (Kouzarides, 2007). The modification is predominantly found at the transcription start site of active loci (Sims and Reinberg, 2006). In Figure 34, this methylation mark on the *myoD* locus correlated with the *myoD* transcription. It is detectable during the basal transcription phase in the blastula stage embryos (NF9) at the promoter and exon 1. As the mRNA amount increases until neurula stage, the methylation mark increases and spreads also into gene exon3 and into the 5'Region of the locus. While *myoD* transcription drops off in the tailbud stage embryos (NF30) as shown by RNA *in situ* hybridization (see Figure 29), also the H3K4me2 mark decreases. Compared to the MyoD P amplicon, virtually no H3K4me2 mark was detected at the inactive TH/bZIP promoter. The GAPDH amplicon shows also hardly any H3K4me2. One possible explanation for this is in regard to the GAPDH probe that the H3K4me2 is predominantly enriched at the transcription sstart site. The signal to noise ratio is again significant (Figure 34B). The signal is up to 214-fold higher than IgG background. Again this shows the good quality of this antibody. From this ChIP analysis, I concluded that the H3K4me2 histone mark correlates very well with the intensity of the *myoD* transcription during the tested developmental stages.

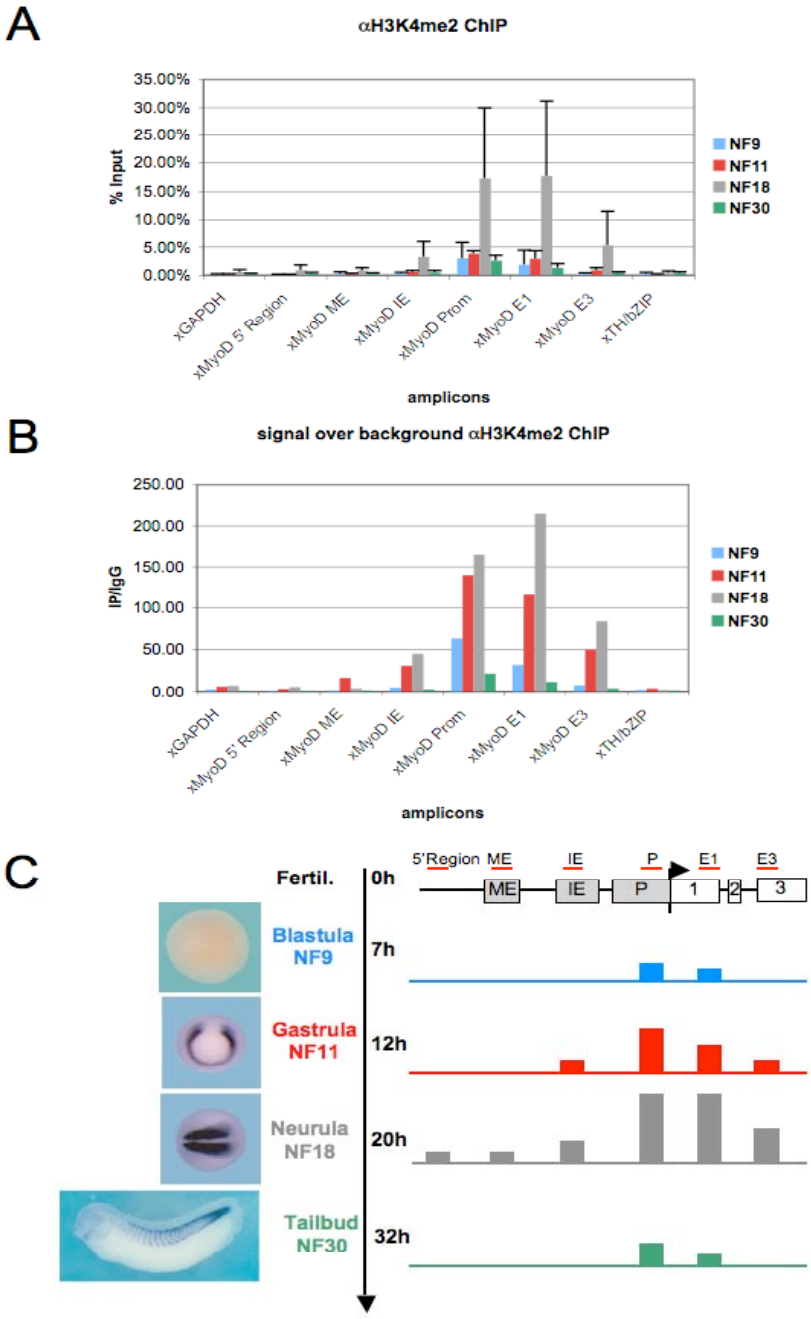

Figure 34: Dimethylated lysine 4 on histone H3 (H3K4me2) is enriched at the promoter and exon1 during active *myoD* transcription.

A) The chart of the ChIP against dimethylated lysine 4 on Histone H3 (H3K4me2) is plotted as % of Input. The analyzed stages and amplicons were described previously (see Figure 28 & 31). The standard deviations reflect 4 individual experiments. **B)** This chart shows the signal over background ratio. Division of average % Input (IP) by average % Input (IgG) calculates this quotient. **C)** A diagram of the graph in A of the ChIP results in arbitrary units. The y-axis gives a time scale of the analyzed stage with pictures of a *myoD* mRNA *in situ* hybridization. The x-axis shows the *myoD* locus from 5' to the 3' end plus the amplicons as red bars.

Hyperacetylation of histones is a hallmark for actively transcribed genes (Turner, 2007). These acetylations are set by histone acetyltransferases (HATs) like CBP/p300, HBO1 and TIP60 (Kouzarides, 2007). The HAT activity of PCAF and p300 is important for the induction of *myoD* expression in mouse cell lines as well as in *Xenopus laevis* (Puri et al., 1997; Steinbach, 1998). The acetylation of Histone H4 (H4ac) is enriched at the promoter of *myoD* throughout all analyzed stages compared to the other analyzed MyoD amplicons. From gastrula stage onwards, the modifications spread towards the 5'Region of the locus (Figure 35A&C). In agreement with published data, the coding sequence of GAPDH is not hyperacetylated (Myers et al., 2001). In contrast to this, *TH/bZIP* appears to be acetylated, probably reflecting basal acetylation levels. However, this was not detected by Sachs and Shi perhaps due to the lower sensitivity of the endpoint PCR they used (Sachs and Shi, 2000). The signal:noise ratio is up to 13x higher than IgG background (Figure 35B). This suggests that the antibody precipitates not as good as the previously discussed one αH3K4me2. Furthermore, this could also reflect the high turnover rate of the acetylation marks due to histone deacetylase (HDAC) activity. As a result, I concluded that H4ac is enriched at the promoter and that it spreads into the 5'Region of the locus after the induction and during the maintenance phase of transcription most likely in *myoD* expressing cells.

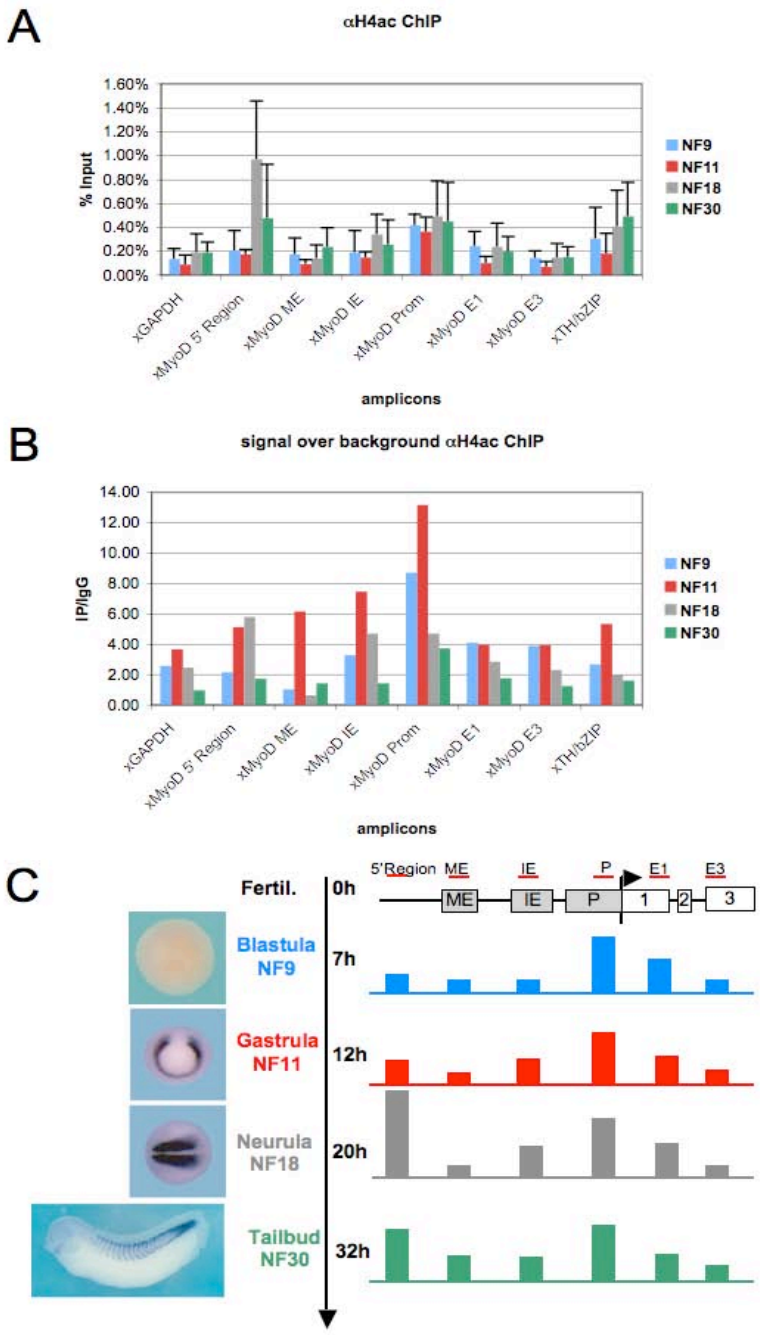

Figure 35: Pan-acetylation of histone H4 is enriched at the *myoD* promoter and spreads into the 5'Region.

A) The chart of the ChIP against pan-acetylated Histone H4 (H4ac) is plotted as % of Input. The analyzed stages and amplicons were described previously (see Figure 28 & 31). The standard deviations reflect 4 individual experiments. **B)** This chart shows the signal over background ratio. Division of average % Input (IP) by average % Input (IgG) calculates this quotient. **C)** A diagram of the graph in A of the αH4ac ChIP results in arbitrary units. The y-axis gives a time scale of analyzed stage with pictures of a *myoD* mRNA *in situ* hybridization. The x-axis shows the *myoD* locus from 5' to the 3' end plus the amplicons as red bars.

Dimethylation of lysine 9 on histone H3 (H3K9me2) is put in place by HMTs like SUVAR39 or G9a and is a hallmark of silent loci (Kouzarides, 2007). Figure 36 shows the ChIP analysis for this modification. H3K9me2 is almost not detectable at the *myoD* locus. It is slightly increased at the 5'Region, but this is still low compared to the control amplicons TH/bZIP and GAPDH. TH/bZIP and GAPDH both show a strong enrichment of H3K9me2 in the neurula stage. This might perhaps reflect the time point, when the heterochromatin starts to form. Also the signal: noise levels of the *myoD* amplicons are low compared to GAPDH and TH/bZIP (Figure 36B). This fact raises the questions, whether the IP displays only background or whether the IgG control is a not a suitable control after all due to background deriving from chromatin binding to unspecific IgG. In summary, this experiment suggests that H3K9me2-mediated repression is not involved in *myoD* silencing in non-muscle cells.

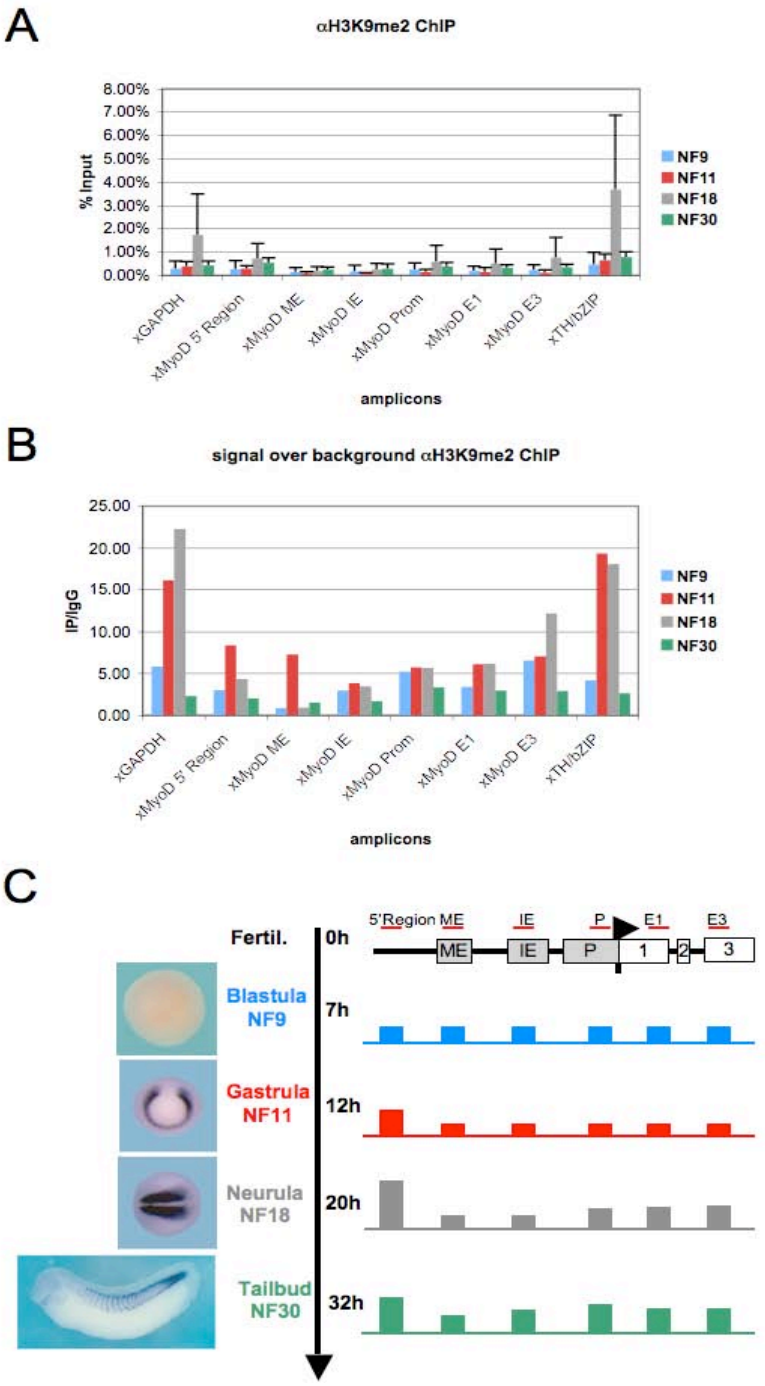

Figure 36: The dimethylation of lysine 9 on histone H3 (H3K9me2) is undetectable on the *myoD* locus.

A) The chart of the ChIP against dimethylated lysine 9 on Histone H3 (H3K9me2) is plotted as % of Input. The analyzed stages and amplicons were described previously (see Figure 28 & 31). The standard deviations reflect 4 individual experiments. **B)** This chart shows the signal over background ratio. Division of average % Input (IP) by average % Input (IgG) calculates this quotient. **C)** A diagram of the graph in A of the αH3K9me2 ChIP results in arbitrary units. The y-axis gives a time scale of analyzed stage with pictures of a *myoD* mRNA *in situ* hybridization. The x-axis shows the *myoD* locus from 5' to the 3' end plus the amplicons as red bars.

Polycomb-mediated repression is marked by trimethylation of lysine 27 on histone H3 (H3K27me3). This methylation is put in place by the histone methyltransferase Enhancer of Zeste (Ehz), a component of the Polycomb-related complexes (PRC) (Levine et al., 2004) (see 2.4.3.2). In Figure 37, this modification was detectable in neurula and tailbud stage embryos at the entire *myoD* locus. This might indicate a role during establishment of the stably repressed state in cells, which do not express the *myoD* gene. The largest enrichment of H3K27me3 was detected at the 5'Region, suggesting again a functional role of this region (see αH4ac ChIP). The spreading of the H3K27me3 modification along the entire *myoD* locus is consistent with published αH3K27me3 ChIPs (Bracken et al., 2006), again arguing for a role of PcG proteins in the repression of the *myoD* locus. The signal:noise ratio was again very low. Once more, this questions the IgG control, since the H3K27me3 modification is absent in earlier stage and emerges from neurula stage on the *myoD* locus as well as the two control loci. This suggests an overall role of Polycomb-mediated repression, starting at some point in development between gastrula (NF11) and neurula stage embryos (NF18).

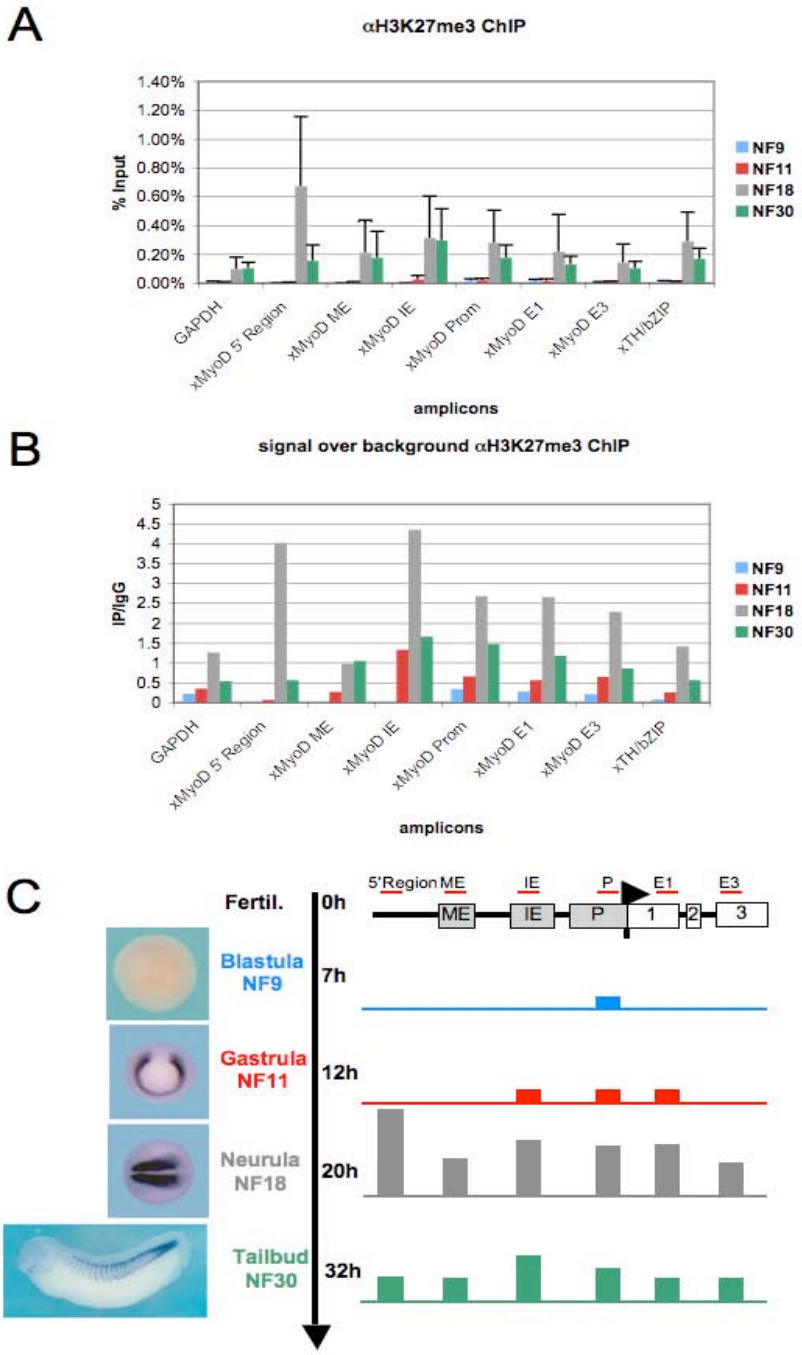

Figure 37: Polycomb-mediated repression might be involved in *myoD* silencing.

A) The chart of the ChIP against trimethylated lysine 27 on Histone H3 (H3K27me3) is plotted as % of Input. The analyzed stages and amplicons were described previously (see Figure 28 & 31). The standard deviations reflect 4 individual experiments. **B)** This chart shows the signal over background ratio. Division of average % Input (IP) by average % Input (IgG) calculates this quotient. **C)** A diagram of the graph in A of the αH3K27me3 ChIP results in arbitrary units. The y-axis gives a time scale of analyzed stages with pictures of a *myoD* mRNA *in situ* hybridization. The x-axis shows the *myoD* locus from 5' to the 3' end plus the amplicons as red bars.

These previous ChIP analyses were performed with lysates of whole embryos consisting of a mixture of *myoD* expressing and non-expressing cells. In order to distinguish these two populations of cells, ChIPs with animal cap explants were performed (also see Figure 19). Figure 38A displays the average of two individual IPs rather in contrast to the previous experiment, where 4 IPs were performed. Nevertheless, the ChIP against histone H3 suggests that the density of nucleosomes in *myoD* non-expressing cells in untreated explants is higher than at the actively transcribed locus in activin treated explants. MyoD E1 shows an exception, which might have technical reasons.

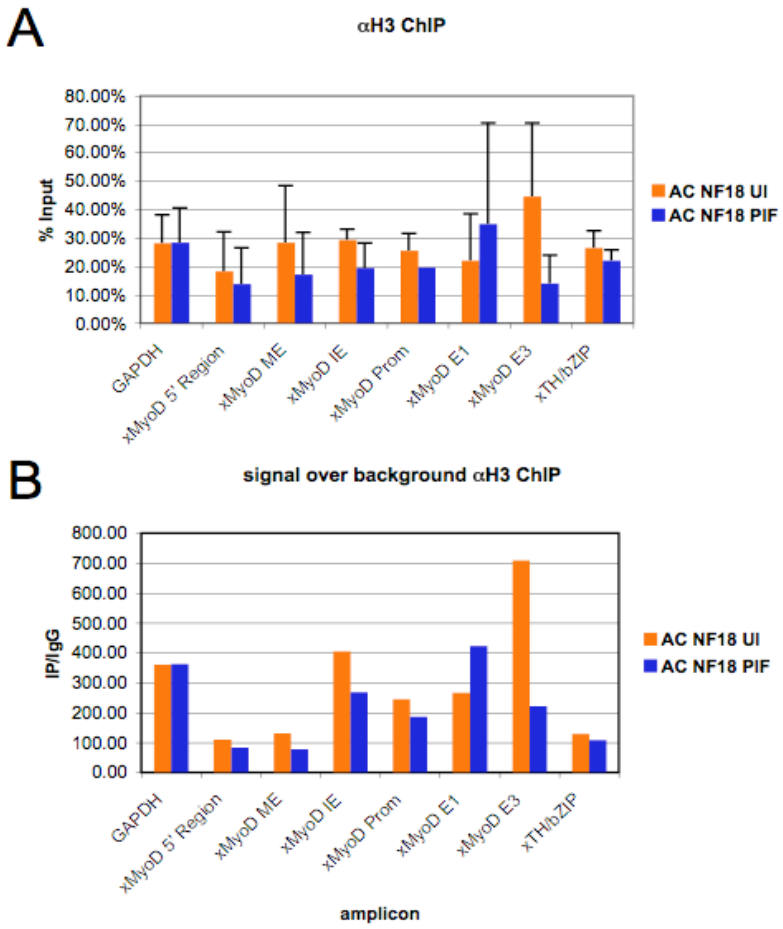

Figure 38: Nucleosomal densities of the *myoD* locus in *myoD* expressing and non-expressing animal cap explants.

A) The chart of the αHistone H3 ChIP is plotted as % of Input. AC NF18 UI: 100eeq untreated, neurula stage (NF18) animal cap explants with *myoD* non-expressing cells AC NF18 PIF: 100eeq activin-treated, neurula stage (NF18) animal cap explants with *myoD* expressing cells (also see Figure 19). The standard deviations reflect 2 individual experiments. **B)** This chart shows the signal over background ratio. Division of average % Input (IP) by average % Input (IgG) calculates this ratio.

Although great efforts were undertaken to cut the animal cap explants, the ChIP against the four histone modifications H3K4me2, H4ac, H3K9me2 and H3K9me3 failed, because the enrichment of the amplicons was below the IgG background and thus inconsistent (data not shown). These reasons also apply to the ChIP against MyoD with the antibody MYO 6C8 in animal caps explants as well in whole embryo lysates (data not shown).

From these ChIP analyses, I recapitulated that at first the nucleosomal density at the ME is remarkably lower compared to exon 1 and exon 3. Second, the nucleosomal densities appear to be very dynamic over the analyzed stages. Third, the αH3 ChIP from animal cap explants suggests that the nucleosomes are less condensed in *myoD* expressing cells. Fourth, the active marks H3K4me2 and H4ac are detectable on the promoter of *myoD,* likely on the transcribed gene. Fifth, the mark for facultative heterochromatin H3K9me2 is virtually not detectable in the stages used for the ChIP analysis. Control amplicons show this modification in the neurula stage (NF18). Sixth, the hallmark for constitutive heterochromatin H3K27me3 appears at neurula stage and thus Polycomb-mediated repression seems to be involved in the regulation of the *myoD* locus. As a summary I draw the conclusion that all analyzed histone modification followed their published patterns (for review see (Kouzarides, 2007)).

4.2.5 CHD4 binds to the *sip1* gene

The chromatin remodeling ATPases CHD4 shows a highly tissue specific expression (Linder et al., 2004). Further loss- and gain-of-function analyses of CHD4 revealed that it is important for the positioning of the mesoderm/neuroectoderm boundary, which is marked by the expression of *Xbra* in the mesoderm and *sip1* in the neuroectoderm. This studied showed that CHD4 negatively influences *sip1* expression (Linder et al., 2007). In order to obtain evidence for a direct regulation of *sip1* by CHD4 ChIP experiments of mid-gastrula stage 11 were performed. The structural organization of the mouse *sip1* locus has been described recently (Nelles et al., 2003), including the presence of nine untranslated and alternatively spliced exons (U1 – U9), and the nucleotide sequence of two putative promoter regions located upstream of U1 and U4/U5, respectively (see Figure 39A). Exons U5, E1 and E2 were identified by sequence conservation between *Xenopus tropicalis* (genome assembly v4.1, scaffold 232)

and mouse *sip1* genomic DNA sequences (Nelles et al., 2003). Among these elements, cDNA (Eisaki et al., 2000) and genomic *sip1* DNA sequences from *Xenopus* showed high sequence similarity for exons U5, E1 and E2, while shorter stretches of clearly conserved DNA sequence extended into the promoter region upstream of U5 (see Figure 39A). Based on this information, TaqMan amplicons, which were located at xU5, xE1 and xE2 of the *Xenopus sip1* gene, were designed. They cover approximately 90kb of the transcribed 5' portion of the *sip1* gene (Table 6, Figure 39A).

Amplicon	Baseline	Thres hold	Slope	Intercept	Correlation of PCR triplicates R2
xU5	3 to 16	0.3	-3,252112	30.446922	0.997565
xE1	3 to 17	0.2	-3.202356	30.003592	0.997568
xE2	3 to 18	0.2	-3.426923	30.491692	0.99917

Table 6: Additional amplicons at the *sip1* locus for αChd4 ChIP with Douncer protocol

The relative occupancy of CHD4 protein at the *sip1* locus was calculated the following way:

1. Average of Ct value (PCR duplicates): Av Ct
2. Calculation of relative DNA amounts via standard curve: $y=10^{((\text{Av Ct} - \text{Intercept})/\text{slope})}$
3. Normalization to input: y / Input DNA amount = z
4. Normalization to GAPDH: z / z(GAPDH)
5. Average of 3 independent IPs plus standard deviation

For the IP of the Chd4 protein, a mixture of αCHD4 monoclonal antibodies CH4-N 3A11, CH4-N 5H4, CH4-N 5A2, CH4-C 7C9 and CH4-C 7E8 was used. This ChIP analysis indicates that CHD4 binding was more than three-fold enriched at the xE1 amplicon, i.e. within the 5' part of the transcribed gene body compared to U5 and E2 (Figure 39B). Furthermore, among all tested regions, amplicon E1 showed the highest CHD4 occupancy. The standard deviations of this ChIP analysis are rather low, because the standard deviations

reflect independent IPs of the same lysate. Based on this result, the *sip1* gene was identified as a direct target of CHD4.

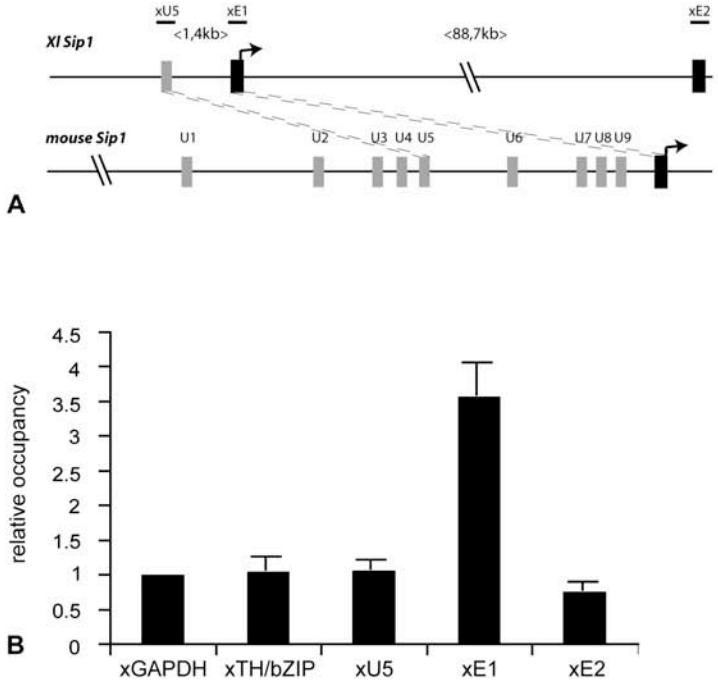

Figure 39: CHD4 binds to the *Sip1* gene.

(**A**) The cartoon depicts the organization of *Xenopus* and mouse *sip1* gene loci around the first translated exon E1 (AUG indicated by arrow). While Exons U5 and E1 are highly conserved in sequence (connected by dashed lines), mouse exons U6-U9 are apparently not conserved in *Xenopus*. Black bars indicate the relative positions of the ChIP amplicons xU5, xE1, and xE2 for *Xenopus*. Not drawn to scale, however, absolute distances between ChIP probes are given in brackets. (**B**) Chromatin immunoprecipitations were performed on midgastrula stage *Xenopus* embryos (NF11), using a rat monoclonal antibody mix against xCHD4 protein followed by real-time PCR analysis. They reveal preferential binding of endogenous xCHD4 protein to E1 (n=3 experiments). The relative xCHD4 occupancy was normalized to the xGAPDH amplicon; xTH/bZIP is a silent gene, which becomes activated during metamorphosis. Error bars: mean standard deviation. This figure is published as Figure 4 in (Linder et al., 2007).

4.2.6 ChIP data quality assessment

The ChIP analyses of histone modifications at the *myoD* locus have very high standard deviation, although the ChIP analyses were performed with highest accurateness. I took great care of the following issues: First, great efforts were made to optimize all protocol parameters. Second, the embryos were handpicked and thoroughly staged. Third, the maximal available sample material and the highest possible replicate number were exploited. This led to the collection of about 12000 embryos for the ChIP analysis against the histone modifications. However, it should be noted that ChIPs with many antibodies are

just above the noise. In most of the cases the standard deviations are large. So, why is it not possible to evaluate the data in a statistically relevant fashion?

In order to address this question, I assessed the Douncer ChIP method by comparing it to ChIP methods of other species, which are carried out at the Department of Molecular Biology of the Adolf-Butenandt-Institut, LMU München. This comparison revealed significant differences with regard to genome size and complexity, cell heterogeneity, cell number and PCR efficiency. At first, the size of the genomes was compared. The different species are listed in Table 6. The DNA amounts were deduced from the base number and plotted as % to *Xenopus laevis*. I considered *Xenopus laevis* as diploid, since it is allotetraploid. This means that it has a diploid chromosome set, but each chromosome has been duplicated and thus has twice the size of a *Xenopus tropicalis* chromosomes. The non-allelic genome copies derived from this duplication can be distinguished in their nucleotide sequence. Only about 68% of the highly expressed, no-allelic gene copies have the same function, whereas low expressed ones have only in 38% of the cases an expression paralog (Morin et al., 2006).

Considering the number of bases the *Xenopus laevis* genome has the largest size. The baker yeast *Saccharomyces cerevisiae* has about a 1000-fold less genome size, the fruit fly *Drosophila melanogaster* 34-fold less. The mammalian mouse and human genomes have only 55% of the size of the *Xenopus* genome.

species	**bases**	**DNA weight per nucleus in pg**	**compared to *Xenopus***	**ploidity**
Yeast	$6.2x10^6$	0.00682	0.11%	haploid
Drosophila	$1.7x10^8$	0.187	2.94%	diploid
Mouse	$6x10^9$	7	55.56%	diploid
Human	$6x10^9$	7	55.56%	diploid
Xenopus laevis	$12x10^9$	12.8	---	allotetraploid/ diploid

Table 7: Genome complexity of ChIP model organisms

The ploidity of *Xenopus laevis* was calculated as diploid, because the term “allotetraploid” reflects the existence of two non-allelic copies of each gene, which differ in their DNA

sequence and frequently expression patterns. Source for *Xenopus*, human and mouse: www.bio.nagoya-u.ac.jp:8000/compG01.html, yeast and *Drosophila*: http://users.rcn.com/jkimball.ma.ultranet/BiologyPages/G/GenomeSizes.html

In a second step, the individual ChIP protocols were compared. Comparing the cell numbers per IP showed that the *Xenopus* cell numbers per IP are approximately 2-10-fold less than the other the ChIP of the other species (see Table 7). As the *Xenopus* ChIPs were performed with whole embryos, the ChIP lysates consist of a heterogeneous cell population. This is an additional difficulty, because this number per IP describes the total number of applied cells. Therefore, the actual cell number expressing e.g. *myoD* is much less and can only be estimated.

Another import issue of the ChIP method is the real-time PCR (also see 4.2.1.3). In Table 7, the Ct values of 10.000 copies of ChIP input DNA were compared. TaqMan-based PCR analysis of murine and *Xenopus* ChIPs need around 28 cycles to reach the threshold with 10000 genomic copies. The yeast Ct value is at around 25 cycles. This reflects about a 10-fold less sensitive PCR, which is most likely due to the lower complexity of the yeast genome.

Comparing SYBR Green based ChIP quantifications with TaqMan based ones, another important fact was discovered. SYBR Green based real-time PCR of Drosophila and human cell culture cells show the Ct values at around 21 to 23 cycles, the TaqMan based at 25-28. This suggests that the SYBR Green PCR is more efficient on mock ChIP DNA than the TaqMan-based real-time PCR technology. This could be due to the damage of the DNA, which may happen during the ChIP procedure. The TaqMan technology requires the binding of a specific fluorescence-labeled oligonucleotide within the PCR amplicon and might therefore be more sensitive to DNA damage.

species	ChIP protocol type	Cell number per IP	Ct value of Input of 10.000 copies	real-time PCR method
Xenopus NF9	Douncer ChIP	$1,6x10^6$	28,56	TaqMan
Xenopus NF11	Douncer ChIP	$4,7x10^6$	28,56	TaqMan
Xenopus NF18	Douncer ChIP	$4,3x10^6$	28,56	TaqMan
Xenopus NF30	Douncer ChIP	$9,2x10^6$	28,56	TaqMan
Xenopus NF18 AC PIF	Douncer ChIP	$8,8x10^5$	28,56	TaqMan
Xenopus NF18 AC UI	Douncer ChIP	$7,3x10^5$	28,56	TaqMan
human breast cancer cell line	In Situ ChIP	$1x10^7$	21,5	SYBR Green
mouse 3T3 Cells	In Situ ChIP	$5x10^6$	28,14	TaqMan
Drosophila adults	Douncer ChIP	$1x10^7$	23,66	SYBR Green
Drosophila embryos	In Situ ChIP	$3,3x10^7$	21	SYBR Green
yeast	In Situ ChIP	$3,3x10^7$	25,15	TaqMan

Table 8: Comparison of the ChIP protocols of different species

For a comparison of the Douncer ChIP and In Situ ChIP methods see Figure 25. For a detailed description of the two different real-time PCR techniques see chapter 4.2.1.3. For a description of the Ct value see Figure 23. The Ct values of the *Xenopus* stages are equal, because they were calculated as the mean Ct value of described standard curves (see chapter 4.2.1.3).

Comparing SYBR Green and TaqMan PCR techniques directly by using the same primer set of the TH/bZIP amplicons showed that the TaqMan fluorescence (Ct=29.83) is detected 5.42 cycles later that the SYBR Green fluorescence (Ct=24.41) (data not shown). Comparing the primer set of the MyoD P, which has a quencher molecule that binds to the minor groove of the DNA helix, showed that the TaqMan fluorescence (Ct=34.1) is detected 8.1 cycles

later than the SYBR Green fluorescence (Ct=26.0). This suggests that the PCR reaction of SYBR Green is more efficient for the ChIP analysis, because the fluorescence is up to 8 cycles earlier detectable. This might help to decrease the standard deviations of the ChIP, because the PCR efficiency is increased and thus might decrease the detection limit.

Apart from the technical problems, there are also biological parameters, which contribute to the high standard deviations. First of all, an important difference to ChIP with cell lines is that the ChIPs of *Xenopus* embryos are performed with a heterogeneous material. Although the embryos were staged thoroughly, the embryos were the offspring of wild(-type) animals with a heterogenetic background. In order to balance this fact, one should attempt to have 2-3 independent IPs of the same male and female combinations.

The most important issue is the limitation of the sample material. In the *Xenopus* ChIP, approximately 10-fold less cells are used in total than the other protocols. This number reflects the total cell number of the heterogeneous cell population, thus the actual number of desired protein-DNA interaction per cell is much lower. Another limitation regarding the detection limit of the desired protein-DNA interactions is the fact that genomic DNA works 20x better than ChIP DNA. So if I assume to detect for example 2000 copies, in reality only 100 copies are detectable. Taken these restrictions together, our ChIP assay seems to be in most of the cases at the level of detection. Nevertheless, our established ChIP protocol is able to show trends of the *in vivo* situation.

5 Discussion

How a complex organism can develop out of a single cell, this question has puzzled developmental biologists since more than a century. Developmental processes were studied with genetic and interference analyses. With these approaches, developmentally important genes were identified and hierarchies of these genes were established, but it was not possible to determine, whether the influences were direct or not. Therefore, one of the major challenges within this quest is still to understand how the genetic information is interpreted to guide the unidirectional process of development. Alterations of histone modifications, changes in the protein composition binding to DNA, or the remodeling of nucleosomes have been proven to be important for the establishment and the inheritance of tissue-specific transcription profiles. A method to study this direct protein association to a specific genomic locus is the chromatin immunoprecipitation (ChIP).

In this study, I have established the two following protocols for ChIP analyses in *Xenopus laevis* embryos: the In Situ ChIP and the Douncer ChIP (also see Figure 25). I addressed three different developmental scenarios. First of all, I investigated the chromatin evolvement during myoblasts determination and differentiation. Successful ChIP analyses with the In Situ ChIP protocol were performed against the serum response factor SRF on the *myoD* locus. With the Douncer ChIP protocol, a time course study was performed in order to understand which and when histone modification marks appear during muscle cell determination and differentiation on the *myoD* locus. Secondly, I attempted to study the chromatin readout upon Wnt/β-catenin signal stimulation at the Wnt target and organizer gene *siamois* and the muscle determination factor *myf5.* Therefore, I generated rat monoclonal antibodies directed against the Lef/Tcf transcription factors Lef1 and Tcf1. Thirdly, I proofed the influence of CHD4 on the positioning of the neuroectoderm/mesoderm boundary in the gastrula to be direct via ChIP.

5.1 Technical aspects of ChIP

The ChIP assay involves five major steps: (I) fixation of DNA bound *in situ*, (II) the shearing of the chromatin, (III) the immunoprecipitation of the desired

chromatin-associated protein, (IV) the purification of the DNA, and (V) the quantification of the DNA via PCR. In the ideal case, the fixed chromatin has an average size of about 500 to 1000bp. The antigen epitope is easily accessible to the specific antibody, the affinity of the antibody is very high and thus the precipitation efficiency is large; i.e. it lies within the range of 2-10% compared to the input.

Nevertheless, the ChIP assay has a variety of limitations. First of all, ChIP is not a quantitative assay. It shows qualitative differences, but it does not offer absolute numbers. A major disadvantage of the assay is its complexity, as it involves many crucial steps. The success of the ChIP depends very much on the abundance of the desired protein-DNA adducts under investigation, on the well-established preparation of the chromatin lysate, on the quality and the affinity of the antibody and on the efficiency of the real-time PCR. Furthermore, it depends on the chosen controls and on the thoughtful interpretation of the data.

In this study, I showed that it is possible to investigate histone modifications and chromatin-associated factors in developing *Xenopus* embryos. Subsequently, I have discussed the technical aspects of the ChIP method and considered my established ChIP protocols and my generated data.

5.1.1 Comparison of ChIP methods

5.1.1.1 Preparation of chromatin lysates

The In Situ ChIP protocol (see 3.9.2) is the protocol type, which is most commonly used for ChIPs (see e.g. www.epigenome-noe.net/researchtools/protocols.php). In this protocol, the chromatin is fixed in intact cells by adding formaldehyde into the culture medium. Subsequently, the cells are lysed and the chromatin is sheared with the FRENCH Press. The cell debris is removed via centrifugation. The ChIP lysate, originating from this preparation, is rather crude. Other protocols purify nuclei, extract the chromatin afterwards (for *Xenopus* neurula stage embryos e.g. (Morgan et al., 2004; Sachs and Shi, 2000)) and thereby get rid of the majority of the cytoplasmic and other proteins, which are not associated with the nucleus. Since such preparations of nuclei usually have a low yield (20-30%), too many embryos would be necessary for this kind of protocol. Especially very young embryos of blastula stage have only about 15,000 cells (also see Table 5). The Douncer ChIP protocol (see 3.9.3 and 4.2.3) avoids the preparation of nuclei, but removes a lot of the soluble

protein fraction and fatty acids by fixation of the chromatin during mechanical lysis with a Douncer in a low salt and low detergent-containing buffer. The chromatin remains in the insoluble portion of the slurry. Subsequently, it is washed several times and eluted afterwards with a buffer containing SDS and N-Lauroylsarcosine. The chromatin is subsequently sheared by sonication.

The chromatin fixation under mechanical lysis is the major disadvantage of the Douncer ChIP protocol. Although all steps were performed with maximal accurateness, slight differences of the cell lysis might lead to variation of the chromatin fixation. The fixation of the chromatin *in situ* is probably more consistent.

The Douncer ChIP protocol has two important benefits over the In Situ ChIP protocol. First of all, the lysate preparation involves several washing steps. Thereby, a great portion of the maternally stored, non-chromatin incorporated yolk storage portion of the antigen becomes eliminated and does not interfere with the IP of the chromatin-associated portion of the antigen. Secondly, the material loss with the FRENCH Press used for the In Situ ChIP is circumvented by the Douncer ChIP protocol, which shears the chromatin via sonication and thus does not need the transfer of the lysate into a new test tube. A crucial disadvantage of the FRENCH Press is its dead volume of approximately 12%. Since the amount of embryonic material is limiting, it was crucial to decrease the loss of lysate. This was achieved by switching the chromatin shearing with the FRENCH Press to the sonicator Bioruptor. This change resulted in a yield up to 25% more lysate.

5.1.1.2 Selection of Antibodies

Polyclonal antibodies are the most commonly used reagents for IPs. Their advantage is that they contain a mixture of antibodies binding to several sites at the target protein. However, because of this, antisera are also prone to cross-react with unrelated proteins. Therefore, their avidity for the antigen is usually high. Because polyclonal antibodies form multivalent interactions with their antigen, their disadvantage is that this can lead to unspecific interactions with other proteins (Harlow E, 1988). By contrast, monoclonal antibodies bind only to one epitope of the antigen. This results in a very high specificity and thus in rather low background. Given that the antibodies bind to only one epitope, the affinity to the epitope can be very low. Therefore, it is crucial to evaluate the

antibodies in regard to their IP efficiency (Harlow E, 1988). Ideally, it was my aim to generate several antibodies against the same target protein, which were tested individually in regard to their cross-reactivity and avidity. By mixing these monoclonal antibodies, they should combine the advantages of the monoclonal and the advantages of the polyclonal antibodies. In order to raise several monoclonal antibodies, rats were immunized with full-length proteins. This should stimulate a complex immune response, which is directed against different antigenic regions of the target protein. Therefore, rat monoclonal antibodies were raised in collaboration with the laboratory of Dr. Elisabeth Kremmer (GSF München). Here, rat monoclonal antibodies against the MyoD protein and the Lef/Tcf transcription factors were raised and successfully tested in Western blot analysis, immunocytochemistry (ICC), immunofluorescence (IF), immunoprecipitation (IP) and ChIP-type IPs (see chapter 4.1). Immunoprecipitation efficiency of formaldehyde-fixed antigens of the αMyoD antibody MYO 6C8 is above 50% of the input sample. For the αLef1 antibodies LEF 3D4 and LEF 5F12 and the αTcf1 Tcf1 2F4 the efficiency is still within 15-20% of the input sample. Therefore, it can be concluded that the generated antibodies are suitable for ChIP assays. However, ChIP analyses with these generated antibodies failed so far. The reasons for the so far unsuccessful ChIPs are presumably not due to the precipitation efficiency of the antibodies and will be discussed below in the discussion part of the biological aspects (see 5.2.2).

5.1.1.3 ChIP controls

It is important to control the ChIP on two levels: the IP control determines the specificity of the observed signal and the PCR controls show the background level of the unspecific DNA co-precipitation. For the control of the IP, equivalent IgG amounts of the specific antibody of either unspecific rabbit IgG were used. In ChIPs with the rat monoclonal antibodies, of the bridging antibody rabbit-αrat IgG were used as the IP control. In Figure 30, the average IgG background was plotted as the percentage of input. None of the amplicons adhered to a greater extend to the ProteinA-sepharose beads than the other amplicons. Due to the large standard deviation, it is apparent that there are huge variations in the unspecific precipitation of this control. This might suggest that also the specific IPs with different lysate preparations have great variations in their precipitation efficiency. Although it was taken great care concerning the

experimental accuracy, this could be due to slight differences in the preparation of the lysate. To circumvent this problem, independent IPs of the same chromatin lysate preparation should be used for the calculation, which should improve the height of the standard deviations (see 4.2.5, Figure 39).

Another important issue is the precise quantification of the IP sample. In order to do so, unrelated control amplicons are necessary. Here, I used control amplicons derived from the *gapdh* and *th/bZIP* gene. The GAPDH amplicons is located within the coding region of the constitutively expressed housekeeping gene. The TH/bZIP amplicon is situated at the promoter region of a thyroid hormone responsive gene, which is silent throughout embryogenesis until metamorphosis. The expression profiles for these two control genes differ from the analyzed genes *myoD, siamois, myf5* and *sip1,* which are developmentally regulated during early embryogenesis. Therefore, they are good controls for the ChIP analyses representing both constitutively active and transcriptionally silent single copy gene loci.

5.1.1.4 Real-time PCR techniques

In this study, the TaqMan-based real-time PCR was performed to quantify the relative DNA enrichment of the ChIP sample (see chapter 4.2.1.3). The TaqMan technology is based on a fluorescence-labeled oligonucleotide, which binds sequence-specifically within the PCR amplicon. In the intact oligonucleotide, a quencher disrupts the signal emission of the fluorescent dye. During the elongation of DNA polymerase, the TaqMan oligonucleotide is degraded by the 5' nuclease activity of the DNA polymerase. As a consequence, the quenching is abolished and the fluorescent signal becomes detectable. I have chosen this PCR method, because the TaqMan probes hybridize very specifically to their target sequence. This minimizes the signal detection due to mis-priming or primer-dimer artifacts, which occurs in other real-time PCR methods such as the SYBR Green PCR. This fluorescent dye intercalates unspecifically into any double-stranded DNA. Nevertheless, comparing SYBR Green-based ChIP analyses with TaqMan-based ones revealed that the SYBR Green PCR is more efficient on ChIP Input DNA than the TaqMan PCR (see chapter 4.2.6). This became apparent by comparing the Ct values, which indicate the cycle numbers, when the amplification curve crosses the threshold (see Figure 21). On one and the same DNA template the Ct values of the SYBR Green PCR are detectable

around cycles 21-23, the TaqMan PCR at around cycle 28 (see Table 7). Comparing the PCR performance with identical primer sets by the TaqMan and SYBR Green techniques confirmed this.

Based on these facts, I conclude that the TaqMan-based real-time PCR technology has the advantage that it has very high sequence specificity. However, the SYBR Green technology is more efficient on DNA, which was treated under ChIP conditions. Therefore, the SYBR Green technology should be preferred for subsequent ChIP analyses. Nevertheless, the SYBR Green method needs to be thoroughly established to exclude PCR products due to mis-priming or primer-dimer artifacts.

5.1.1.5 Abundance of the investigated protein-DNA association

The success of a ChIP experiment directly interdepends with the abundance of the investigated protein-DNA interactions. Therefore, it is important to determine cell number used for the ChIP experiments. In chapter 4.2.6 Table 7, the cell numbers per IP were summarized and compared. ChIPs with *Xenopus* embryos applied around $5x10^6$ cells in total, whereas ChIP in *Drosophila*, yeast and cell culture cell lines used about $1x10^7$ cells. This demonstrated that the cell numbers per *Xenopus* ChIP are about 2 to 10-fold lower than in other ChIP protocols. If the desired protein-DNA interactions are only rare abundant, it is likely that they are below the level of detection. Since the embryonic material is limiting, it is not possible to increase the amount of embryos per IP and thus the amount of precipitated DNA. Therefore, linker-mediated linear amplification of the precipitated DNA might be an option to overcome the PCR limitation. Farnham and colleagues used a protocol to amplify their ChIP DNA in a linear fashion (O'Geen et al., 2006). Their assay might be used for our ChIP protocol to amplify the precipitated DNA, and thus might help to decrease the variations of the real-time PCR replicates, which frequently led to inconsistent ChIP results (see αLef/Tcf ChIP chapter 4.2.2, αMyoD ChIP chapter 4.2.4).

5.1.1.6 Quantification and representation of the ChIP data

Important issues of the ChIP are the quantification of the enriched DNA fragments and the representation of data. Two different quantification approaches were used for this project. For the analysis of the αSRF ChIP at the

myoD locus, the ΔΔCt method was used. This calculation method requires almost ideal slopes of all standard curves, because it calculates the ratio between different samples by subtraction of the Ct values and subsequent conversion with the PCR equation 2^n (see chapter 4.2.1.3). For the quantification of the ChIP against the histone modification, the relative DNA amounts were determined via the standard curve and plotted as the percentage of the input DNA sample (see chapter 4.2.3). Some ChIPs are quantified by subtraction of the IgG background prior to the normalization to the input DNA sample (personal communication Attila Nemeth, University of Regensburg). But this subtraction leads to irregular variability of the normalization ratios. Therefore, the ChIPs in this analysis were plotted without taking the IgG control into account.

Nevertheless, I evaluated the relative impact of non-specific binding by dividing the % input of the IP by the % input of the IgG. This revealed that in some cases, e.g. with αH3 or αH3K4me2 antibodies, the precipitated DNA amounts were several hundred fold over IgG background level. In other cases, e.g. the αH3K27me3 antibody, this difference between the specific precipitation and the background was only up to four fold. This difference reflects the discrepancy in the epitope avidity of the antibodies. In spite of this, the IP with unspecific IgG is an important control to interpret the specificity of the observed signal.

There is no commonly accepted standard, how ChIP data should be controlled and represented. The data can in principle be plotted as the average of the PCR replicates or as the average of individual IPs. The ChIP data in chapter 4.2.4 are plotted as average of four individual IPs of independent chromatin lysate preparations. I have chosen this conservative way of data representation, because I believe that this is close to the *in vivo* situation. A compromise to reduce high standard deviations is to display the average of independent IPs of the same lysate.

Taking the variations of the biological material, the IP and the PCR into consideration, the ChIP quantification by plotting the data as % input is the method of choice for my future ChIP experiments. Furthermore, IP replicates of the same lysate should be performed in order to avoid different IP efficiencies due to slight differences in the lysate preparation.

5.1.1.7 Conclusions

In this project, two different ChIP protocols were adapted for *Xenopus laevis* embryos. Both approaches were successful with some antibodies, but also failed with others. They have the discussed advantages and disadvantages. For early developmental stages until the tailbud stage (NF30), the Douncer ChIP is more suitable, because the lysate preparation removes maternal, non-chromatin incorporated storage proteins, which could otherwise interfere in the IP with the chromatin-bound fraction of the antigens. Recapitulating this technical part of the discussion, I come to the conclusion that I have established a reliable ChIP method, which is able to show qualitative trends. However, there is room for further technical improvement like changing the real-time PCR staining technique or amplification of the precipitated DNA.

5.2 Biological results of this project

5.2.1 Regulation of the MyoD locus

The basic helix-loop-helix protein MyoD is a transcription factor that promotes skeletal muscle formation in *Xenopus laevis*. Its expression is activated at the early gastrula stage and is restricted to the gastrula mesoderm and the somites of neurula and tailbud embryos (Hopwood et al., 1989) (also see Figure 2). Several growth factor signaling cascades have been shown to be important for muscle development (for review see e.g. (Pownall et al., 2002)), yet a direct link like a transcription factor binding to the *myoD* locus upon induction was not identified until now. Transcriptional repressors of *myoD* are better understood. It was shown that the globular domain of the somatic linker histones is sufficient for direct gene specific transcriptional repression (Lee et al., 2004; Steinbach et al., 1997; Vermaak et al., 1998). In subsequent studies, the *Xenopus myoD* locus was cloned, sequenced and analyzed with a transgenic reporter gene assays to determine regulatory elements (Otto, 2000; Xiao, 2003). Two enhancer elements were mapped, which are important for the induction and the maintenance of the *myoD* transcription. Based on this study, ChIP analyses at the *myoD* locus were performed during this project to gain a better understanding of these regulatory elements.

5.2.1.1 Histone ChIP

Observations like the involvement of H1 in transcriptional silencing (Steinbach et al., 1997) suggested a contribution of chromatin in the regulation of the *myoD* gene expression. In order to study the chromatin environment during the various phases of *myoD* expression, a time course of histone modifications was carried out (see chapter 4.2.4, Figures 33-38). The modifications are mainly found on the N-terminal tails of the core histones. The best-studied covalent modifications are methylations, acetylations and phosphorylations (Kouzarides, 2007).

As a prerequisite for the analysis of histone modifications, I investigated the nucleosomal densities of the *myoD* locus (see Figure 33). I showed by characterization of the nucleosomal loading that the nucleosomal density at the maintenance enhancer is remarkably lower compared to exon 1 and exon 3. Furthermore, the αH3 ChIP of animal cap explants suggests that the chromatin is less condensed in *myoD*-expressing cells compared to *myoD* non-expressing cells. This “open” chromatin conformation at the active locus is in accordance to published data (Nemeth and Langst, 2004). Unexpectedly, the nucleosomal densities appear to be very dynamic over the analyzed stages. In the blastula and neurula stage it appears rather condensed, in the gastrula and in the tailbud stage less condensed. This is a phenomenon, which was not described so far. The biological relevance of this observation will have to be analyzed further.

The results of time course of the different analyzed histone modifications are summarized in Figure 40. The active marks H3K4me2 and H4ac are detectable throughout all analyzed stage on the promoter of *myoD*. In all likelihood, they were detected on the actively transcribed gene, since these modifications can be correlated with the *myoD* expression pattern (see Figure 40, upper lane) (Hopwood et al., 1989; Rupp and Weintraub, 1991). The only exception was H3K4me2. In the tailbud stage, the *myoD* expression decreases and therefore the histone modification marks disappear. The increase of H3K4me2 at the promoter of *myoD* until the neurula stage is in consistence with previously described data (Nightingale et al., 2006). The importance of histone acetylation for the *myoD* locus was described previously. It was shown that over expression of histone acetyl-transferases PCAF and P300 leads to earlier *myoD* induction (Puri et al., 1997). My ChIP results support these data, since I see an

enrichment of H4ac on the *myoD* promoter prior to the gene induction. Unexpectedly, H4ac was enriched at the 5'Region amplicon in the neurula stage. This acetylation mark might suggest the transcription of a non-coding RNA. These RNAs are known to be involved in gene silencing (Yang and Kuroda, 2007). A second indication for the existence of transcription of non-coding RNAs was made by the identification of highly repetitive DNA region upstream of the maintenance enhancer (Xiao, 2003). This sequence is very similar to a reported repetitive sequence motive *Flirt* (Spohr et al., 1981). If a non-coding RNA plays a role in the silencing of *myoD*, remains to be elucidated.

The mark for constitutive heterochromatin H3K9me2 is almost not detectable in the stages used for the ChIP analysis (see Figure 36). Therefore, an involvement of histone methyltransferases SUVAR39 or G9a in the repression of the *myoD* gene is highly unlikely. However, the control amplicons show this modification in the neurula stage (NF18), suggesting that this way of repression exists in *Xenopus*. In addition, G9a-meditated repression was described already for *Xenopus laevis* oocytes (Stewart et al., 2006).

The histone modification H3K27me3, correlated with Polycomb-mediated repression, appears at neurula stage on the *myoD* locus. Furthermore, a potential YY1 binding site is found at the *myoD* promoter. YY1 is the vertebrate homolog of the *Drosophila* Polycomb group (PcG) protein Pleiohomeotic. The over-expression of a dominant-negative YY1-EnR inhibits the *myoD* expression (Xiao, 2003). This suggests that PcG proteins are involved in the transcriptional repression of *myoD*. Moreover, it is described for mouse cell lines that Ezh2 regulates muscle gene expression (Caretti et al., 2004). In addition, it was shown that the PcG group protein Suz12 is bound the gene body the *myoD* locus in ES cells. Upon differentiation into muscle cells, the binding of Suz12 to the *myoD* locus together was lost. Furthermore, also the H3K27me3 mark disappears (Lee et al., 2006). Interestingly, PcG members are expressed in somites (Showell and Cunliffe, 2002). Taking all these evidences into consideration, they suggest that Polycomb-mediated repression is also involved in the silencing of *myoD* in *Xenopus*. Further analysis will be needed to determine the players and the entry site. A potential candidate for the entry factor is YY1.

embryonic stage	Blastula NF9	Gastrula NF11	Neurula NF18	Tailbud NF30
ISH				
myoD expression	basal and ubiquitous pre-induction	high in preinvoluted mesoderm post-induction	high in paraxial mesoderm	high in myocytes
histone modification	H4ac H3K4me2	H4ac H3K4me2	H4ac H3K4me2 H3K27me3	H4ac H3K27me3

Figure 40: Summary of the analyzed histone modifications at the *myoD* locus

Top row indicates the embryonic stages analyzed by ChIP. Second row shows the mRNA expression pattern of *myoD* with *in situ* Hybridization (ISH) (see 3.5.6). Third row describes the *myoD* expression pattern. Fourth row shows the detected histone marks, marks for active transcription in green, for repressed transcription in red. The histone modifications are listed after the Brno nomenclature (Turner, 2005)

From the above discussion, it can be concluded that the histone modification pattern detected at the *myoD* locus correlates with the mRNA expression pattern (see Figure 40). The hallmarks for active transcription H4ac and H3K4me2 are detectable on the *myoD* locus in stages, which express *myoD*. The hallmark for silent loci H3K27me3 is detectable in from neurula stage on, which is the stage, when the *myoD* transcription is maintained. In addition, the hallmarks for active transcription H4ac and H3K4me2 can be detected at the *myoD* locus prior to the gene induction during the phase of basal *myoD* transcription. However, it is not possible to draw mechanistic insights concerning the activation of *myoD* by any growth factor signaling cascades. With regard to the transcriptional silencing I hypothesize that Polycomb-mediated repression is involved in the *myoD* regulation.

Interesting for future experiments are the following observation by Fisher and colleagues. They showed that H3K27me3 was found together with H3K9ac and H3K4me2 on one nucleosome (Azuara et al., 2006) on some developmentally important gene loci in human and murine ES cells. This phenomenon of bivalent histone modifications could not be detected at the *myoD*

locus. There are several reasons, why this phenomenon was not observed. The bivalent modification pattern might only exist during the early cleavage stages. Furthermore, it might be specific for mammals, which have evolved extra-embryonic tissue parts. Apart from the histone modifications, also the characterization of the chromatin architecture by mapping DNaseI hypersensitive sites and/or histone positioning in the promoter region and the enhancer is important. Moreover, histone variants like H3.3 might be involved in the regulation of active transcription (Kimura, 2005). Recently, Ren and colleagues could show that in HeLa cells enhancers can be mapped by the existence of the histone modification H3K4me1, DNaseI hypersensitive sites and shortage of Histone H3 (Heintzman et al., 2007). Further ChIP studies with additional antibodies like H3K4me1 and earlier embryonic stages might also help to understand further details of the *myoD* regulation.

5.2.1.2 αSRF ChIP

Transgenic reporter gene assays indicated that a SRF binding site in the maintenance enhancer is important for maintaining the *myoD* reporter gene expression (Xiao, 2003). Neighboring E-boxes and Lef/Tcf binding sites are not necessary for this maintenance function. These data were supported with ChIP analysis, which proofed that SRF is bound to the *myoD* maintenance enhancer in neurula-stage somite explants, but not in blastula stage animal cap explants (Nentwich, 2003). Here, we have extended this analysis by comparing a more homogenous tissue sample of muscle-induced activin-treated animal cap explants with ectodermal, non-induced animal cap explants (see chapter 4.2.1.4, Figure 23). This αSRF ChIP analyses could confirm the earlier ChIP analysis and determined in addition that SRF is preferentially bound to the *myoD* maintenance enhancer exclusively in *myoD*-expressing cells. Furthermore, an additional SRF binding site was discovered in the second intron shortly before the third exon. The function of this site is unknown until now. Future analysis with the REMI transgenic reporter approach (also see chapter 2.2.1) will have to reveal the functional properties of the newly discovered SRF binding site.

How the SRF transcription factor gains access to its binding site during active *myoD* transcription is still unknown. Cooper and colleagues mapped SRF binding sites in various different human cell lines (Cooper et al., 2007). Although they have analyzed several histone modifications and the DNA methylation, only

few of these sites they were correlated with these epigenetic marks. The same is true for the histone modifications analyzed in this study. Neither the hallmarks for active chromatin H4ac and H3K4me2, nor hallmarks for silent loci H3K9me2 and H3K27me3 are enriched at the *myoD* maintenance enhancer. The only obvious difference of this site is that it appears to be poor in nucleosomes compared to the promoter or exon1 (see Figure 33). Whether this has any functional relevance for the binding of the SRF to the *myoD* maintenance enhancer, remains to be elucidated. Besides a possible epigenetic mechanism for the recruitment of SRF to its tissue specific target site, it is more likely due to signaling events through auxiliary factors. Components of the ternary complex factor TCF like Elk or Ets, which are responsible for stabilizing SRF at immediate early gene *egr1* (Panitz et al., 1998), could be excluded due to the lack of the required binding sequence. One candidate for this DNA binding co-factor could be the myocardin-related protein MAL. Treisman and colleagues showed that MAL becomes translocated into the nucleus upon Rho-actin signaling (Miralles et al., 2003). In a subsequent analysis, they showed that SRF and MAL form a complex in a signal-dependent manner. Furthermore, DNA binding and distortion is necessary for optimal interaction between SRF and MAL, which directly contacts DNA flanking the SRF binding site (Zaromytidou et al., 2006). It is unknown, whether the binding of MAL to the DNA is sequence-specific or not. Therefore, it is not possible to predict the binding of MAL together with SRF at the SRF site in the maintenance enhancer by sequence analysis. An additional support of this hypothesis is that the expression of *myoD* in murine C2C12 myoblasts depends on Rho-actin signaling (Dhawan and Helfman, 2004). However, it remains to be determined, whether MAL could be the signaling dependent co-factor, which helps to target or stabilize SRF to the *myoD* locus.

5.2.1.3 αMyoD ChIP

The MyoD autocatalysis is important for the *myoD* induction (Steinbach et al., 1998; Thayer et al., 1989). Fifteen potential E-boxes were identified by sequence comparison on the *myoD* locus. Three of them are located in the promoter and in the first exon and were shown to be able to support autocatalysis of the gene (Lun et al., 1997). The *in vivo* binding of MyoD to its own locus could not be shown yet. Therefore, rat monoclonal antibodies against MyoD were generated (see chapter 4.1.1, Figure 12) in order to perform ChIP

experiments. The antibodies MYO 6C8, MYO 5A9 and MYO 7F11 were raised. The antibody MYO 6C8 was identified as the most suitable for ChIP analyses. Although the antibody showed a good IP efficiency under formaldehyde-fixed ChIP condition, the time course ChIP analysis failed. Apart from the above-discussed technical reasons (see chapter 5.1.1 and following chapters), several biological reasons are conceivable. First of all, it is not known for how long after induction MyoD autocatalysis is required. Basal *myoD* expression is detectable from the start of the zygotic transcription at the mid-blastula stage (NF8) on (Rupp and Weintraub, 1991). The second reason could be that MyoD protein is only transiently bound to its target sites. Thus, it might be impossible to fix it to the DNA. The third possibility is that the antigen is very low abundant. Therefore, the precipitation efficiency might be below the background noise and as a consequence not detectable by real-time PCR.

5.2.2 Lef/Tcf transcription factors co-precipitate under ChIP-type IP conditions

The canonical Wnt/β-catenin signaling is one of the most important signaling cascades throughout embryonic development and adulthood. Its extracellular and cytoplasmic signal transmission is very well understood (see Figure 4). Upon Wnt stimulation the central, signal transmitting molecule β-catenin enters the nucleus and binds to its interaction partners like the Lef/Tcf proteins (for review e.g. (Moon et al., 2002; Wang and Wynshaw-Boris, 2004)). However, the signal transmission within the nucleus after the stabilization is less well studied. Therefore, antibodies against the transcription factors Lef1, Tcf1 and Tcf3 were raised in order to analyze, which of them and when they are bound to their sites at the Wnt target genes *siamois* or *myf5*. They were tested for their ability to detect their antigen by immunoblotting, immunofluorescence, immunocytochemistry, IP, and ChIP-type IP. Their specificity was tested in IPs and ChIP-type IPs. In native IPs (see Figure 16 & 17), the antibodies precipitated very specifically their antigen. Unexpectedly, under formaldehyde-fixed condition they precipitated apart from their specific antigen also the other Lef/Tcf family members (see Figure 18). I investigated this co-precipitation further with the bimolecular fluorescence complementation assay (Hu et al., 2002). Unfortunately in non-formaldehyde fixed samples, I could not detect any direct or short-range interaction among Lef/Tcf proteins. This analysis and the native Co-IP suggest

that the Lef/Tcfs do not interact directly with each other. However, they appear to be components of a large complex either in the nucleus or in the cytoplasm. Yet in this study, Lef1 and Tcf1 were localized in the nucleus (see Figures Appendix 3-8). So if they are present in the nucleus, they might be part of mediator complexes (Heintzman and Ren, 2007) and thereby trigger transcriptional processes. Another fact, which argues for a supercomplex, is the clustering of functional Lef/Tcf binding sites, typically associated with Wnt target gene promoters. For example, the *siamois* promoter harbors five Lef/Tcf binding sites within of 311bp (Brannon et al., 1997). However, further analyses will be needed to test this hypothesis. Co-immunoprecipitation experiments with components of the mediator complex like the TRAP220/MED1 subunit (Roeder, 2005) might help to determine the association of the Lef/Tcf proteins to a supercomplex. Furthermore, also components of the preinitiation complex (PIC) like TFIID (Chadick and Asturias, 2005) or hallmarks of active RNA polymerase II transcription like the phosphorylated C-terminal domain of RNA polymerase II are candidates for components of a mediator supercomplex associated upon Wnt target activation.

5.2.3 CHD4 binds to the *sip1* locus at exon 1

During gastrulation the three germlayers are formed. In *Xenopus*, the border between neuroectoderm and mesoderm is marked by the transcription factors *sip1* and *Xbra,* respectively (Papin et al., 2002; Wardle and Smith, 2006). A potential mechanisms for this border formation might be repression of *Xbra* mediated by Sip1 (Lerchner et al., 2000; Papin et al., 2002). On the other hand, the *sip1* gene expression was found to be under the regulation of CHD4 (Linder et al., 2007). In order to prove a direct regulation, I performed a ChIP analysis with CHD4 antibodies at the *sip1* locus. My results (see Figure 39) identified the *sip1* gene as a direct target of CHD4 in gastrula stage embryos (NF11), the stage, when the neuroectoderm/mesoderm boundary is formed. CHD4 was exclusively enriched at the first transcribed exon, but not at the untranslated exon U5 or at the 80kb downstream located transcribed exon 2. The binding of CHD4 to the locus might either be local at the exon E1 or might be spread along the locus. Further analysis will be necessary like ChIP-on-chip experiments with a tilling array to investigate the association of CHD4 to the *sip1* locus in detail with a high resolution.

In comparison to the ChIPs against the histone modifications, the standard deviations of this ChIP are low. This could be due to two technical reasons. First, a mixture of five monoclonal antibodies against different parts of CHD4 was used. This helped to increase the stability between the antibodies and the target protein. Second, in this ChIP assay we performed three independent IPs of the same lysate. This excludes variations of the lysate, which could lead to large standard deviations.

The direct binding of CHD4 to the *sip1* locus suggests for a binding at the active locus rather than the silent one, because over-expression of CHD4 protein reduced *sip1* mRNA levels in animal caps (Linder et al., 2007). This is in contrast to the prevailing opinion that the CHD4 containing NuRD complex is correlated with repressed loci (Bowen et al., 2004). However, *Drosophila* Mi-2/CHD4 is co-localized with activated RNA polymerase II in salivary gland polytene chromosome (Srinivasan et al., 2005). Furthermore, the human Mi-2 protein was shown be important for the re-initiation of the transcription elongation (Mellor, 2006a). Due to my observations and the cited publication, I suggest that CHD4 is involved in restricting *sip1* expression at the activated locus. Yet the subcomposition of the CHD4 protein complex and its recruitment to the *sip1* gene remains to be elucidated.

5.2.4 Conclusions

The examples discussed above illustrate that the two ChIP protocols, which I have adapted for the use in *Xenopus laevis*, provide biological information. The established ChIP protocols were successfully employed in *Xenopus laevis* embryos for different approaches. But the success of the experiments depends very much on the precipitation efficiency of the antibody and abundance of the protein-DNA interaction under investigation. Therefore, I come to the conclusion that our ChIP data are able to show qualitative trends of the association of proteins to specific genomic loci.

5.3 Outlook

In order to investigate how the genetic information is interpreted on the level of the chromatin template during cellular differentiation, I have established and adapted two ChIP protocols for *Xenopus laevis*. They provide a powerful tool to study the direct interaction of proteins with specific genomic loci in early frog embryos. Future ChIP approaches will help to gain further insight into the regulation of key regulators of *Xenopus* development.

For instance, the window of myogenic competence is very likely determined by the chromatin composition. Somatic linker histone variants were shown to be rate limiting for the induction of *myoD* (Steinbach et al., 1997). ChIP analyses with maternal and somatic linker histones would be very useful to gain more insights into the induction processes of the gene.

Moreover, Polycomb-group (PcG) of proteins are important negative regulators of *myoD* in mice and humans (Caretti et al., 2004; Lee et al., 2006). Therefore, members of the PcG protein family are candidate negative regulators of the *Xenopus myoD* locus. ChIP approaches with components of the PcG of proteins like Suz12, Eed or YY1 would support the understanding of the regulation of the skeletal muscle regulator *myoD*.

Furthermore, CHD4 was shown to be important for the positioning of the neuroectoderm/mesoderm germlayer boundary (Linder et al., 2007) by constraining the expression of the neuroectoderm marker *sip1*. A continuative αCHD4 ChIP approach with SYBR Green amplicons located on the entire *sip1* locus would help to understand how CHD4 is involved in quantitative transcription control.

In general, ChIP is a potent technology to study direct physical interactions of proteins and DNA. By genetic and interference analyses in contrast, regulatory hierarchies can be determined, but it is not possible to determine, whether the regulation is direct or not. For *Xenopus laevis,* which is the best understood model organism concerning the early embryonic vertebrate development, connections of genetic regulatory networks were investigated in detail (Loose and Patient, 2004). The ChIP technology will provide important data to hardwire the regulatory networks in *Xenopus*, which promote differentiation processes. In addition, if the properties of chromatin and associated factors on exemplary gene loci like *myoD* and *sip1* over the period of embryonic

development is identified, cell fate determination processes will be better understood.

6 Abbreviations

ATP	adenosine triphosphate
bHLH	basic helix-loop-helix
bp	base pairs
cDNA	complementary DNA
ChIP	chromatin immunoprecipitation
Ct	Cycle number, when the threshold is crossed (real-time PCR, see Figure 21)
DEPC	diethlypryocarbonate
ddH_2O	double-distilled water
DNA	deoxyribonucleic acid
eeq	embryo equivalents
e.g.	exempli gratia, for example
EST	expressed sequence tag
et al.	et alii, and others
etc.	et cetera
g	gram
GFP	green fluorescent protein
GST	glutathione S-transferase
h	hour
HAT	histone acetyltransferase
HDAC	histone deacetylase
H3K4me2	example for abbreviation of histone modification, here: dimethylation of lysine 4 on Histone H3
HMG	high mobility group
hpf	hours post fertilization
ICC	immunocytochemistry
i.e.	id est, it is
IF	immunofluorescence
IP	immunoprecipitation
l	liter
kDa	kilodaltons
min	minutes

M	molar
MBT	mid-blastula transition
ml	milliliter
mM	millimolar
mRNA	messenger ribonucleic acid
NF	*Xenopus* developmental stages according to the normal table of staging of *Xenopus laevis* (Daudin) after (Niewkoop and Faber, 1994)
ng	nanogram
nm	nanometer
NTPs	nucleotide triphosphate mixture containing adenosine, guanidine, uridine and cytosine
OD	optical density
PCR	polymerase chain reaction
pmol	picomol
REMI	restriction enzyme-mediated integration
RNA	ribonucleic acid
rpm	revolutions per minute
RT	room temperature
RT-PCR	reverse transcription polymerase chain reaction
SDS	sodium dodecyl sulfate
SDS-PAGE	sodium dodecyl sulfate polyacrylamide gelelectrophoresis
sec	seconds
TSA	Trichostatin A
UV	ultraviolet
WB	Western blot analysis
µg	microgram
µl	microliter
µM	micromolar

7 References

Alberts, B., Jonhanson, J., Lewis, J., Raff, M., Roberts, K. and Walter, P. (2004) *Molekularbiologie der Zelle*. WILEY-VCH, Weinheim.

Allfrey, V.G., Faulkner, R. and Mirsky, A.E. (1964) Acetylation and Methylation of Histones and Their Possible Role in the Regulation of Rna Synthesis. *Proc Natl Acad Sci U S A*, **51**, 786-794.

Allis CD, J.T., Reinberg D, Caparros ML. (2007) *Epigenetics*. Cold Spring Harbor Laboratory Press, Cold Spring Harbor, New York, USA.

Ariizumi, T. and Asashima, M. (2001) In vitro induction systems for analyses of amphibian organogenesis and body patterning. *Int J Dev Biol*, **45**, 273-279.

Azuara, V., Perry, P., Sauer, S., Spivakov, M., Jorgensen, H.F., John, R.M., Gouti, M., Casanova, M., Warnes, G., Merkenschlager, M. and Fisher, A.G. (2006) Chromatin signatures of pluripotent cell lines. *Nat Cell Biol*, **8**, 532-538.

Bader, D., Masaki, T. and Fischman, D.A. (1982) Immunochemical analysis of myosin heavy chain during avian myogenesis in vivo and in vitro. *J Cell Biol*, **95**, 763-770.

Becker, P.B. and Horz, W. (2002) ATP-dependent nucleosome remodeling. *Annu Rev Biochem*, **71**, 247-273.

Bernstein, B.E., Mikkelsen, T.S., Xie, X., Kamal, M., Huebert, D.J., Cuff, J., Fry, B., Meissner, A., Wernig, M., Plath, K., Jaenisch, R., Wagschal, A., Feil, R., Schreiber, S.L. and Lander, E.S. (2006) A bivalent chromatin structure marks key developmental genes in embryonic stem cells. *Cell*, **125**, 315-326.

Bernstein, E. and Hake, S.B. (2006) The nucleosome: a little variation goes a long way. *Biochem Cell Biol*, **84**, 505-517.

Bork, P. and Koonin, E.V. (1993) An expanding family of helicases within the 'DEAD/H' superfamily. *Nucleic Acids Res*, **21**, 751-752.

Bouazoune, K. and Brehm, A. (2006) ATP-dependent chromatin remodeling complexes in Drosophila. *Chromosome Res*, **14**, 433-449.

Bowen, N.J., Fujita, N., Kajita, M. and Wade, P.A. (2004) Mi-2/NuRD: multiple complexes for many purposes. *Biochim Biophys Acta*, **1677**, 52-57.

Bracken, A.P., Dietrich, N., Pasini, D., Hansen, K.H. and Helin, K. (2006) Genome-wide mapping of Polycomb target genes unravels their roles in cell fate transitions. *Genes Dev*, **20**, 1123-1136.

Brackertz, M., Boeke, J., Zhang, R. and Renkawitz, R. (2002) Two highly related p66 proteins comprise a new family of potent transcriptional repressors interacting with MBD2 and MBD3. *J Biol Chem*, **277**, 40958-40966.

Brackertz, M., Gong, Z., Leers, J. and Renkawitz, R. (2006) p66alpha and p66beta of the Mi-2/NuRD complex mediate MBD2 and histone interaction. *Nucleic Acids Res*, **34**, 397-406.

Brannon, M., Gomperts, M., Sumoy, L., Moon, R.T. and Kimelman, D. (1997) A beta-catenin/XTcf-3 complex binds to the siamois promoter to regulate dorsal axis specification in Xenopus. *Genes Dev*, **11**, 2359-2370.

Brannon, M. and Kimelman, D. (1996) Activation of Siamois by the Wnt pathway. *Dev Biol*, **180**, 344-347.

Braunstein, M., Rose, A.B., Holmes, S.G., Allis, C.D. and Broach, J.R. (1993) Transcriptional silencing in yeast is associated with reduced nucleosome acetylation. *Genes Dev*, **7**, 592-604.

Brown, D.D., Wang, Z., Furlow, J.D., Kanamori, A., Schwartzman, R.A., Remo, B.F. and Pinder, A. (1996) The thyroid hormone-induced tail resorption program during Xenopus laevis metamorphosis. *Proc Natl Acad Sci U S A*, **93**, 1924-1929.

Brown, J.L., Mucci, D., Whiteley, M., Dirksen, M.L. and Kassis, J.A. (1998) The Drosophila Polycomb group gene pleiohomeotic encodes a DNA binding protein with homology to the transcription factor YY1. *Mol Cell*, **1**, 1057-1064.

Brutlag, D., Schlehuber, C. and Bonner, J. (1969) Properties of formaldehyde-treated nucleohistone. *Biochemistry*, **8**, 3214-3218.

Bultman, S., Gebuhr, T., Yee, D., La Mantia, C., Nicholson, J., Gilliam, A., Randazzo, F., Metzger, D., Chambon, P., Crabtree, G. and Magnuson, T. (2000) A Brg1 null mutation in the mouse reveals functional differences among mammalian SWI/SNF complexes. *Mol Cell*, **6**, 1287-1295.

Caretti, G., Di Padova, M., Micales, B., Lyons, G.E. and Sartorelli, V. (2004) The Polycomb Ezh2 methyltransferase regulates muscle gene expression and skeletal muscle differentiation. *Genes Dev*, **18**, 2627-2638.

Chadick, J.Z. and Asturias, F.J. (2005) Structure of eukaryotic Mediator complexes. *Trends Biochem Sci*, **30**, 264-271.

Chanas, G., Lavrov, S., Iral, F., Cavalli, G. and Maschat, F. (2004) Engrailed and polyhomeotic maintain posterior cell identity through cubitus-interruptus regulation. *Dev Biol*, **272**, 522-535.

Cheng, D., Cote, J., Shaaban, S. and Bedford, M.T. (2007) The arginine methyltransferase CARM1 regulates the coupling of transcription and mRNA processing. *Mol Cell*, **25**, 71-83.

Chiba, H., Muramatsu, M., Nomoto, A. and Kato, H. (1994) Two human homologues of Saccharomyces cerevisiae SWI2/SNF2 and Drosophila brahma are transcriptional coactivators cooperating with the estrogen receptor and the retinoic acid receptor. *Nucleic Acids Res*, **22**, 1815-1820.

Christian, J.L., McMahon, J.A., McMahon, A.P. and Moon, R.T. (1991) Xwnt-8, a Xenopus Wnt-1/int-1-related gene responsive to mesoderm-inducing growth factors, may play a role in ventral mesodermal patterning during embryogenesis. *Development*, **111**, 1045-1055.

Cooper, S.J., Trinklein, N.D., Nguyen, L. and Myers, R.M. (2007) Serum response factor binding sites differ in three human cell types. *Genome Res*, **17**, 136-144.

Cremer, T., Cremer, M., Dietzel, S., Muller, S., Solovei, I. and Fakan, S. (2006) Chromosome territories--a functional nuclear landscape. *Curr Opin Cell Biol*, **18**, 307-316.

Cuthbert, G.L., Daujat, S., Snowden, A.W., Erdjument-Bromage, H., Hagiwara, T., Yamada, M., Schneider, R., Gregory, P.D., Tempst, P., Bannister, A.J. and Kouzarides, T. (2004) Histone deimination antagonizes arginine methylation. *Cell*, **118**, 545-553.

Darken, R.S. and Wilson, P.A. (2001) Axis induction by wnt signaling: Target promoter responsiveness regulates competence. *Dev Biol*, **234**, 42-54.

Davis, R.L., Weintraub, H. and Lassar, A.B. (1987) Expression of a single transfected cDNA converts fibroblasts to myoblasts. *Cell*, **51**, 987-1000.

Dedon, P.C., Soults, J.A., Allis, C.D. and Gorovsky, M.A. (1991) A simplified formaldehyde fixation and immunoprecipitation technique for studying protein-DNA interactions. *Anal Biochem*, **197**, 83-90.

Delmas, V., Stokes, D.G. and Perry, R.P. (1993) A mammalian DNA-binding protein that contains a chromodomain and an SNF2/SWI2-like helicase domain. *Proc Natl Acad Sci U S A*, **90**, 2414-2418.

Dhawan, J. and Helfman, D.M. (2004) Modulation of acto-myosin contractility in skeletal muscle myoblasts uncouples growth arrest from differentiation. *J Cell Sci*, **117**, 3735-3748.

Dimitrov, S., Almouzni, G., Dasso, M. and Wolffe, A.P. (1993) Chromatin transitions during early Xenopus embryogenesis: changes in histone H4 acetylation and in linker histone type. *Dev Biol*, **160**, 214-227.

Dworkin-Rastl, E., Kandolf, H. and Smith, R.C. (1994) The maternal histone H1 variant, H1M (B4 protein), is the predominant H1 histone in Xenopus pregastrula embryos. *Dev Biol*, **161**, 425-439.

Eisaki, A., Kuroda, H., Fukui, A. and Asashima, M. (2000) XSIP1, a member of two-handed zinc finger proteins, induced anterior neural markers in Xenopus laevis animal cap. *Biochem Biophys Res Commun*, **271**, 151-157.

Eisen, J.A., Sweder, K.S. and Hanawalt, P.C. (1995) Evolution of the SNF2 family of proteins: subfamilies with distinct sequences and functions. *Nucleic Acids Res*, **23**, 2715-2723.

Elgin, S.C. and Grewal, S.I. (2003) Heterochromatin: silence is golden. *Curr Biol*, **13**, R895-898.

Engländer, H. (1962) Die Differenzierungsleistungen des Triturus- und Amlystoma-Ektoderms unter der Einwirkung von Knochenmark. *Wilhelm Roux' Archiv. Entwickl.-Mech. Org*, **154**, 143-159.

Evan, G.I., Lewis, G.K., Ramsay, G. and Bishop, J.M. (1985) Isolation of monoclonal antibodies specific for human c-myc proto-oncogene product. *Mol Cell Biol*, **5**, 3610-3616.

Fagotto, F. and Gumbiner, B.M. (1994) Beta-catenin localization during Xenopus embryogenesis: accumulation at tissue and somite boundaries. *Development*, **120**, 3667-3679.

Feng, Q., Cao, R., Xia, L., Erdjument-Bromage, H., Tempst, P. and Zhang, Y. (2002) Identification and functional characterization of the p66/p68 components of the MeCP1 complex. *Mol Cell Biol*, **22**, 536-546.

Feng, Q. and Zhang, Y. (2001) The MeCP1 complex represses transcription through preferential binding, remodeling, and deacetylating methylated nucleosomes. *Genes Dev*, **15**, 827-832.

Ficzycz, A., Eskiw, C., Meyer, D., Marley, K.E., Hurt, M. and Ovsenek, N. (2001) Expression, activity, and subcellular localization of the Yin Yang 1 transcription factor in Xenopus oocytes and embryos. *J Biol Chem*, **276**, 22819-22825.

Finnin, M.S., Donigian, J.R., Cohen, A., Richon, V.M., Rifkind, R.A., Marks, P.A., Breslow, R. and Pavletich, N.P. (1999) Structures of a histone deacetylase homologue bound to the TSA and SAHA inhibitors. *Nature*, **401**, 188-193.

Fischle, W., Wang, Y. and Allis, C.D. (2003) Histone and chromatin cross-talk. *Curr Opin Cell Biol*, **15**, 172-183.

Flemming, W. (1882) *Zellsubstanz, Kern und Zelltheilung*. Vogel, Leipzig.

Fujita, N., Jaye, D.L., Geigerman, C., Akyildiz, A., Mooney, M.R., Boss, J.M. and Wade, P.A. (2004) MTA3 and the Mi-2/NuRD complex regulate cell fate during B lymphocyte differentiation. *Cell*, **119**, 75-86.

Fujita, N., Jaye, D.L., Kajita, M., Geigerman, C., Moreno, C.S. and Wade, P.A. (2003) MTA3, a Mi-2/NuRD complex subunit, regulates an invasive growth pathway in breast cancer. *Cell*, **113**, 207-219.

Gebhardt, D.O. and Nieuwkoop, P.D. (1964) The Influence of Lithium on the Competence of the Ectoderm in Ambystoma Mexicanum. *J Embryol Exp Morphol*, **12**, 317-331.

Gelius, B., Wade, P., Wolffe, A., Wrange, O. and Ostlund Farrants, A.K. (1999) Characterization of a chromatin remodelling activity in Xenopus oocytes. *Eur J Biochem*, **262**, 426-434.

Gilbert, S.F. (2006) *Develpomental Biology*. Sinauer Asscociates, Inc, Sunderland, MA,USA.

Gilmour, D.S. and Lis, J.T. (1984) Detecting protein-DNA interactions in vivo: distribution of RNA polymerase on specific bacterial genes. *Proc Natl Acad Sci U S A*, **81**, 4275-4279.

Gilmour, D.S., Rougvie, A.E. and Lis, J.T. (1991) Protein-DNA cross-linking as a means to determine the distribution of proteins on DNA in vivo. *Methods Cell Biol*, **35**, 369-381.

Goldberg, A.D., Allis, C.D. and Bernstein, E. (2007) Epigenetics: a landscape takes shape. *Cell*, **128**, 635-638.

Gorbalenya, A.E., Koonin, E.V., Donchenko, A.P. and Blinov, V.M. (1989) Two related superfamilies of putative helicases involved in replication, recombination, repair and expression of DNA and RNA genomes. *Nucleic Acids Res*, **17**, 4713-4730.

Grainger, R.M. and Gurdon, J.B. (1989) Loss of competence in amphibian induction can take place in single nondividing cells. *Proc Natl Acad Sci U S A*, **86**, 1900-1904.

Green, J.B., New, H.V. and Smith, J.C. (1992) Responses of embryonic Xenopus cells to activin and FGF are separated by multiple dose thresholds and correspond to distinct axes of the mesoderm. *Cell*, **71**, 731-739.

Grewal, S.I. and Jia, S. (2007) Heterochromatin revisited. *Nat Rev Genet*, **8**, 35-46.

Grobstein, C. (1953) Morphogenetic interaction between embryonic mouse tissues separated by a membrane filter. *Nature*, **172**, 869-870.

Grunz, H. (1968) Experimentelle Untersuchungen über die Kompetenzverhältnisse füherer Entwicklungstadien des Amphibien-Ektoderms *Wilhelm Roux' Archiv* **160**, 344-374.

Grunz, H. (1969) Hemmung der Reaggregation dissozierter Amphibienzellen durch Inhibition der RNS- und Proteinsynthese. *Wilhelm Roux' Archiv*, **163**, 184-196.

Grunz H. (1970) Abhängigkeit der Kompetenz des Amphibien-Ektoderms von der Proteinsynthese. *Wilhelm Roux' Archiv*, **168**, 91-102.

Grunz, H., McKeehan, W.L., Knochel, W., Born, J., Tiedemann, H. and Tiedemann, H. (1988) Induction of mesodermal tissues by acidic and basic heparin binding growth factors. *Cell Differ*, **22**, 183-189.

Grunz, H. and Tacke, L. (1986) Embryonic induction in amphibians. *Prog Clin Biol Res*, **217A**, 135-138.

Hansen, J.C. (2002) Conformational dynamics of the chromatin fiber in solution: determinants, mechanisms, and functions. *Annu Rev Biophys Biomol Struct*, **31**, 361-392.

Harlow E, L.D. (1988) *Antibodies- A Laboratory Manual*. Cold Spring Harbor Laboratory.

Heasman, J. (2006) Patterning the early Xenopus embryo. *Development*, **133**, 1205-1217.

Hecht, A., Strahl-Bolsinger, S. and Grunstein, M. (1996) Spreading of transcriptional repressor SIR3 from telomeric heterochromatin. *Nature*, **383**, 92-96.

Hecht, A., Vleminckx, K., Stemmler, M.P., van Roy, F. and Kemler, R. (2000) The p300/CBP acetyltransferases function as transcriptional coactivators of beta-catenin in vertebrates. *Embo J*, **19**, 1839-1850.

Heintzman, N.D. and Ren, B. (2007) The gateway to transcription: identifying, characterizing and understanding promoters in the eukaryotic genome. *Cell Mol Life Sci*, **64**, 386-400.

Heintzman, N.D., Stuart, R.K., Hon, G., Fu, Y., Ching, C.W., Hawkins, R.D., Barrera, L.O., Van Calcar, S., Qu, C., Ching, K.A., Wang, W., Weng, Z., Green, R.D., Crawford, G.E. and Ren, B. (2007) Distinct and predictive chromatin signatures of transcriptional promoters and enhancers in the human genome. *Nat Genet*, **39**, 311-318.

Heitz, E. (1928) Das Heterochromatin der Moose. *Jahrb Wiss Botanik*, **69**, 762-818.

Henikoff, S. (2000) Heterochromatin function in complex genomes. *Biochim Biophys Acta*, **1470**, O1-8.

Hopwood, N.D., Pluck, A. and Gurdon, J.B. (1989) MyoD expression in the forming somites is an early response to mesoderm induction in Xenopus embryos. *Embo J*, **8**, 3409-3417.

Hopwood, N.D., Pluck, A., Gurdon, J.B. and Dilworth, S.M. (1992) Expression of XMyoD protein in early *Xenopus laevis* embryos. *Development*, **114**, 31-38.

Houston, D.W., Kofron, M., Resnik, E., Langland, R., Destree, O., Wylie, C. and Heasman, J. (2002) Repression of organizer genes in dorsal and ventral Xenopus cells mediated by maternal XTcf3. *Development*, **129**, 4015-4025.

Hovanes, K., Li, T.W., Munguia, J.E., Truong, T., Milovanovic, T., Lawrence Marsh, J., Holcombe, R.F. and Waterman, M.L. (2001) Beta-catenin-sensitive isoforms of lymphoid enhancer factor-1 are selectively expressed in colon cancer. *Nat Genet*, **28**, 53-57.

Hu, C.D., Chinenov, Y. and Kerppola, T.K. (2002) Visualization of interactions among bZIP and Rel family proteins in living cells using bimolecular fluorescence complementation. *Mol Cell*, **9**, 789-798.

Ilyin, Y.V. and Georgiev, G.P. (1969) Heterogeneity of deoxynucleoprotein particles as evidencec by ultracentrifugation of cesium chloride density gradient. *J Mol Biol*, **41**, 299-303.

Iyer, V.R., Horak, C.E., Scafe, C.S., Botstein, D., Snyder, M. and Brown, P.O. (2001) Genomic binding sites of the yeast cell-cycle transcription factors SBF and MBF. *Nature*, **409**, 533-538.

Jackson, V. (1978) Studies on histone organization in the nucleosome using formaldehyde as a reversible cross-linking agent. *Cell*, **15**, 945-954.

Jenuwein, T. and Allis, C.D. (2001) Translating the histone code. *Science*, **293**, 1074-1080.

Jerzmanowski, J. (2004) *The linker histones. In Chromatin Structure and Dynamics: State-of-the-Art.* Elsevier B.V., London.

Kennison, J.A. and Tamkun, J.W. (1988) Dosage-dependent modifiers of polycomb and antennapedia mutations in Drosophila. *Proc Natl Acad Sci U S A*, **85**, 8136-8140.

Khavari, P.A., Peterson, C.L., Tamkun, J.W., Mendel, D.B. and Crabtree, G.R. (1993) BRG1 contains a conserved domain of the SWI2/SNF2 family necessary for normal mitotic growth and transcription. *Nature*, **366**, 170-174.

Kimura, H. (2005) Histone dynamics in living cells revealed by photobleaching. *DNA Repair (Amst)*, **4**, 939-950.

Klose, R.J., Gardner, K.E., Liang, G., Erdjument-Bromage, H., Tempst, P. and Zhang, Y. (2007) Demethylation of histone H3K36 and H3K9 by Rph1: a vestige of an H3K9 methylation system in Saccharomyces cerevisiae? *Mol Cell Biol*.

Konig, A., Gradl, D., Kuhl, M. and Wedlich, D. (2000) The HMG-box transcription factor XTcf-4 demarcates the forebrain-midbrain boundary. *Mech Dev*, **93**, 211-214.

Kornberg, R.D. (1974) Chromatin structure: a repeating unit of histones and DNA. *Science*, **184**, 868-871.

Kouzarides, T. (2007) Chromatin modifications and their function. *Cell*, **128**, 693-705.

Kunz, M., Herrmann, M., Wedlich, D. and Gradl, D. (2004) Autoregulation of canonical Wnt signaling controls midbrain development. *Dev Biol*, **273**, 390-401.

Kwon, H.J. and Chung, H.M. (2003) Yin Yang 1, a vertebrate polycomb group gene, regulates antero-posterior neural patterning. *Biochem Biophys Res Commun*, **306**, 1008-1013.

Langst, G. and Becker, P.B. (2001) Nucleosome mobilization and positioning by ISWI-containing chromatin-remodeling factors. *J Cell Sci*, **114**, 2561-2568.

Latinkic, B.V., Cooper, B., Smith, S., Kotecha, S., Towers, N., Sparrow, D. and Mohun, T.J. (2004) Transcriptional regulation of the cardiac-specific MLC2 gene during Xenopus embryonic development. *Development*, **131**, 669-679.

Latinkic, B.V., Cooper, B., Towers, N., Sparrow, D., Kotecha, S. and Mohun, T.J. (2002) Distinct enhancers regulate skeletal and cardiac muscle-specific expression programs of the cardiac alpha-actin gene in Xenopus embryos. *Dev Biol*, **245**, 57-70.

Latinkic, B.V., Umbhauer, M., Neal, K.A., Lerchner, W., Smith, J.C. and Cunliffe, V. (1997) The Xenopus Brachyury promoter is activated by FGF and low concentrations of activin and suppressed by high concentrations of activin and by paired-type homeodomain proteins. *Genes Dev*, **11**, 3265-3276.

Laurent, M.N., Blitz, I.L., Hashimoto, C., Rothbacher, U. and Cho, K.W. (1997) The Xenopus homeobox gene twin mediates Wnt induction of goosecoid in establishment of Spemann's organizer. *Development*, **124**, 4905-4916.

Lee, D.Y., Teyssier, C., Strahl, B.D. and Stallcup, M.R. (2005) Role of protein methylation in regulation of transcription. *Endocr Rev*, **26**, 147-170.

Lee, H., Habas, R. and Abate-Shen, C. (2004) MSX1 cooperates with histone H1b for inhibition of transcription and myogenesis. *Science*, **304**, 1675-1678.

Lee, T.I., Jenner, R.G., Boyer, L.A., Guenther, M.G., Levine, S.S., Kumar, R.M., Chevalier, B., Johnstone, S.E., Cole, M.F., Isono, K., Koseki, H., Fuchikami, T., Abe, K., Murray, H.L., Zucker, J.P., Yuan, B., Bell, G.W., Herbolsheimer, E., Hannett, N.M., Sun, K., Odom, D.T., Otte, A.P., Volkert, T.L., Bartel, D.P., Melton, D.A., Gifford, D.K., Jaenisch, R. and Young, R.A. (2006) Control of developmental regulators by Polycomb in human embryonic stem cells. *Cell*, **125**, 301-313.

Leikola, A. (1965) On the loss of mesodermal competence of the Triturus gastrula ectoderm in vivo. *Experientia*, **21**, 458-459.

Lerchner, W., Latinkic, B.V., Remacle, J.E., Huylebroeck, D. and Smith, J.C. (2000) Region-specific activation of the Xenopus brachyury promoter involves active

repression in ectoderm and endoderm: a study using transgenic frog embryos. *Development*, **127**, 2729-2739.

Levine, S.S., King, I.F. and Kingston, R.E. (2004) Division of labor in polycomb group repression. *Trends Biochem Sci*, **29**, 478-485.

Linder, B., Cabot, R.A., Schwickert, T. and Rupp, R.A. (2004) The SNF2 domain protein family in higher vertebrates displays dynamic expression patterns in Xenopus laevis embryos. *Gene*, **326**, 59-66.

Linder, B., Mentele, E., Mansperger, K., Straub, T., Kremmer, E. and Rupp, R.A. (2007) CHD4/Mi-2beta activity is required for the positioning of the mesoderm/neuroectoderm boundary in Xenopus. *Genes Dev*, **21**, 973-983.

Liu, F., van den Broek, O., Destree, O. and Hoppler, S. (2005) Distinct roles for Xenopus Tcf/Lef genes in mediating specific responses to Wnt/{beta}-catenin signalling in mesoderm development. *Development*, **132**, 5375-5385.

Loose, M. and Patient, R. (2004) A genetic regulatory network for Xenopus mesendoderm formation. *Dev Biol*, **271**, 467-478.

Luger, K., Mader, A.W., Richmond, R.K., Sargent, D.F. and Richmond, T.J. (1997) Crystal structure of the nucleosome core particle at 2.8 A resolution. *Nature*, **389**, 251-260.

Lun, Y., Sawadogo, M. and Perry, M. (1997) Autoactivation of Xenopus MyoD transcription and its inhibition by USF. *Cell Growth Differ*, **8**, 275-282.

McKendry, R., Hsu, S.C., Harland, R.M. and Grosschedl, R. (1997) LEF-1/TCF proteins mediate wnt-inducible transcription from the Xenopus nodal-related 3 promoter. *Dev Biol*, **192**, 420-431.

Mellor, J. (2006a) Dynamic nucleosomes and gene transcription. *Trends Genet*, **22**, 320-329.

Mellor, J. (2006b) It takes a PHD to read the histone code. *Cell*, **126**, 22-24.

Miralles, F., Posern, G., Zaromytidou, A.I. and Treisman, R. (2003) Actin dynamics control SRF activity by regulation of its coactivator MAL. *Cell*, **113**, 329-342.

Misteli, T. (2007) Beyond the sequence: cellular organization of genome function. *Cell*, **128**, 787-800.

Molenaar, M., Roose, J., Peterson, J., Venanzi, S., Clevers, H. and Destree, O. (1998) Differential expression of the HMG box transcription factors XTcf-3 and XLef-1 during early xenopus development. *Mech Dev*, **75**, 151-154.

Moon, R.T., Bowerman, B., Boutros, M. and Perrimon, N. (2002) The promise and perils of Wnt signaling through beta-catenin. *Science*, **296**, 1644-1646.

Morgan, M.J., Woltering, J.M., In der Rieden, P.M., Durston, A.J. and Thiery, J.P. (2004) YY1 regulates the neural crest-associated slug gene in Xenopus laevis. *J Biol Chem*, **279**, 46826-46834.

Morin, R.D., Chang, E., Petrescu, A., Liao, N., Griffith, M., Chow, W., Kirkpatrick, R., Butterfield, Y.S., Young, A.C., Stott, J., Barber, S., Babakaiff, R., Dickson, M.C., Matsuo, C., Wong, D., Yang, G.S., Smailus, D.E., Wetherby, K.D., Kwong, P.N., Grimwood, J., Brinkley, C.P., 3rd, Brown-John, M., Reddix-Dugue, N.D., Mayo, M., Schmutz, J., Beland, J., Park, M., Gibson, S., Olson, T., Bouffard, G.G., Tsai, M., Featherstone, R., Chand, S., Siddiqui, A.S., Jang, W., Lee, E., Klein, S.L., Blakesley, R.W., Zeeberg, B.R., Narasimhan, S., Weinstein, J.N., Pennacchio, C.P., Myers, R.M., Green, E.D., Wagner, L., Gerhard, D.S., Marra, M.A., Jones, S.J. and Holt, R.A. (2006) Sequencing and analysis of 10,967 full-length cDNA clones from Xenopus laevis and Xenopus tropicalis reveals post-tetraploidization transcriptome remodeling. *Genome Res*, **16**, 796-803.

Muchardt, C. and Yaniv, M. (1993) A human homologue of Saccharomyces cerevisiae SNF2/SWI2 and Drosophila brm genes potentiates transcriptional activation by the glucocorticoid receptor. *Embo J*, **12**, 4279-4290.

Murray, K. (1964) The Occurrence of Epsilon-N-Methyl Lysine in Histones. *Biochemistry*, **3**, 10-15.

Myers, F.A., Evans, D.R., Clayton, A.L., Thorne, A.W. and Crane-Robinson, C. (2001) Targeted and extended acetylation of histones H4 and H3 at active and inactive genes in chicken embryo erythrocytes. *J Biol Chem*, **276**, 20197-20205.

Nelles, L., Van de Putte, T., van Grunsven, L., Huylebroeck, D. and Verschueren, K. (2003) Organization of the mouse Zfhx1b gene encoding the two-handed zinc finger repressor Smad-interacting protein-1. *Genomics*, **82**, 460-469.

Nemeth, A. and Langst, G. (2004) Chromatin higher order structure: opening up chromatin for transcription. *Brief Funct Genomic Proteomic*, **2**, 334-343.

Nentwich, O. (2003) Die Rolle von SRF und assoziierter Proteine in der frühen Embryonalentwicklung von *Xenopus laevis*. *Fakultät für Biologie*. Eberhard-Karls-Universität Tübingen, Tübingen, Vol. PhD.

Niewkoop, P.D. and Faber, J. (1994) *Normal Table of Xenopus laevis (daudin)*. GARLAND PUBLISHING ,INC., New York & London.

Nightingale, K.P., O'Neill, L.P. and Turner, B.M. (2006) Histone modifications: signalling receptors and potential elements of a heritable epigenetic code. *Curr Opin Genet Dev*, **16**, 125-136.

Nitta, K.R., Tanegashima, K., Takahashi, S. and Asashima, M. (2004) XSIP1 is essential for early neural gene expression and neural differentiation by suppression of BMP signaling. *Dev Biol*, **275**, 258-267.

O'Geen, H., Nicolet, C.M., Blahnik, K., Green, R. and Farnham, P.J. (2006) Comparison of sample preparation methods for ChIP-chip assays. *Biotechniques*, **41**, 577-580.

Orlando, V., Strutt, H. and Paro, R. (1997) Analysis of chromatin structure by in vivo formaldehyde cross-linking. *Methods*, **11**, 205-214.

Otto, A. (2000) Transkritptionelle Regulation des *Xenopus myoD* Gens - eine *cis*-Element-Analyse in transgenen Froschembryonen. *Fakultät fü Biologie*. Eberhard-Karls-Universität Tübingen, Tübingen, Vol. PhD.

Panitz, F., Krain, B., Hollemann, T., Nordheim, A. and Pieler, T. (1998) The Spemann organizer-expressed zinc finger gene Xegr-1 responds to the MAP kinase/Ets-SRF signal transduction pathway. *Embo J*, **17**, 4414-4425.

Papin, C., van Grunsven, L.A., Verschueren, K., Huylebroeck, D. and Smith, J.C. (2002) Dynamic regulation of Brachyury expression in the amphibian embryo by XSIP1. *Mech Dev*, **111**, 37-46.

Park, J.I., Kim, S.W., Lyons, J.P., Ji, H., Nguyen, T.T., Cho, K., Barton, M.C., Deroo, T., Vleminckx, K., Moon, R.T. and McCrea, P.D. (2005) Kaiso/p120-catenin and TCF/beta-catenin complexes coordinately regulate canonical Wnt gene targets. *Dev Cell*, **8**, 843-854.

Paro, R. and Hogness, D.S. (1991) The Polycomb protein shares a homologous domain with a heterochromatin-associated protein of Drosophila. *Proc Natl Acad Sci U S A*, **88**, 263-267.

Phillips, D.M. (1963) The presence of acetyl groups of histones. *Biochem J*, **87**, 258-263.

Pickart, C.M. and Cohen, R.E. (2004) Proteasomes and their kin: proteases in the machine age. *Nat Rev Mol Cell Biol*, **5**, 177-187.

Pownall, M.E., Gustafsson, M.K. and Emerson, C.P., Jr. (2002) Myogenic regulatory factors and the specification of muscle progenitors in vertebrate embryos. *Annu Rev Cell Dev Biol*, **18**, 747-783.

Prigent, C. and Dimitrov, S. (2003) Phosphorylation of serine 10 in histone H3, what for? *J Cell Sci*, **116**, 3677-3685.

Pukrop, T., Gradl, D., Henningfeld, K.A., Knochel, W., Wedlich, D. and Kuhl, M. (2001) Identification of two regulatory elements within the high mobility group box transcription factor XTCF-4. *J Biol Chem*, **276**, 8968-8978.

Puri, P.L., Sartorelli, V., Yang, X.J., Hamamori, Y., Ogryzko, V.V., Howard, B.H., Kedes, L., Wang, J.Y., Graessmann, A., Nakatani, Y. and Levrero, M. (1997) Differential roles of p300 and PCAF acetyltransferases in muscle differentiation. *Mol Cell*, **1**, 35-45.

Randazzo, F.M., Khavari, P., Crabtree, G., Tamkun, J. and Rossant, J. (1994) brg1: a putative murine homologue of the Drosophila brahma gene, a homeotic gene regulator. *Dev Biol*, **161**, 229-242.

Reinke, H. and Horz, W. (2003) Histones are first hyperacetylated and then lose contact with the activated PHO5 promoter. *Mol Cell*, **11**, 1599-1607.

Ren, B., Robert, F., Wyrick, J.J., Aparicio, O., Jennings, E.G., Simon, I., Zeitlinger, J., Schreiber, J., Hannett, N., Kanin, E., Volkert, T.L., Wilson, C.J., Bell, S.P. and Young, R.A. (2000) Genome-wide location and function of DNA binding proteins. *Science*, **290**, 2306-2309.

Robinson, P.J. and Rhodes, D. (2006) Structure of the '30 nm' chromatin fibre: a key role for the linker histone. *Curr Opin Struct Biol*, **16**, 336-343.

Roeder, R.G. (2005) Transcriptional regulation and the role of diverse coactivators in animal cells. *FEBS Lett*, **579**, 909-915.

Roel, G., Hamilton, F.S., Gent, Y., Bain, A.A., Destree, O. and Hoppler, S. (2002) Lef-1 and Tcf-3 transcription factors mediate tissue-specific Wnt signaling during Xenopus development. *Curr Biol*, **12**, 1941-1945.

Roel, G., van den Broek, O., Spieker, N., Peterson-Maduro, J. and Destree, O. (2003) Tcf-1 expression during Xenopus development. *Gene Expr Patterns*, **3**, 123-126.

Rosa, F., Roberts, A.B., Danielpour, D., Dart, L.L., Sporn, M.B. and Dawid, I.B. (1988) Mesoderm induction in amphibians: the role of TGF-beta 2-like factors. *Science*, **239**, 783-785.

Rupp, R.A., Singhal, N. and Veenstra, G.J. (2002) When the embryonic genome flexes its muscles. *Eur J Biochem*, **269**, 2294-2299.

Rupp, R.A., Snider, L. and Weintraub, H. (1994) Xenopus embryos regulate the nuclear localization of XMyoD. *Genes Dev*, **8**, 1311-1323.

Rupp, R.A. and Weintraub, H. (1991) Ubiquitous MyoD transcription at the midblastula transition precedes induction-dependent MyoD expression in presumptive mesoderm of X. laevis. *Cell*, **65**, 927-937.

Ruthenburg, A.J., Allis, C.D. and Wysocka, J. (2007) Methylation of lysine 4 on histone H3: intricacy of writing and reading a single epigenetic mark. *Mol Cell*, **25**, 15-30.

Sachs, L.M. and Shi, Y.B. (2000) Targeted chromatin binding and histone acetylation in vivo by thyroid hormone receptor during amphibian development. *Proc Natl Acad Sci U S A*, **97**, 13138-13143.

Saeki, H., Ohsumi, K., Aihara, H., Ito, T., Hirose, S., Ura, K. and Kaneda, Y. (2005) Linker histone variants control chromatin dynamics during early embryogenesis. *Proc Natl Acad Sci U S A*, **102**, 5697-5702.

Saha, A., Wittmeyer, J. and Cairns, B.R. (2006) Chromatin remodelling: the industrial revolution of DNA around histones. *Nat Rev Mol Cell Biol*, **7**, 437-447.

Sambrook, J., Fritsch, E.F. and Mainatis, T. (1989) *Molecular Cloning. A laboratory manual*. Cold Spring Harbour Laboratory Press, New York.

Santos-Rosa, H. and Caldas, C. (2005) Chromatin modifier enzymes, the histone code and cancer. *Eur J Cancer*, **41**, 2381-2402.

Satijn, D.P., Hamer, K.M., den Blaauwen, J. and Otte, A.P. (2001) The polycomb group protein EED interacts with YY1, and both proteins induce neural tissue in Xenopus embryos. *Mol Cell Biol*, **21**, 1360-1369.

Schneider, S., Steinbeisser, H., Warga, R.M. and Hausen, P. (1996) Beta-catenin translocation into nuclei demarcates the dorsalizing centers in frog and fish embryos. *Mech Dev*, **57**, 191-198.

Schohl, A. and Fagotto, F. (2002) Beta-catenin, MAPK and Smad signaling during early Xenopus development. *Development*, **129**, 37-52.

Schuettengruber, B., Chourrout, D., Vervoort, M., Leblanc, B. and Cavalli, G. (2007) Genome regulation by polycomb and trithorax proteins. *Cell*, **128**, 735-745.

Schulze, E. and Schulze, B. (1995) The vertebrate linker histones H1 zero, H5, and H1M are descendants of invertebrate "orphon" histone H1 genes. *J Mol Evol*, **41**, 833-840.

Seo, S., Herr, A., Lim, J.W., Richardson, G.A., Richardson, H. and Kroll, K.L. (2005a) Geminin regulates neuronal differentiation by antagonizing Brg1 activity. *Genes Dev*, **19**, 1723-1734.

Seo, S., Richardson, G.A. and Kroll, K.L. (2005b) The SWI/SNF chromatin remodeling protein Brg1 is required for vertebrate neurogenesis and mediates transactivation of Ngn and NeuroD. *Development*, **132**, 105-115.

Servetnick, M. and Grainger, R.M. (1991) Changes in neural and lens competence in Xenopus ectoderm: evidence for an autonomous developmental timer. *Development*, **112**, 177-188.

Sheng, G., dos Reis, M. and Stern, C.D. (2003) Churchill, a zinc finger transcriptional activator, regulates the transition between gastrulation and neurulation. *Cell*, **115**, 603-613.

Showell, C. and Cunliffe, V.T. (2002) Identification of putative interaction partners for the Xenopus Polycomb-group protein Xeed. *Gene*, **291**, 95-104.

Sims, R.J., 3rd and Reinberg, D. (2006) Histone H3 Lys 4 methylation: caught in a bind? *Genes Dev*, **20**, 2779-2786.

Singhal, N. (2005) The role of *Xenopus* Brg1, a conserved subunit of SWI/SNF class remodeling complexes, during early frog development. *Fakultät für Biologie*. Ludwig-Maximilians-Universität München, München, Vol. PhD.

Slack, J.M. (2002) Conrad Hal Waddington: the last Renaissance biologist? *Nat Rev Genet*, **3**, 889-895.

Smith, W.C. and Harland, R.M. (1992) Expression cloning of noggin, a new dorsalizing factor localized to the Spemann organizer in Xenopus embryos. *Cell*, **70**, 829-840.

Sokol, S., Christian, J.L., Moon, R.T. and Melton, D.A. (1991) Injected Wnt RNA induces a complete body axis in Xenopus embryos. *Cell*, **67**, 741-752.

Sokol, S., Wong, G.G. and Melton, D.A. (1990) A mouse macrophage factor induces head structures and organizes a body axis in Xenopus. *Science*, **249**, 561-564.

Solomon, M.J., Larsen, P.L. and Varshavsky, A. (1988) Mapping protein-DNA interactions in vivo with formaldehyde: evidence that histone H4 is retained on a highly transcribed gene. *Cell*, **53**, 937-947.

Solomon, M.J. and Varshavsky, A. (1985) Formaldehyde-mediated DNA-protein crosslinking: a probe for in vivo chromatin structures. *Proc Natl Acad Sci U S A*, **82**, 6470-6474.

Spohr, G., Reith, W. and Sures, I. (1981) Organization and sequence analysis of a cluster of repetitive DNA elements from Xenopus laevis. *J Mol Biol*, **151**, 573-592.

Srinivasan, S., Armstrong, J.A., Deuring, R., Dahlsveen, I.K., McNeill, H. and Tamkun, J.W. (2005) The Drosophila trithorax group protein Kismet facilitates an early step in transcriptional elongation by RNA Polymerase II. *Development*, **132**, 1623-1635.

Stancheva, I., Collins, A.L., Van den Veyver, I.B., Zoghbi, H. and Meehan, R.R. (2003) A mutant form of MeCP2 protein associated with human Rett syndrome cannot be displaced from methylated DNA by notch in Xenopus embryos. *Mol Cell*, **12**, 425-435.

Standley, H.J., Destree, O., Kofron, M., Wylie, C. and Heasman, J. (2006) Maternal XTcf1 and XTcf4 have distinct roles in regulating Wnt target genes. *Dev Biol*, **289**, 318-328.

Stark, J., Andl, T. and Millar, S.E. (2007) Hairy math: insights into hair-follicle spacing and orientation. *Cell*, **128**, 17-20.

Steinbach, O. (1998) Epigenetische Kontrolle von Entwicklungsprozessen bei Wirbeltieren - eine Fallstudie am Beispiel der myoD-Induktion bei Xenopus laevis. *Fakultät für Chemie und Pharmacie*. Universität Tübingen, Tübingen, Vol. Ph.d.

Steinbach, O.C., Ulshofer, A., Authaler, A. and Rupp, R.A. (1998) Temporal restriction of MyoD induction and autocatalysis during Xenopus mesoderm formation. *Dev Biol*, **202**, 280-292.

Steinbach, O.C., Wolffe, A.P. and Rupp, R.A. (1997) Somatic linker histones cause loss of mesodermal competence in Xenopus. *Nature*, **389**, 395-399.

Stern, C.D. (2005) Neural induction: old problem, new findings, yet more questions. *Development*, **132**, 2007-2021.

Stern, M., Jensen, R. and Herskowitz, I. (1984) Five SWI genes are required for expression of the HO gene in yeast. *J Mol Biol*, **178**, 853-868.

Stewart, M.D., Sommerville, J. and Wong, J. (2006) Dynamic regulation of histone modifications in Xenopus oocytes through histone exchange. *Mol Cell Biol*, **26**, 6890-6901.

Strahl-Bolsinger, S., Hecht, A., Luo, K. and Grunstein, M. (1997) SIR2 and SIR4 interactions differ in core and extended telomeric heterochromatin in yeast. *Genes Dev*, **11**, 83-93.

Sudarsanam, P. and Winston, F. (2000) The Swi/Snf family nucleosome-remodeling complexes and transcriptional control. *Trends Genet*, **16**, 345-351.

Tamkun, J.W. (1995) The role of brahma and related proteins in transcription and development. *Curr Opin Genet Dev*, **5**, 473-477.

Tamkun, J.W., Deuring, R., Scott, M.P., Kissinger, M., Pattatucci, A.M., Kaufman, T.C. and Kennison, J.A. (1992) brahma: a regulator of Drosophila homeotic genes structurally related to the yeast transcriptional activator SNF2/SWI2. *Cell*, **68**, 561-572.

Taylor, S.M. and Jones, P.A. (1982) Changes in phenotypic expression in embryonic and adult cells treated with 5-azacytidine. *J Cell Physiol*, **111**, 187-194.

Thayer, M.J., Tapscott, S.J., Davis, R.L., Wright, W.E., Lassar, A.B. and Weintraub, H. (1989) Positive autoregulation of the myogenic determination gene MyoD1. *Cell*, **58**, 241-248.

Toivonen, S. (1953) Knochenmark als mesodermaler Induktor im Implantatsversuche bei Triturus. *Atch.Soc. zool.-bot. fenn. "Vanamo"*, **7**, 113-121.

Torres-Padilla, M.E., Parfitt, D.E., Kouzarides, T. and Zernicka-Goetz, M. (2007) Histone arginine methylation regulates pluripotency in the early mouse embryo. *Nature*, **445**, 214-218.

Turner, B.M. (2005) Reading signals on the nucleosome with a new nomenclature for modified histones. *Nat Struct Mol Biol*, **12**, 110-112.

Turner, B.M. (2007) Defining an epigenetic code. *Nat Cell Biol*, **9**, 2-6.

Unhavaithaya, Y., Shin, T.H., Miliaras, N., Lee, J., Oyama, T. and Mello, C.C. (2002) MEP-1 and a homolog of the NURD complex component Mi-2 act together to maintain germline-soma distinctions in C. elegans. *Cell*, **111**, 991-1002.

Van de Wetering, M., Castrop, J., Korinek, V. and Clevers, H. (1996) Extensive alternative splicing and dual promoter usage generate Tcf-1 protein isoforms with differential transcription control properties. *Mol Cell Biol*, **16**, 745-752.

Van Lente, F., Jackson, J.F. and Weintraub, H. (1975) Identification of specific crosslinked histones after treatment of chromatin with formaldehyde. *Cell*, **5**, 45-50.

van Noort, M. and Clevers, H. (2002) TCF transcription factors, mediators of Wnt-signaling in development and cancer. *Dev Biol*, **244**, 1-8.

Vermaak, D., Steinbach, O.C., Dimitrov, S., Rupp, R.A. and Wolffe, A.P. (1998) The globular domain of histone H1 is sufficient to direct specific gene repression in early Xenopus embryos. *Curr Biol*, **8**, 533-536.

Verschueren, K., Remacle, J.E., Collart, C., Kraft, H., Baker, B.S., Tylzanowski, P., Nelles, L., Wuytens, G., Su, M.T., Bodmer, R., Smith, J.C. and Huylebroeck, D. (1999) SIP1, a novel zinc finger/homeodomain repressor, interacts with Smad proteins and binds to 5'-CACCT sequences in candidate target genes. *J Biol Chem*, **274**, 20489-20498.

von Zelewsky, T., Palladino, F., Brunschwig, K., Tobler, H., Hajnal, A. and Muller, F. (2000) The C. elegans Mi-2 chromatin-remodelling proteins function in vulval cell fate determination. *Development*, **127**, 5277-5284.

Waddington, C.H. (1942) *Endeavor*, **1**, 18-20.

Waddington, C.H. (1957) *The Strategy of the Genes; a Diacussion of Some Aspects of Theoretical Biology* Allen & Unwin, London.

Wade, P.A., Jones, P.L., Vermaak, D. and Wolffe, A.P. (1999) Purification of a histone deacetylase complex from Xenopus laevis: preparation of substrates and assay procedures. *Methods Enzymol*, **304**, 715-725.

Wang, J. and Wynshaw-Boris, A. (2004) The canonical Wnt pathway in early mammalian embryogenesis and stem cell maintenance/differentiation. *Curr Opin Genet Dev*, **14**, 533-539.

Wardle, F.C. and Smith, J.C. (2006) Transcriptional regulation of mesendoderm formation in Xenopus. *Semin Cell Dev Biol*, **17**, 99-109.

Waterborg, J.H. (2001) Dynamics of histone acetylation in Saccharomyces cerevisiae. *Biochemistry*, **40**, 2599-2605.

Wolpert, L., Beddington, B., Brockes, J., Jessell, T., Lawrence, P. and Meyerowitz, E. (1998) *Principles of Development*. Current Biology Publications, London.

Woodage, T., Basrai, M.A., Baxevanis, A.D., Hieter, P. and Collins, F.S. (1997) Characterization of the CHD family of proteins. *Proc Natl Acad Sci U S A*, **94**, 11472-11477.

Xiao, L. (2003) Transcriptional Regulation of the *Xenopus MyoD* Gene. *Fakultät für Biologie*. Ludwig-Maximilians-Universität München, München, Vol. Ph.d.

Yamagoe, S., Kanno, T., Kanno, Y., Sasaki, S., Siegel, R.M., Lenardo, M.J., Humphrey, G., Wang, Y., Nakatani, Y., Howard, B.H. and Ozato, K. (2003) Interaction of histone acetylases and deacetylases in vivo. *Mol Cell Biol*, **23**, 1025-1033.

Yang, J., Mei, W., Otto, A., Xiao, L., Tao, Q., Geng, X., Rupp, R.A. and Ding, X. (2002) Repression through a distal TCF-3 binding site restricts Xenopus myf-5 expression in gastrula mesoderm. *Mech Dev*, **115**, 79-89.

Yang, P.K. and Kuroda, M.I. (2007) Noncoding RNAs and intranuclear positioning in monoallelic gene expression. *Cell*, **128**, 777-786.

Zaromytidou, A.I., Miralles, F. and Treisman, R. (2006) MAL and ternary complex factor use different mechanisms to contact a common surface on the serum response factor DNA-binding domain. *Mol Cell Biol*, **26**, 4134-4148.

Zeng, L. and Zhou, M.M. (2002) Bromodomain: an acetyl-lysine binding domain. *FEBS Lett*, **513**, 124-128.

8 Appendix

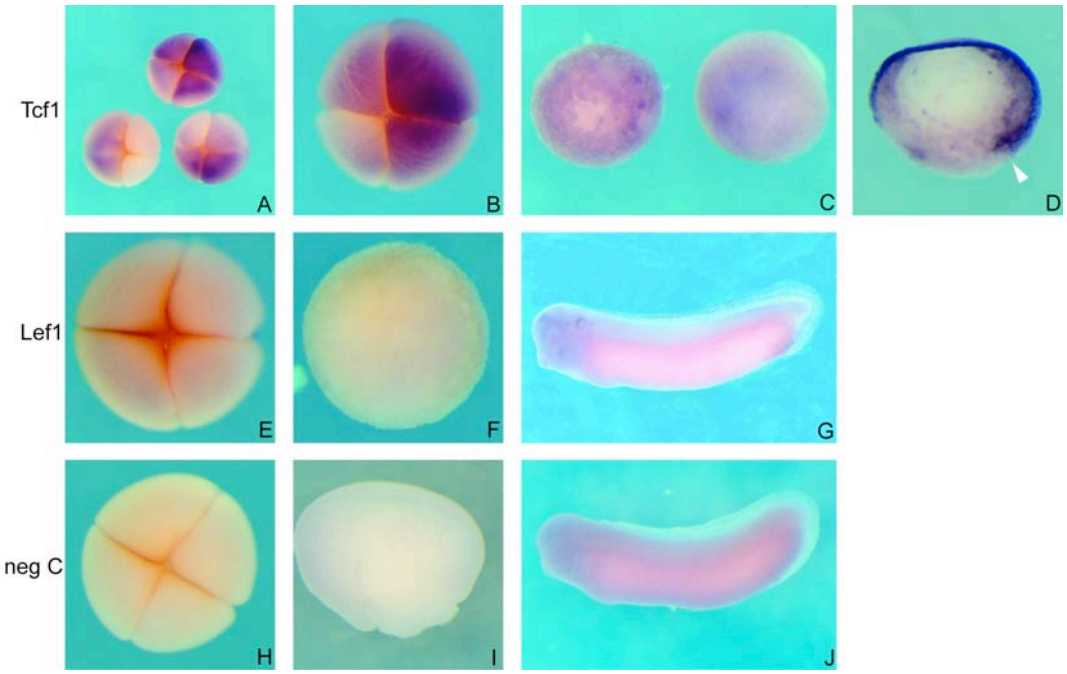

Appendix Figure 1: Protein expression patterns of Lef1 and Tcf1 in embryos
A-D: Immunocytochemistry (ICC, see 3.7.2) with αTcf1 antibody Tcf1 2F4; E-G: Immunocytochemistry (ICC) with αLef1 antibody LEF 3D4; H-J: negative control of ICC without primary antibody. A, B, E, H: 4-cell stage embryos; C,F: blastula NF8; D,F,I: gastrula NF11; G,J: tailbud NF 30. White arrowhead in D marks the bastopore lip on the dorsal side of the embryo.

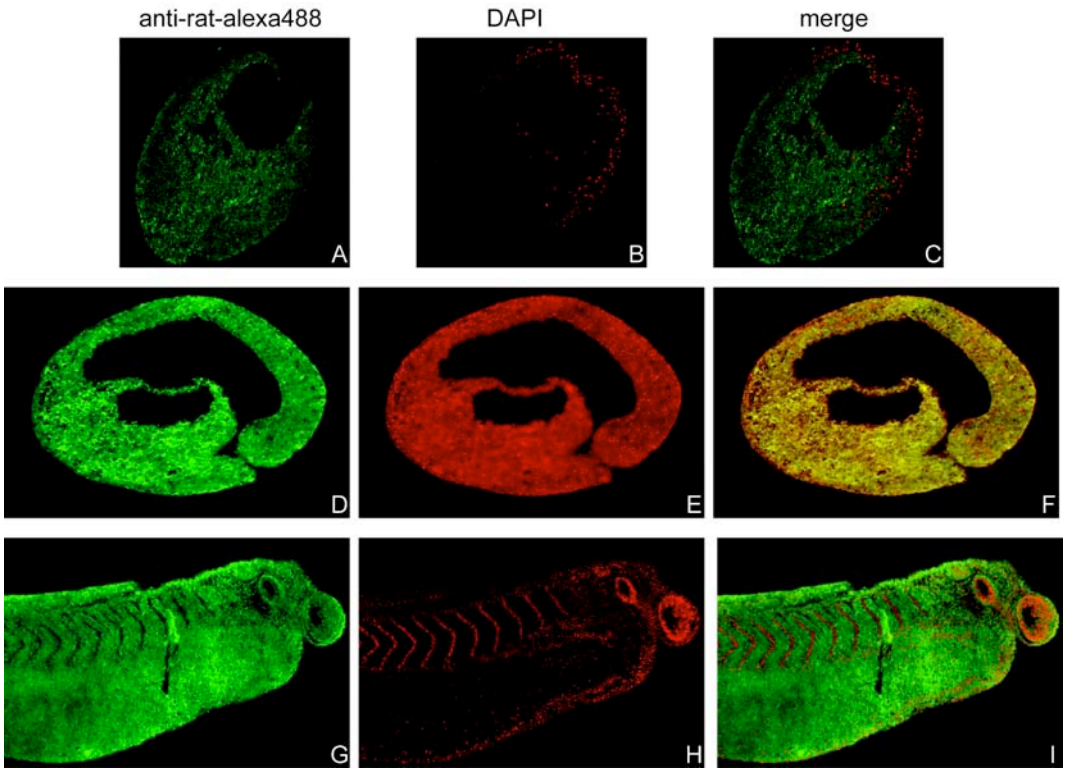

Appendix Figure 2: Control of immunofluorescence study of Lef1 and Tcf1

Immunofluoresence (IF, see 3.7.3) on paraffin sections with secondary antibody alone. A,D,G: background fluorescence of anti-rat-alexa488; B,E,H: DAPI staining of DNA, C,F,I: merged alexa and DNA stain. Yellow are the overlays. A-C: gastrula NF11 dorsal to the right, animal to the top, D-F: neurula NF 18, anterior to the front, dorsal to the top; G-I: tailbud NF 28, anterior to the right, dorsal to the top.

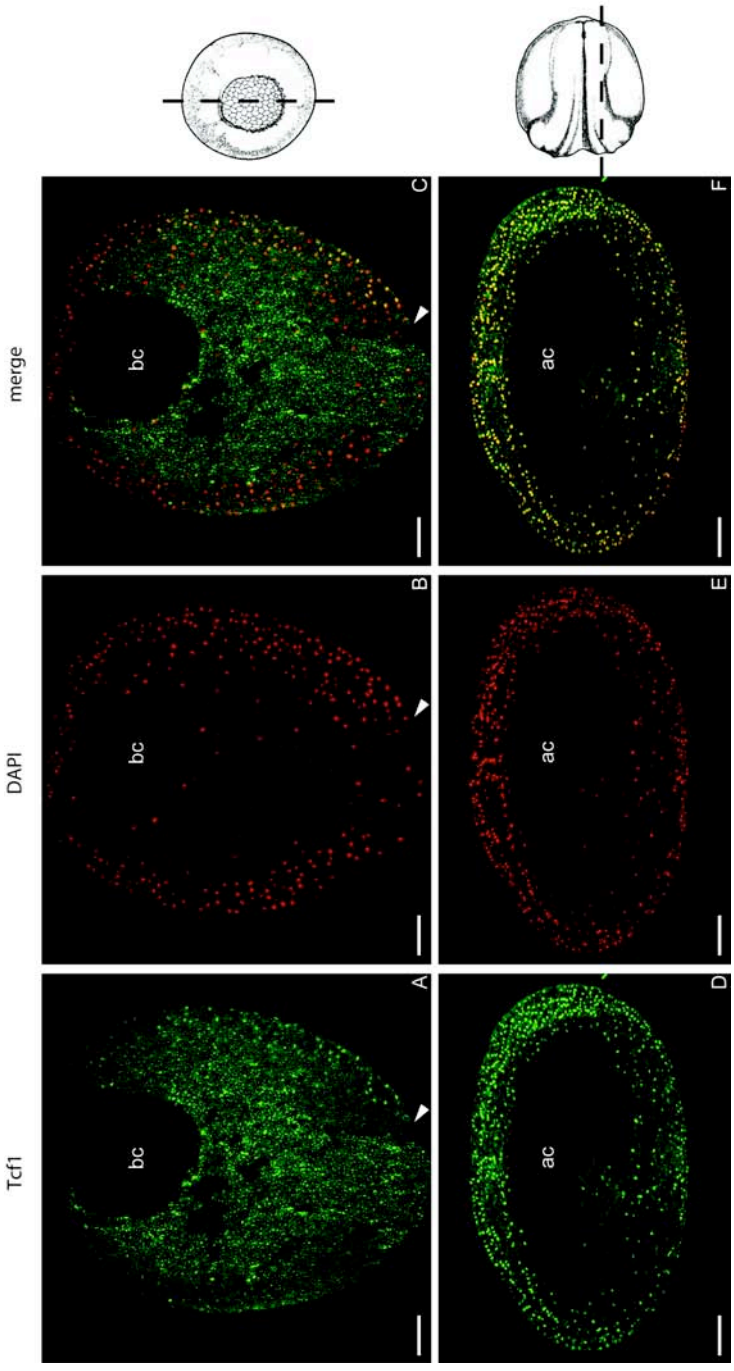

Appendix Figure 3: Protein expression pattern of Tcf1 in paraffin sections of gastrula NF11 and neurula NF15
Immunofluoresence analysis (IF, see 3.7.3) on paraffin sections of Tcf1. A,D: Tcf1 stain with antibody Tcf1 2F4; B,E: DNA stain with DAPI; C, F: merged pictures. A-C: gastrula NF11 dorsal to the right, animal to the top, bc: blastocoel; white arrow head: dorsal blastopore lip. D-F: neurula NF 18, anterior to the front, dorsal to the top, ac: archenteron. Scale bar is 200µM. Sketch on the right hand side marks the section planes.

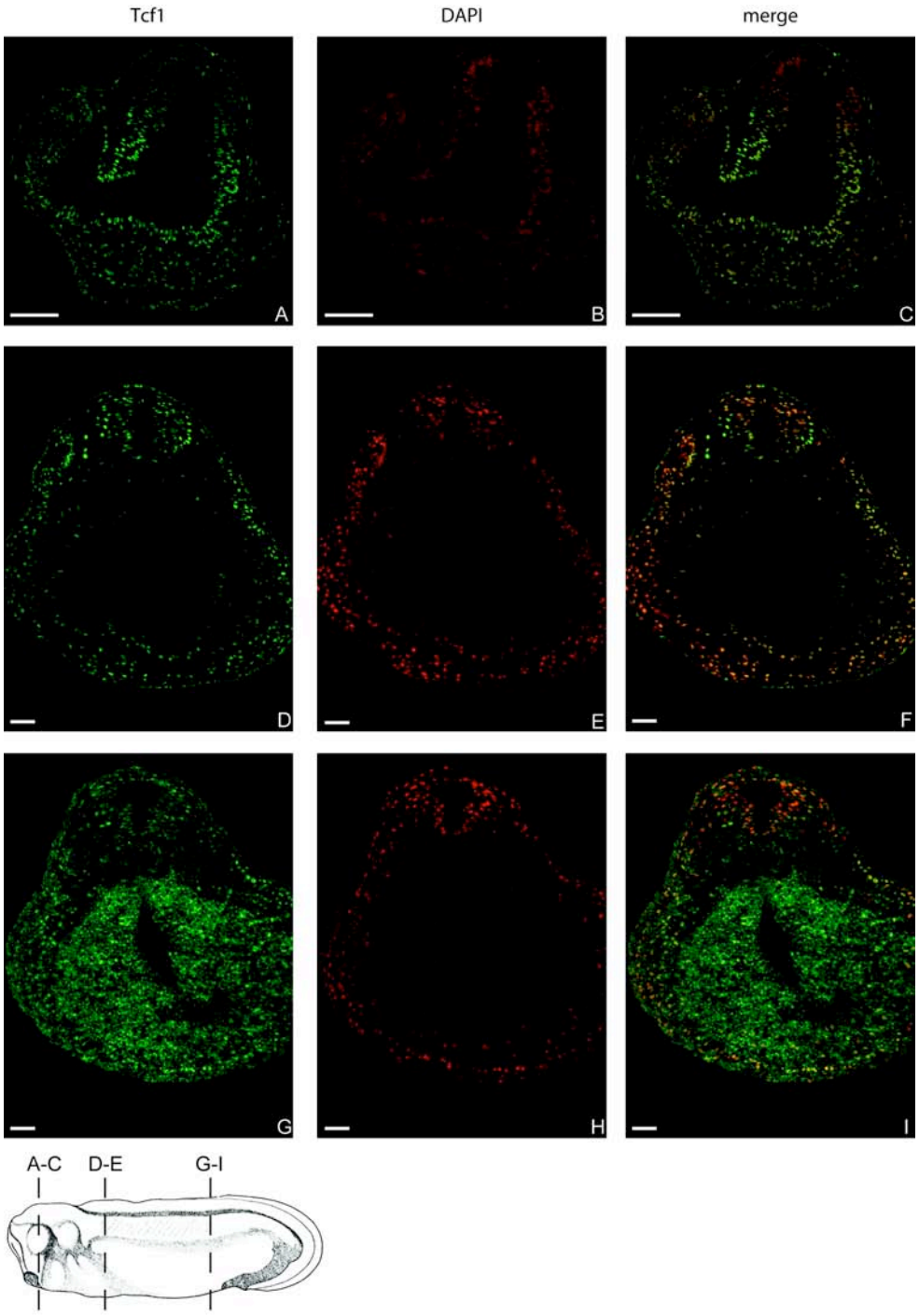

Appendix Figure 4: Protein expression pattern of Tcf1 in cross sections of head, anterior and posterior trunk of a tailbud NF27

Immunofluoresence analysis (IF, see 3.7.3) on paraffin sections of Tcf1. A,D,G: Tcf1 stain with antibody Tcf1 2F4; B,E,H: DNA stain with DAPI; C,F,I: merged pictures. A-C: Sections of the head including midbrain, eyes and cement gland, D-F: Section of the anterior trunk. G-I: Section of the posterior trunk. Scale bar is 100µM. Sketch on the bottom marks the section planes.

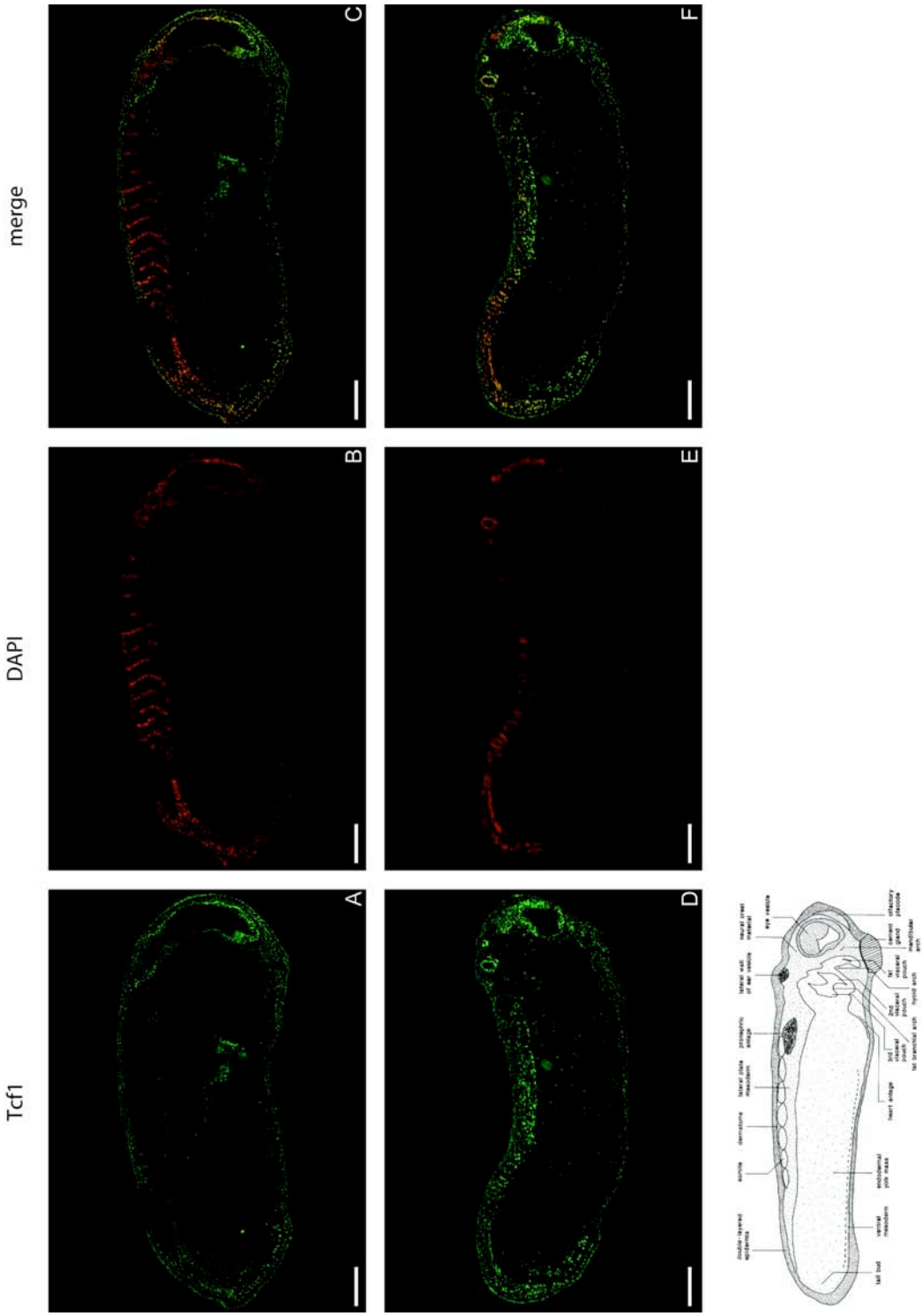

Appendix Figure 5: Protein expression pattern of Tcf1 in longitudinal sections of a tailbud NF27

Immunofluoresence analysis (IF, see 3.7.3) on paraffin sections of Tcf1. A,D: Tcf1 stain with antibody Tcf1 2F4; B,E: DNA stain with DAPI; C,F: merged pictures. A-C,D-F: longitudinal sections of a tailbud embryos. Scale bar is 500µM. Sketch on the bottom marks the section plain.

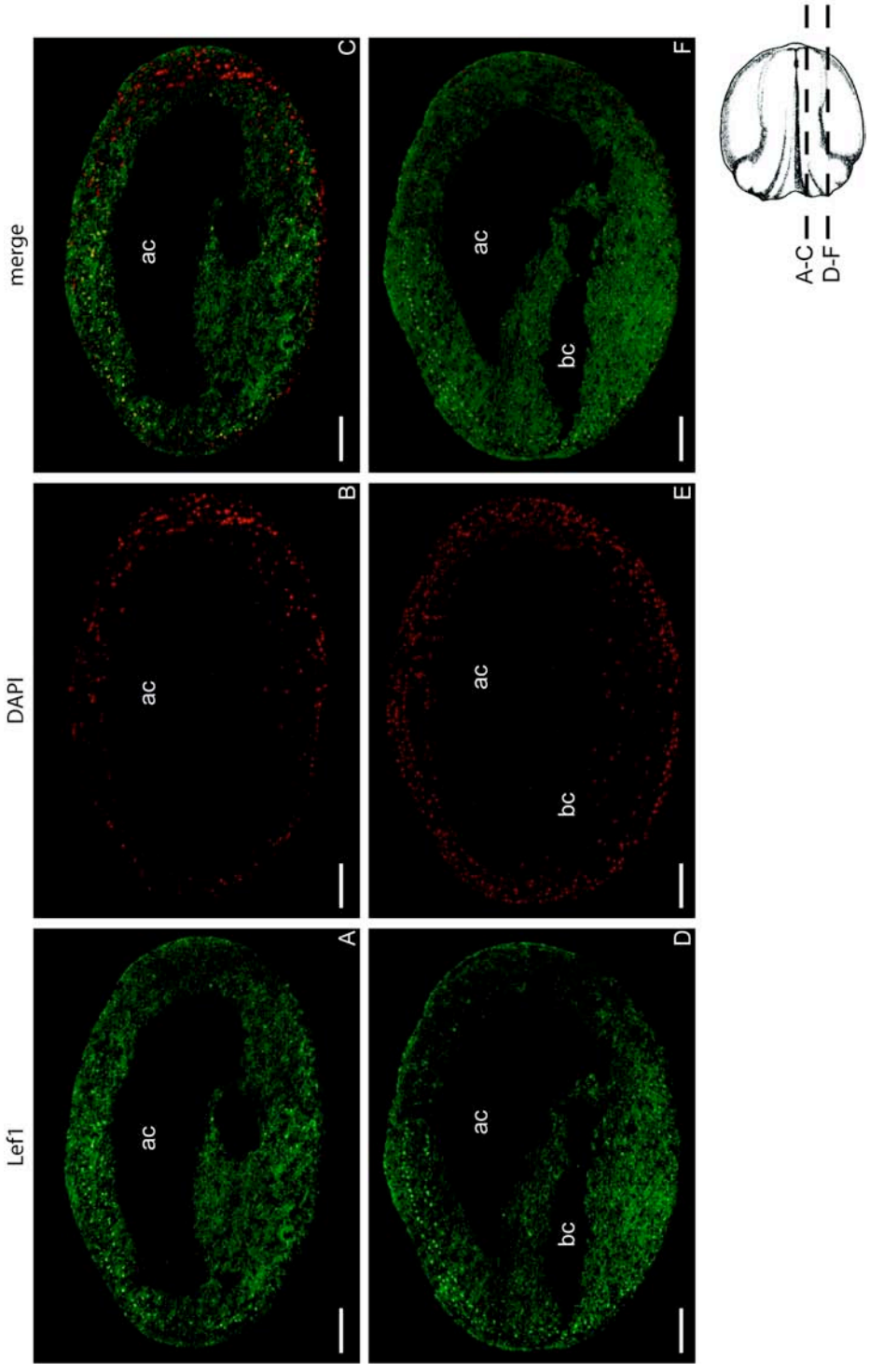

Appendix Figure 6: Protein expression pattern of Lef1 in paraffin sections of neurula NF15

Immunofluoresence analysis (IF, see 3.7.3) on paraffin sections of Lef1. A,D: Lef1 stain with antibody LEF 3D4; B,E: DNA stain with DAPI; C, F: merged pictures. A-C, D-F: neurula NF 18, anterior to the front, dorsal to the top, bc: blastocoel ac: archenteron. Scale bar is 200µM. Sketch on the right hand side marks the section planes.

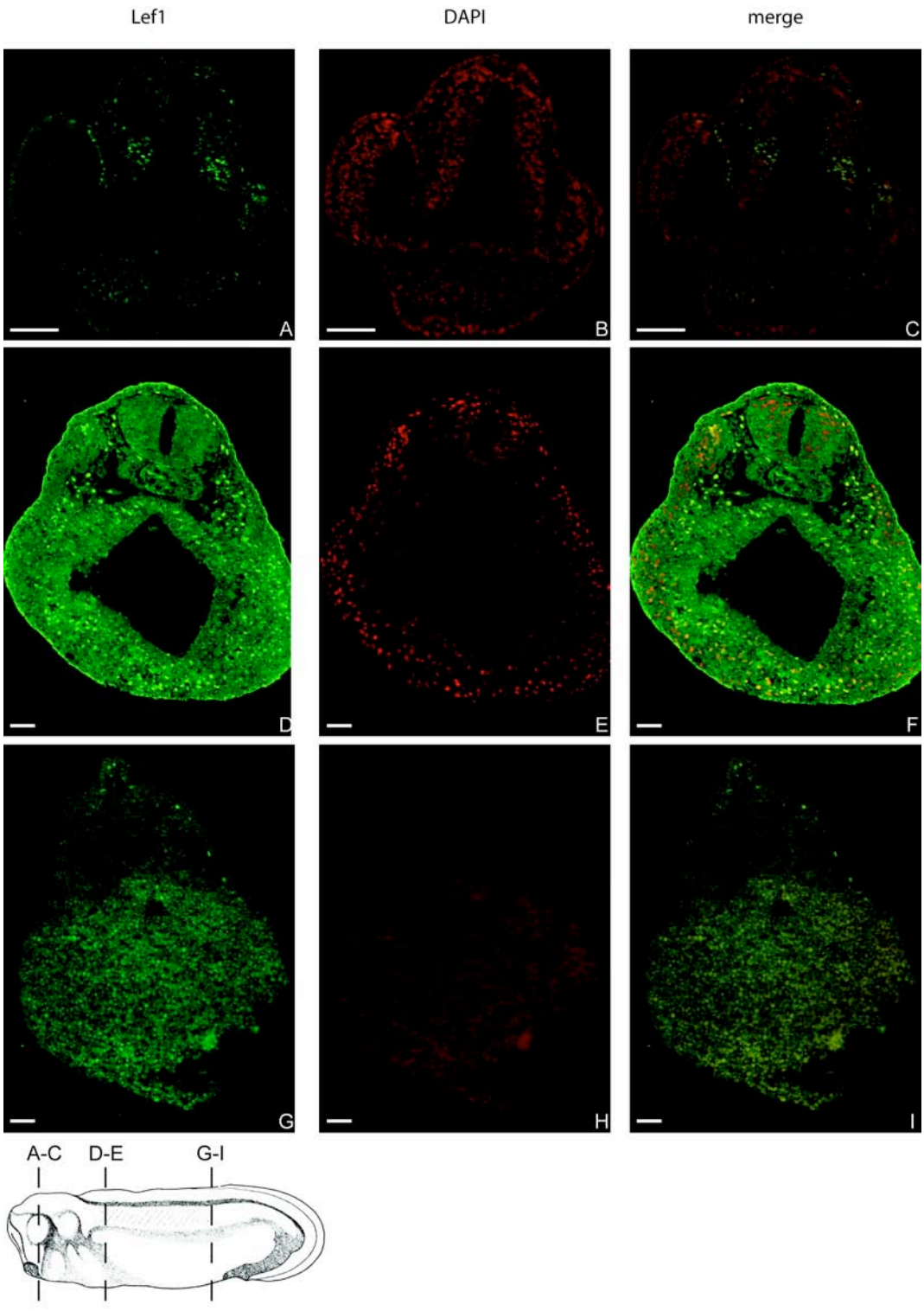

Appendix Figure 7: Protein expression pattern of Lef1 in cross sections of head, anterior and posterior trunk of a tailbud NF27
Immunofluoresence analysis (IF, see 3.7.3) on paraffin sections of Lef1. A,D,G: Lef1 stain with antibody LEF 3D4; B,E,H: DNA stain with DAPI; C,F,I: merged pictures. A-C: Sections of the head including midbrain, eyes and cement gland, D-F: Section of the anterior trunk. G-I: Section of the posterior trunk. Scale bar is 100µM. Sketch on the bottom marks the section planes.

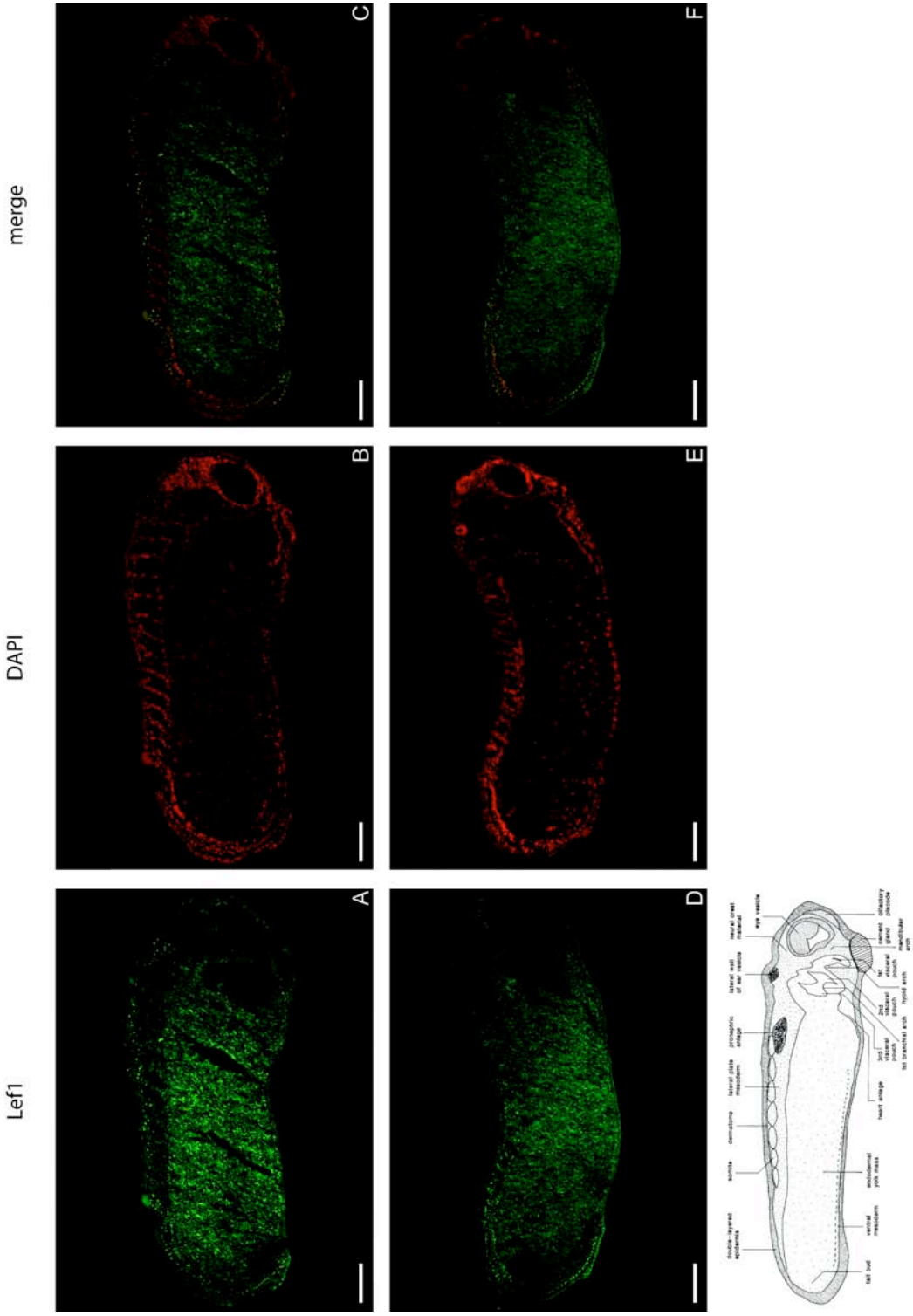

Appendix Figure 8: Protein expression pattern of Lef1 in longitudinal sections of a tailbud NF27
Immunofluoresence analysis (IF, see 3.7.3) on paraffin sections of Lef1. A,D: Lef1 stain with antibody LEF 3D4; B,E: DNA stain with DAPI; C,F: merged pictures. A-C,D-F: longitudinal sections of a tailbud embryos. Scale bar is 500µM. Sketch on the bottom marks the section planes.

Danksagung

Ich danke…

Prof. Dr. Ralph AW Rupp für die Überlassung dieser herausfordernden Arbeit, für seine gute Betreuung und für die wissenschaftliche Freiheit, die er mir gewährt hat.

Prof. Dr. Peter Becker für die Vertretung dieser Arbeit vor der Fakultät und für wertvolle Verbesserungsvorschläge im Rahmen von Laborseminaren und PhD-Mentoratssitzungen.

Dr. Elisabeth Kremmer (GSF München) und ihren Mitarbeitern für die Kooperation bei der Herstellung der monoklonalen Antikörper. Außerdem danke ich Alice Sulz für die Unterstützung bei den Paraffinschnitten.

den weiteren Mitgliedern meines PhD-Mentorats Dr. Gregor Gilfillan und Dr. Aloys Schepers für wichtige Tipps und Hilfestellungen. Des Weiteren danke ich Angelika Mitterweger, Dr. Matthias Prestl, Dr. Hans Reinke und Dr. Oliver Nentwich für Ihre Hilfe und Diskussionsbereitschaft bei „ChIP“-Fragen.

Prof. Dr. Herbert Steinbeisser für die großzügige Hilfestellung beim Froschnotstand und seine Diskussionsbereitschaft. Ich danke auch Dr. Dietmar Gradl für seine fortwährende Diskussionsbereitschaft und die Kooperation beim Lef/Tcf-Projekt. Des Weiteren danke ich Klaus-Michael Kürner für die Gewährung von Unterschlupf während meines Aufenthalts in Heidelberg und für sein offenes Ohr.

Prof. Dr. Axel Imhof, Prof. Dr. Gustav Klobeck, Dr. Britta Linder-Stuart, Dr. Alyos Schepers und Annette Scharf für die Korrektur dieser Arbeit.

allen Mitarbeitern des Instituts für das freundliche und hilfsbereite Arbeitsumfeld.

natürlich ganz besonders meinen KollegInnen Barbara, Britta, Edith, Laura, Markus, Sabine und Tobias für den vielen Spaß, den wir hatten und dafür, dass ihr immer ein offenes Ohr hattet. Vielen Dank an Edith, vor allem aber an Barbara für Eure Hilfsbereitschaft und Unterstützung bei diversen Projekten und „Notfällen“. Vielen Dank an Britta für Deine Hilfestellungen bei vielen Projekten. Vielen Dank natürlich an Sabine. Ohne deinen herrlichen Humor und deine Lebensberatung wäre vieles nicht so einfach gewesen. Und natürlich vielen Dank an den Salatclub, ohne Eure Kreationen wäre ich verhungert.

meinen Freunden für viele schöne Wandertouren, Radltouren und schöne Stunden in Biergärten und im Lochhamer’s, die ein guter Ausgleich zum Arbeitsalltag waren.

meinen Eltern und meiner Familie für all ihre Unterstützung und meinem Freund Markus für seinen liebevollen Beistand in allen Lebenslagen.

Lebenslauf

geboren am 14.November 1976 in Stuttgart-Bad Cannstatt

09/87 – 06/96	**Remstalgymnasium Weinstadt** Mathematisch-naturwissenschaftlicher Zweig Abschluss: Abitur
10/96 – 09/98	**Eberhardt-Karls-Universität Tübingen** **Studiengang Biologie Diplom** Vordiplom
10/98 – 06/99	**University of Sussex, Brighton/England** **ERASMUS-Austauschstudium in Biological Sciences** Certificate in Life Sciences
07/99 – 03/02	**Eberhardt-Karls-Universität Tübingen** **Studiengang Biologie Diplom** Diplomarbeit “Untersuchungen zum Einfluss des Wnt/PKC-Signaltransduktionsweges auf die Proteinphosphorylierung in *Xenopus* Embryonen” Abschluss: Diplom-Biologin
05/02 – 12/02	**Ludwig-Maximilians-Universität München** **Adolf-Butenandt-Institut,** Wissenschaftliche Mitarbeiterin Abteilung Physiologische Chemie Untersuchungen zur Rolle von kleinen G-Proteinen auf das polarisierte Wachstum des filamentösen Pilzes *Neurospora crassa*
01/03 – heute	**Ludwig-Maximilians-Universität München** **Fakultät für Biologie** Promotionsstudentin am Adolf-Butenandt-Institut, Abteilung Molekularbiologie Doktorarbeit “Analysis of Developmental Epistasis by Chromatin Immunoprecepitation in *Xenopus laevis*”